



Prepared for:
Rijkswaterstaat
Dienst Getijdewateren

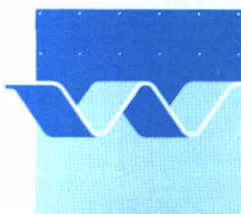
Wave conditions along the Dutch coast

AFGEHANDELD

Part A: Text, tables and appendices
Report on numerical model studies
July 1993

	bibliotheek postbus 177 - 2600 MH Delft waterloopkundig laboratorium/WL
BB	VERVALEN 62253
WL	
EXPL	 R0000988

Wave conditions along the Dutch coast



delft hydraulics

Executive summary

The proposed new "Act on the Sea Defence" ("Wet op de Waterkering") prescribes a 5 yearly evaluation of the safety of the coastal defence of the Netherlands. Rijkswaterstaat (Directorate-General for Public Works and Water Management) is at this moment studying the aspects required for a probabilistic approach. This includes both the input parameters and the method for the safety analysis. An important element in this analysis are the hydraulic boundary conditions (water levels, wave conditions, wind and currents). The HYDRA-project was set-up by the Tidal Waters Division of Rijkswaterstaat (further referred to as RWS-DGW) to provide the hydraulic input parameters for this safety analysis along the coast and in the estuaries of the Netherlands. Because of the increasing importance of probabilistic methods in failure analysis, the HYDRA-project has two goals:

- to provide the multi-dimensional statistics of the hydraulic conditions in deeper water (approximately NAP -20 m contour line)
- to select a procedure to compute the hydraulic conditions along a dike-ring in a uniform way.

The whole HYDRA-project consists of a larger number of separate studies related to the deep water statistics, analysis of wave measurements, wave modelling in the nearshore zone and translation of the deep water statistics to the constructions.

In their letter of 29 May 1991, RWS-DGW invited Delft Hydraulics (DH) to submit a proposal for a reconnaissance study for numerical modelling of the wave conditions in shallow water using the numerical model HISWA. On 12 July 1991 DH submitted a joint proposal of DH and the Group Fluid Mechanics of the Faculty of Civil Engineering of the Delft University of Technology (TUD), author of the HISWA-model. The proposal included:

- set-up of HISWA-models of the area between IJmuiden and Texel,
- a sensitivity study to assess the importance of a large number of parameters on the wave height and wave period near the NAP -5 m contour line,
- validation and calibration of the model against measured wave conditions,
- trial computations to determine the wave conditions during design conditions along the NAP -5 m contour line for points with a spacing of 200 m.

TUD participated in the project for support in the model set-up and the interpretation of the results and for some research on the formulations and implementation of the model, because of irregularities in the results encountered in an earlier study for RWS-DGW. In their letter of October 14, 1991, reference AO/915594, Rijkswaterstaat commissioned Delft Hydraulics to carry out these studies including a number of the optional items of the proposal under contract number DG-377.

Aspects like the proposed schematisations, boundary conditions and interim results were regularly discussed during progress meetings attended by all parties involved.

From the studies carried out in the framework of the HYDRA-project to select the methodology to compute the wave conditions nearshore from the conditions at the NAP -20 m contour line, we draw the following conclusions:

- Irregularities in the results of HISWA in earlier studies were caused by numerical instabilities. These instabilities are to a large extent suppressed in a recent test version and will be implemented together with a few other improvements in the next release of the program. See Chapter 3 and Appendix A.
- Limitation of the wave height by the water depth is the most significant factor in the shallow nearshore zone along the coast and in the entrance of the tidal inlet. The water level is therefore an important parameter in the computations (Sections 4.4.3 and 4.5.6).
- In the shallow water zone wave breaking is the most important physical phenomenon. The computational results are rather sensitive to the choice of the parameters describing this process, such as the shallow water breaking coefficient and the frequency change by breaking (Sections 4.4.12, 4.4.13 and 4.5.6).
- In the tidal inlet the current conditions have also a considerable effect on the wave height (Section 4.4.9) and are in the tidal channels the dominating factor in the total uncertainty (Section 4.5.6).
- Considering that the measurements sometimes show large variations, the computed wave heights and periods show fair agreement with the measured conditions in the Egmond profile. Bottom friction appears to be rather well computed; shallow water wave breaking is the most critical point for calibration (Chapter 5).
- For the tidal inlet a good, complete set of data for verification is not available. For the area of the Wadden Sea just behind the tidal inlet the wind speed is the most important parameter for calibration of the model. Accounting for the difference in temperature between sea and air in the wind speed used in the computations, improves the agreement between computed and measured wave height (Chapter 5).
- The computational results at the NAP -10 m contour lines are fairly constant along the coast. Near the tidal inlet, in the area sheltered by the shoals of the outer delta, the wave height and period decrease (Chapter 6).
- Along the closed coast the most seaward bar in the computational area causes an irregular position of the NAP -5 m line in the cross-shore profile, leading to variations in the wave height along the NAP -5 m contour line generated by HISWA. For future computations we suggest a position between the NAP -10 m and NAP -5 m contour lines for the output points (Chapter 6).
- Between the NAP -10 m and NAP -5 m lines in the Egmond profile the total uncertainty in the significant wave height is about 0.55 m (H_s between 6 and 5 m) and in the mean wave period about 1.7 s (T_m between 10 and 9 s).
Near the coast at Den Helder the total uncertainty in the significant wave height is also about 0.55 m ($H_s = 1.5$ m) and in the mean wave period 2.5 s ($T_m = 7$ s). See section 4.5.6 and Table 4.7.

Based on the above we conclude that the HISWA model is in principle a suitable tool to compute the nearshore wave conditions from the conditions offshore. The model has, however, a few limitations that are mainly related to the formulation of the dissipation by

wave breaking. This is relevant for the proposed application, because reduction of the wave height by wave breaking due to depth limitation is one of the most important phenomena. This also explains that results along the closed coast are most sensitive for the water level and the wave breaking coefficients. The following points should be noted when using HISWA to assess the wave heights along the coast for design purposes:

- The water level in the model is fixed. Breaking waves induce a set-up of the water level near the coast. This effect and its return-effect on the wave heights may be significant in very shallow water. The wave set-up is not included in the HISWA computations carried out for this study. Results in water shallower than 5 m, should therefore be treated with caution. The wave set-up can be included by applying a different methodology. In a more extensive study the set-up could be calculated using a hydrodynamic model or estimated in another way. The set-up would then be included in the wave propagation computations by modifying the bathymetry for the HISWA models according to the calculated differences in water level. For the presently envisaged application of HISWA to generate boundary conditions for dune erosion computations, neglecting the set-up can be partly avoided. When these dune erosion computations start further offshore most of the set-up will be taken into account, as the 1-dimensional wave propagation model that is included in the dune erosion model (ENDEC), also computes the wave set-up.
- The computed wave heights are rather sensitive to the choice of the shallow water breaking coefficient. Improvement of the breaking formulation reducing the uncertainty in the coefficients for surf breaking, could reduce the total uncertainty in the computed wave conditions.
- The prediction of the wave period in the breaker zone and on underwater bars is rather difficult using a model like HISWA since it is parametric in frequency. In such models a fixed shape of the frequency spectrum is assumed (e.g. a JONSWAP-spectrum), but in the surf-zone the spectral shape does not comply any more with the chosen fixed shape. The change of the wave period in extremely shallow water can better be modelled using fully spectral models, since these models have more degrees of freedom in the spectral shape. In addition such models are able to include the separate effects of depth-limited wave breaking and other non-linear phenomena such as 3-wave interactions. Formulations for the effect on the frequency of the relevant phenomena of wave breaking and 3-wave interactions have only recently been proposed and have not yet been verified.
- The effect of wave breaking on the wave period is also of importance in tidal inlets and estuaries. The wave period is an important parameter in the formulae that are used to compute wave run-up on a dike. We expect that in such areas fully spectral models will give more accurate results. Further the effect of the wind growth after breaking, leading to a bi-modal spectral shape, is better represented in these models. RWS-DGW may consider studies into the suitability of fully spectral models for application in these areas. With HISWA the bi-modal spectrum is best modelled using two computations: one starting in deep water calculating the propagation into the tidal inlet without wave growth and a second run starting on the shallowest parts of the tidal inlet (e.g. Noorderhaaks), to compute the wave height generated by wind action.

Recommended settings

In applications of the HISWA model to compute the wave conditions near the shore for offshore conditions with an exceedance frequency of 10^{-4} , we recommend to use the following schematisations and settings of the internal parameters of HISWA:

- *bottom topography*

In the offshore area variations in time of the bathymetry have a long time scale. Though not explicitly tested in this study we expect that the results near the coast are not very sensitive to small errors in the offshore bathymetry. The long profiles, the HOKU-model or other flow models and nautical maps provide information of sufficient accuracy and detail in this area.

In the coastal zone the bathymetry between the coast and the NAP -10 m contour can change considerably due to a single storm, especially the position of the bar in the profile. It is not known if the results of the dune erosion computations are very sensitive for such changes. This aspect may be the subject of following studies. For the time being it seems adequate to use the most recent available data from the "doorlodigen" and JARKUS-profiles. When the dune erosion computations start near the NAP -10 m line, the bathymetry of the coastal zone is not very critical for the HISWA-computations.

For the wave heights at the seaside of the tidal inlet the depth and location of the Noorderhaaks is of importance, but further into the Wadden Sea the sheltering is mainly caused by the land.

- *computational grids*

In the offshore area which is relatively deep and where variations in depth and wave height occur on a rather large spatial scale, a computational grid with a resolution of 160x400 m is adequate to obtain results with a numerical accuracy in the order of a few centimetres.

In the coastal zone of the closed coast the depth and, consequently, the wave height decreases rapidly. The selected step sizes of 40x100 m in this study seemed a fair choice to describe the bathymetry in this area (bar - trough profile) accurately, as the bathymetry was also given with a resolution of approximately 40 m perpendicular to the shore. Computations carried out by RWS-DGW after completion of the work presented in this report indicate that a smaller step size may be required for reasons of numerical accuracy. This may not be necessary, however, if the dune erosion computations start further offshore (before the most seaward bar in the profile).

The resolution in the area of the Zeegat of 20x65 m was chosen for a proper representation of the bathymetry and for stability of the computation with opposing currents. Computations carried out by RWS-DGW using a smaller spatial resolution showed fairly the same results in the Zeegat van Texel.

- *bottom friction coefficients*

For the bottom friction coefficient for waves we recommend to use the value $c_{fw} = 0.006$. This value has been derived using the theory of Nielson (1979) and Jonsson (1978). The predicted value of the friction coefficient is not very sensitive for small variations in wave height or period for the extreme conditions considered in this study. Close to the coast near Egmond and in the tidal inlet the wave heights are not very sensitive to changes in the friction coefficient we consider to be possible ($0.005 < c_{fw} < 0.007$). The wave period is more affected, mainly because less

dissipation by friction in the offshore area leads to more dissipation by breaking nearshore, while breaking is assumed to affect the mean frequency and friction not. We recommend to switch the effect of bottom friction on the mean wave frequency off, as this is in HISWA modelled in a rather crude way and the effect seems to be counteracted by non-linear interaction between spectral components.

- *wave breaking coefficients*

The formulae to assess the wave breaking coefficients are based on the peak wave period of the spectrum, whereas HISWA uses the mean wave period. We recommend to use corrected values for the deep and shallow water breaking coefficients which account for this difference. For the deep water breaking coefficient (white-capping) the value $\gamma_d = 1.13$ should be used. For the shallow water breaking coefficient (surf breaking) the default value in HISWA is $\gamma_s = 0.80$. Using the formula of Battjes and Stive (1985) and the computed wave conditions before the breaker zone we find an optimal value of $\gamma_s = 0.75$. The results of the validation computations indicate that a lower value of $\gamma_s = 0.70$ may lead to a better agreement with the measured conditions. Recently Roelvink (1993) found that for a slightly modified version of the procedure to compute the dissipation by surf breaking, the optimal value of the breaking coefficient is $\gamma_s = 0.66$. This value has not yet been verified with measurements along the dutch coast. We recommend to use $\gamma_s = 0.75$ for the shallow water breaking coefficient. This will lead to higher values of the wave height in the nearshore area and is therefore a safe value. The recommended values take into account the above mentioned difference in the wave periods.

We recommend to switch the effect of wave breaking on the mean frequency off for the offshore area and the nearshore zone along the closed coast. In the tidal inlet, where growth of the waves due to wind action is an important aspect, switching the effect on the mean frequency off will lead underestimation of the wave height. Taking the effect into account leads to higher wave heights, but the wave period, which is also of importance in wave run-up computations, decreases. For the wave conditions on the seaward side of the tidal inlet we recommend to switch the effect on the mean frequency off too. The effect of wave growth is best assessed with a separate computation using the procedure described above (see page Ex. Sum. 3).

- *current condition*

The current conditions has considerable effect on the wave conditions in the tidal inlet. The highest wave heights occur with an ebb current. The wave periods are also slightly longer. We recommend to use ebb current conditions in the tidal inlets.

Summarizing we recommend:

bathymetry	:	recent data of sufficient detail in relation to variations in depth and to resolution of computational grids
computational grids	:	offshore 160x400 m nearshore less than 40x100 m zeegat 20x65 m
friction coefficients	:	$c_{fw} = 0.006$ frequency change off
breaking coefficients	:	$\gamma_d = 1.13$ (deep water) $\gamma_s = 0.75$ (shallow water) frequency change off
current conditions	:	ebb currents

Contents

List of tables

List of figures

List of notations

1	Introduction	1
2	Description of HISWA	3
2.1	General	3
2.2	Physical background	4
2.2.1	Action balance equation	4
2.2.2	Refraction	5
2.2.3	Wave growth by wind action	5
2.2.4	Bottom dissipation	6
2.2.5	Surf dissipation	6
2.2.6	Current dissipation	7
2.3	Use of HISWA	8
3	Irregular response	9
3.1	Introduction	9
3.2	Approach and results	9
4	Sensitivity study	10
4.1	General	10
4.2	Schematisations	10
4.2.1	Bottom topography	10
4.2.2	Current fields	12
4.2.3	Computational grids	12
4.3	Boundary conditions	14
4.3.1	General	14
4.3.2	Water levels	15
4.3.3	Wave height	15
4.3.4	Wave period	15
4.3.5	Wave direction and directional spreading	16
4.3.6	Wind speed	16
4.3.7	Bottom friction coefficient	17
4.3.8	Frequency change due to bottom friction	17
4.3.9	Wave breaking coefficient	17
4.3.10	Frequency change due to wave breaking	17
4.4	Presentation and discussion of results	18
4.4.1	Output points	18
4.4.2	Reference case	19
4.4.3	Sensitivity for water level	20
4.4.4	Sensitivity for wave height	21
4.4.5	Sensitivity for wave period	21
4.4.6	Sensitivity for wave/wind direction	22
4.4.7	Sensitivity for directional spreading	22

Contents (continued)

4.4.8	Sensitivity for wind speed	23
4.4.9	Sensitivity for current effects	24
4.4.10	Sensitivity for bottom friction coefficient	24
4.4.11	Sensitivity for frequency change due to bottom friction	25
4.4.12	Sensitivity for shallow water breaking coefficient	25
4.4.13	Sensitivity for frequency change due to wave breaking	26
4.4.14	Bottom variability	26
4.5	Combined sensitivity	27
4.5.1	General	27
4.5.2	Method of analysis	28
4.5.3	Method of computation	29
4.5.4	Interdependency between the external parameters	29
4.5.5	The uncertainty of the input parameters	31
4.5.6	Presentation and discussion of the results	31
4.6	Conclusions	34
5	Validation	35
5.1	Storm selection	35
5.2	Computations Egmond profile	35
5.2.1	Description of measurements	35
5.2.2	Schematisation	36
5.2.3	Initial parameter settings	36
5.2.4	Results and calibration	37
5.3	Computations Zeegat van Texel	38
5.3.1	Description of measurements	38
5.3.2	Schematisation	38
5.3.3	Initial parameter settings	38
5.3.4	Results and calibration	39
5.4	Conclusions	40
6	Trial computations	42
6.1	General	42
6.2	Schematisations	42
6.3	Boundary conditions	42
6.4	Discussion of results	43
6.5	Conclusions	44

References

Tables

Figures (see Part B)

Appendix A: Irregularities in HISWA-results

B: Fully spectral propagation scheme

C: Analysis of uncertainty for wave run-up and dike height

List of tables

- 4.1 Boundary conditions HISWA-computations sensitivity study
- 4.2 Averaged mean wave period T_{m01} for a few stations along the Dutch coast (for position see Figure 4.12)
- 4.3 Computed significant wave height, mean wave period and main wave direction of sensitivity runs in selected points in the Egmond profile.
- 4.4 Computed significant wave height, mean wave period and main wave direction of sensitivity runs in selected points in the tidal inlet.
- 4.5 Mean value and standard deviation of primary and related secondary parameters and the assumed interdependency (note: $y = \alpha x$)
- 4.6 Reference values and assumed uncertainty of the input parameters
- 4.7 Absolute and relative uncertainty at two locations in the Egmond profile and one point in the Molengat profile

- 5.1 Wind and wave measurements available for validation in DTBEST-files
- 5.2 Measured wave conditions during storm of December 1982
- 5.3 Boundary conditions validation computations Egmond
- 5.4 Measured and computed wave conditions at offshore and Egmond-stations, storm December 16, 1982
- 5.5 Wave conditions predicted using Hurdle and Stive (1984) for a wind speed of 18 m/s
- 5.6 Wave conditions measured during storm of March 11, 1982
- 5.7 Boundary conditions validation computations Zeegat van Texel
- 5.8 Measured and computed wave conditions at offshore-stations and stations in the Zeegat van Texel, storm November 24, 1981

- 6.1 Boundary conditions trial computations

List of figures

- 4.1 Data sources bathymetry
- 4.2 Comparison long profiles L33 and L35 with corresponding Jarkus-profiles
- 4.3 Effect of averaging on profile representation
- 4.4 Comparison long profile L33 with corresponding section of the Hoku-model
- 4.5 Data points Hoku bathymetry detail outer delta
- 4.6 Data points 250 x 250 bathymetry detail outer delta
- 4.7 Origin of data bathymetry
- 4.8 Waterlevel and windspeed synthetic extreme storm
- 4.9 Current field extreme storm flood conditions
- 4.10 Current field extreme storm ebb conditions
- 4.11 Locations of computational grids
- 4.12 Location wave measuring stations
- 4.13 Expected significant wave height versus storm surge level
- 4.14 Location of output points, lines and areas
- 4.15 Location of output points, lines and areas detail zeegat van Texel
- 4.16 Bottom topography, Run SSS, outer model (in m below NAP)
- 4.17 Bottom topography, Run SSS, zeegat mode (in m below NAP)
- 4.18 Current field, Run SSS, Zeegat model
- 4.19a Significant wave height contours, Run SSS, outer model (in m)
- 4.19b Main wave directions, Run SSS, outer model
- 4.20a Significant wave height contours, Run SSS, Inner model (in m)
- 4.20b Main wave directions, Run SSS, Inner model
- 4.21a Significant wave height contours, Run SSS, Zeegat model (in m)
- 4.21b Main wave directions, Run SSS, Zeegat model
- 4.22a Significant wave height contours, Run SSS, Detail Haaks (in m)
- 4.22b Main wave directions, Run SSS, Detail Haaks
- 4.23a Significant wave height contours, Run SSS, Detail Malzwin (in m)
- 4.23b Main wave directions, Run SSS, Detail Malzwin
- 4.24a Significant wave height Egmond profile comparison buiten and binnen model
- 4.24b Significant wave height Molengat profile comparison buiten and zeegat model
- 4.24c Significant wave height Marsdiep profile comparison of buiten and zeegat model
- 4.24d Significant wave height Breewijd profile comparison buiten and zeegat model
- 4.24e Significant wave height nhpaal 10 profile comparison buiten, binnen and zeegat model
- 4.25a Significant wave height Egmond profile varying water level
- 4.25b Significant wave height Egmond profile varying water level
- 4.25c Mean wave period Egmond profile varying water level
- 4.25d Effect of water level variation Egmond profile
- 4.25e Significant wave height Molengat profile varying water level
- 4.25f Significant wave height Molengat profile varying water level
- 4.25g Significant wave height Marsdiep profile varying water level
- 4.25h Mean wave period Marsdiep profile varying water level
- 4.25i Significant wave height Marsdiep profile varying water level
- 4.25j Mean wave period Marsdiep profile varying water level
- 4.25k Significant wave height Breewijd profile varying water level
- 4.25l Significant wave height Breewijd profile varying water level

List of figures (continued)

- 4.25m Effect of water level variation entrance Wadden Sea
- 4.26a Significant wave height Egmond profile varying incoming wave height
- 4.26b Significant wave height Egmond profile varying incoming wave height
- 4.26c Mean wave period Egmond profile varying incoming wave height
- 4.26d Effect of wave height variation Egmond profile
- 4.26e Significant wave height Molengat profile varying incoming wave height
- 4.26f Significant wave height Molengat profile varying incoming wave height
- 4.26g Significant wave height Marsdiep profile varying incoming wave height
- 4.26h Mean wave period Marsdiep profile varying incoming wave height
- 4.26i Significant wave height Marsdiep profile varying incoming wave height
- 4.26j Mean wave period Marsdiep profile varying incoming wave height
- 4.26k Significant wave height Breewijd profile varying incoming wave height
- 4.26l Significant wave height Breewijd profile varying incoming wave height
- 4.26m Effect of wave height variation entrance Wadden Sea
- 4.27a Significant wave height Egmond profile varying wave period
- 4.27b Mean wave period Egmond profile varying wave period
- 4.27c Wave steepness Egmond profile varying wave period
- 4.27d Significant wave height Egmond profile varying wave period
- 4.27e Mean wave period Egmond profile varying wave period
- 4.27f Effect of wave period variation Egmond profile
- 4.27g Significant wave height Molengat profile varying wave period
- 4.27h Significant wave height Molengat profile varying wave period
- 4.27i Significant wave height Marsdiep profile varying wave period
- 4.27j Mean wave period Marsdiep profile varying wave period
- 4.27k Significant wave height Marsdiep profile varying wave period
- 4.27l Mean wave period Marsdiep profile varying wave period
- 4.27m Significant wave height Breewijd profile varying wave period
- 4.27n Significant wave height Breewijd profile varying wave period
- 4.27o Effect of wave period variation entrance Wadden Sea
- 4.28a Significant wave height Molengat profile varying wave direction
- 4.28b Significant wave height Marsdiep profile varying wave direction
- 4.28c Mean wave period Marsdiep profile varying wave direction
- 4.28d Significant wave height Breewijd profile varying wave direction
- 4.28e Effect of main wave direction entrance Wadden Sea
- 4.29a Significant wave height Egmond profile varying directional spreading
- 4.29b Significant wave height Egmond profile varying directional spreading
- 4.29c Mean wave period Egmond profile varying directional spreading
- 4.29d Effect of directional spreading Egmond profile
- 4.29e Significant wave height Molengat profile varying directional spreading
- 4.29f Significant wave height Molengat profile varying directional spreading
- 4.29g Significant wave height Marsdiep profile varying directional spreading
- 4.29h Mean wave period Marsdiep profile varying directional spreading
- 4.29i Significant wave height Marsdiep profile varying directional spreading
- 4.29j Mean wave period Marsdiep profile varying directional spreading
- 4.29k Significant wave height Breewijd profile varying directional spreading
- 4.29l Significant wave height Breewijd profile varying directional spreading

List of figures (continued)

- 4.29m Effect of directional spreading entrance Wadden Sea
- 4.30a Significant wave height Egmond profile varying wind speed
- 4.30b Significant wave height Egmond profile varying wind speed
- 4.30c Mean wave period Egmond profile varying wind speed
- 4.30d Effect of wind speed variation Egmond profile
- 4.30e Significant wave height Molengat profile varying wind speed
- 4.30f Significant wave height Molengat profile varying wind speed
- 4.30g Significant wave height Marsdiep profile varying wind speed
- 4.30h Mean wave period Marsdiep profile varying wind speed
- 4.30i Significant wave height Marsdiep profile varying wind speed
- 4.30j Mean wave period Marsdiep profile varying wind speed
- 4.30k Significant wave height Breewijd profile varying wind speed
- 4.30l Significant wave height Breewijd profile varying wind speed
- 4.30m Effect of wind speed variation entrance Wadden Sea
- 4.31a Significant wave height Molengat profile varying current conditions
- 4.31b Mean wave period Molengat profile varying current conditions
- 4.31c Significant wave height Marsdiep profile varying current conditions
- 4.31d Mean wave period Marsdiep profile varying current conditions
- 4.31e Significant wave height Breewijd profile varying current conditions
- 4.31f Mean wave period Breewijd profile varying current conditions
- 4.31g Effect of current conditions entrance Wadden Sea
- 4.32a Significant wave height Egmond profile varying bottom friction coefficient
- 4.32b Significant wave height Egmond profile varying bottom friction
- 4.32c Mean wave period Egmond profile varying bottom friction
- 4.32d Effect of friction coefficient Egmond profile
- 4.32e Significant wave height Molengat profile varying bottom friction coefficient
- 4.32f Significant wave height Molengat profile varying bottom friction coefficient
- 4.32g Significant wave height Marsdiep profile varying bottom friction coefficient
- 4.32h Mean wave period Marsdiep profile varying bottom friction coefficient
- 4.32i Significant wave height Marsdiep profile varying bottom friction coefficient
- 4.32j Mean wave period Marsdiep profile varying bottom friction coefficient
- 4.32k Significant wave height Breewijd profile varying bottom friction coefficient
- 4.32l Significant wave height Breewijd profile varying bottom friction coefficient
- 4.32m Effect of friction coefficient entrance Wadden Sea
- 4.33a Significant wave height Egmond profile frequency change friction on/off
- 4.33b Mean wave period Egmond profile frequency change friction on/off
- 4.33c Effect of frequency change friction Egmond profile
- 4.33d Significant wave height Molengat profile frequency change friction on/off
- 4.33e Significant wave height Marsdiep profile frequency change friction on/off
- 4.33f Mean wave period Marsdiep profile frequency change friction on/off
- 4.33g Significant wave height Breewijd profile frequency change friction on/off
- 4.33h Effect of frequency change friction entrance Wadden Sea
- 4.34a Significant wave height Egmond profile varying wave breaking coefficient
- 4.34b Significant wave height Egmond profile varying wave breaking coefficient
- 4.34c Mean wave period Egmond profile varying wave breaking coefficient
- 4.34d Effect of breaking coefficient Egmond profile

List of figures (continued)

- 4.34e Significant wave height Molengat profile varying wave breaking coefficient
- 4.34f Significant wave height Molengat profile varying wave breaking coefficient
- 4.34g Significant wave height Marsdiep profile varying wave breaking coefficient
- 4.34h Mean wave period Marsdiep profile varying wave breaking coefficient
- 4.34i Significant wave height Marsdiep profile varying wave breaking coefficient
- 4.34j Mean wave period Marsdiep profile varying wave breaking coefficient
- 4.34k Significant wave height Breewijd profile varying wave breaking coefficient
- 4.34l Significant wave height Breewijd profile varying wave breaking coefficient
- 4.34m Effect of breaking coefficient entrance Wadden Sea
- 4.35a Significant wave height Egmond profile frequency change breaking on/off
- 4.35b Significant wave height Egmond profile frequency change breaking on/off
- 4.35c Mean wave period Egmond profile frequency change breaking on/off
- 4.35d Effect of frequency change breaking Egmond profile
- 4.35e Significant wave height Molengat profile frequency change breaking on/off
- 4.35f Significant wave height Molengat profile frequency change breaking on/off
- 4.35g Significant wave height Marsdiep profile frequency change breaking on/off
- 4.35h Mean wave period Marsdiep profile frequency change breaking on/off
- 4.35i Significant wave height Marsdiep profile frequency change breaking on/off
- 4.35j Mean wave period Marsdiep profile frequency change breaking on/off
- 4.35k Significant wave height Breewijd profile frequency change breaking on/off
- 4.35l Significant wave height Breewijd profile frequency change breaking on/off
- 4.35m Effect of frequency change breaking entrance Wadden Sea
- 4.36a Bottom variability bathymetry of profiles
- 4.36b Bottom variability relation depth - significant wave height
- 4.37a Significant wave height and mean wave period Egmond profile
- 4.37b Significant wave height Egmond profile, total uncertainty
- 4.37c Significant wave height Egmond profile, normalized uncertainty due to parameters WS, HS and TM
- 4.37d Significant wave height Egmond profile, Normalized uncertainty due to parameters WI and SD
- 4.37e Significant wave height Egmond profile, Normalized uncertainty due to parameters FV, BW and BC
- 4.37f Mean wave period Egmond profile, total uncertainty
- 4.37g Mean wave period Egmond profile, normalized uncertainty due to parameters WS, HS and TM
- 4.37h Mean wave period Egmond profile, normalized uncertainty due to parameters WI and SD
- 4.37i Mean wave period Egmond profile, normalized uncertainty due to parameters FV, BW and BC
- 4.38a Significant wave height and mean wave period Molengat profile
- 4.38b Significant wave height Molengat profile, total uncertainty
- 4.38c Significant wave height Molengat profile, normalized uncertainty due to parameters WS, HS and TM
- 4.38d Significant wave height Molengat profile, normalized uncertainty due to parameters WI, SR and SD

List of figures (continued)

- 4.38e Significant wave height Molengat profile, normalized uncertainty due to parameters FV, BW and BC
- 4.38f Mean wave period Molengat profile, total uncertainty
- 4.38g Mean wave period Molengat profile, normalized uncertainty due to parameters WS, HS and TM
- 4.38h Mean wave period Molengat profile, normalized uncertainty due to parameters WI, SR and SD
- 4.38i Mean wave period Molengat profile, normalized uncertainty due to parameters FV, BW and BC
- 4.39a Significant wave height and mean wave period Marsdiep profile
- 4.39b Significant wave height Marsdiep profile, total uncertainty
- 4.39c Significant wave height Marsdiep profile, normalized uncertainty due to parameters WS, HS and TM
- 4.39d Significant wave height Marsdiep profile, normalized uncertainty due to parameters WI, SR and SD
- 4.39e Significant wave height Marsdiep profile, normalized uncertainty due to parameters FV, BW and BC
- 4.39f Mean wave period Marsdiep profile, total uncertainty
- 4.39g Mean wave period Marsdiep profile, normalized uncertainty due to parameters WS, HS and TM
- 4.39h Mean wave period Marsdiep profile, normalized uncertainty due to parameters WI, SR and SD
- 4.39i Mean wave period Marsdiep profile, normalized uncertainty due to parameters FV, BW and BC

- 5.1a Measured wave height H_{m0} (down) and wave period T_{m01} (uP0, storm December 1982, offshore stations
- 5.1b Measured wave height H_{m0} (down) and wave period T_{m01} (up), storm December 1982, Egmond stations
- 5.2a Measured wind speed (down) and direction (up) storm December 1982, offshore stations
- 5.2b Measured wind speed (down) and direction (up) storm December 1982, Egmond stations
- 5.3 Locations of computational grids validation computations
- 5.4 Significant wave height H_s and mean wave period T_m , 16 December 1982, 0.00 h
- 5.5 Significant wave height H_s and mean wave period T_m , 16 December 1982, 6.00 h
- 5.6 Significant wave height H_s and mean wave period T_m , 16 December 1982, 18.00 h
- 5.7a Variation bathymetry Egmond profile, profile 40.000, 1977-1984
- 5.7b Variation bathymetry Egmond profile, profile 40.500, 1977-1984
- 5.7c Variation bathymetry Egmond profile, profile 41.000, 1977-1984
- 5.8a Measured wave height H_{m0} (down) and wave period T_{m01} (up), storm November 1981, Schulpengat

List of figures (continued)

- 5.8b Measured wave height H_{m0} (down) and wave period T_{m01} (up), storm November 1981, Bollen
- 5.9a Measured wind speed (down) and direction (up) storm November 1981, Schulpengat
- 5.9b Measured wind speed (down) and direction (up) storm November 1981, Bollen
- 5.10 Current field storm 24 November 1981
- 5.11 Amplification factor for effect of air-water temperature difference

- 6.1 Position of NAP -10 m contour HISWA output coast of North-Holland
- 6.2 Position of NAP -5 m contour HISWA output coast of North-Holland
- 6.3 Position of NAP -10 m contour HISWA output coast of Texel
- 6.4 Position of NAP -5 m contour HISWA output coast of Texel
- 6.5a Significant wave height H_s and mean wave period T_m at NAP -10 m contour coast of North-Holland
- 6.5b Main wave direction at NAP -10 m contour coast of North-Holland
- 6.6a Significant wave height H_s and mean wave period T_m at NAP -5 m contour coast of North-Holland
- 6.6b Main wave direction at NAP -5 m contour coast of North-Holland
- 6.7a Significant wave height H_s and mean wave period T_m at NAP -10 m contour coast of Texel
- 6.7b Main wave direction at NAP -10 m contour coast of Texel
- 6.8a Significant wave height H_s and mean wave period T_m at NAP -5 m contour coast of Texel
- 6.8b Main wave direction at NAP -5 m contour coast of Texel
- 6.9a Significant wave height H_s and mean wave period T_m at NAP -10 m contour Coast of North-Holland
- 6.9b Main wave direction at NAP -10 m contour coast of North-Holland
- 6.10a Significant wave height H_s and mean wave period T_m at NAP -5 m contour coast of North-Holland
- 6.10b Main wave direction at NAP -5 m contour coast of North-Holland
- 6.11a Significant wave height H_s and mean wave period T_m at NAP -10 m contour coast of Texel
- 6.11b Main wave direction at NAP -10 m contour coast of Texel
- 6.12a Significant wave height H_s and mean wave period T_m at NAP -5 m contour coast of Texel
- 6.12b Main wave direction at NAP -5 m contour coast of Texel

List of notations

A	wave action density spectrum (E/σ)
A_i	i -th order moment of wave action density spectrum
C_g	group velocity
$C_{x,y,\theta}$	propagation velocities in x , y and θ -direction
c_{fc}	friction coefficient for current
c_{fw}	friction coefficient for waves
E	wave energy density spectrum
E_{tot}	total wave energy
f	wave frequency $1/T$
f_c	critical wave frequency
f_p	peak wave frequency
g	gravitational acceleration
H	wave height
H_m	maximum wave height
H_s	significant wave height, defined as $4\sqrt{m_0}$
h	water depth
k	wave number
\underline{k}	wave number vector
m_0	variance of surface elevation, zero-th order moment of energy density spectrum
n	direction normal to wave direction
Q_b	fraction of breaking waves
S	source term in energy balance equation
T_0, T_1	source terms in action balance equation
T	wave period
T_{m01}	spectral mean wave period
T_p	peak wave period
t^*	dimensionless time of wave growth
U_{bot}	horizontal component of orbital velocity at the sea bed
V	current velocity
α	constant (wave breaking)
γ_d	wave breaking coefficient deep water
γ_s	wave breaking coefficient shallow water
θ	wave direction
π	circular constant
σ	relative frequency
ω	wave frequency ($2\pi f$)

1 Introduction

Rijkswaterstaat (Directorate-General for Public Works and Water Management) is developing procedures for a regular evaluation of the safety of the coastal defence of the Netherlands. The Tidal Waters Division has started several studies concerning the hydraulic boundary conditions along the entire dutch coast in the HYDRA-project. These studies are directed at both the statistical description of the conditions and methods to obtain consistent results along the entire coast. The hydraulic boundary conditions are the input for models evaluating the strength of dikes and dunes. The present study concerns the methodology to compute the wave conditions nearshore (NAP -5 m contour line) from the conditions in deeper water. The aim of the study is to verify the performance of the HISWA-model for wave propagation computations in the area of interest and to analyse the sensitivity of the computed nearshore conditions for a number of external and internal parameters.

The work carried out under the contract for the present studies included:

- investigation into causes of irregularities in HISWA-results and improvement of the HISWA-model,
- set-up of HISWA-models of the area between IJmuiden and Texel including a comparison and synthesis of bathymetry data in the area to be modelled and the determination of the boundary conditions for the reference case,
- a sensitivity study to assess the importance of a large number of parameters on the wave height and wave period near the NAP -5 m contour line; the parameters that were varied are: water level, incoming wave height, incoming wave period, directional spreading of the incoming wave field, wind speed, current conditions in the tidal inlet, bottom friction coefficient, shallow water wave breaking coefficient, frequency change due to wave breaking,
- validation and calibration of the model against measured wave conditions; computations were carried out for conditions measured in the Egmond profile during the storm of 16 December 1982 and for conditions measured in the tidal inlet on 24 November 1981,
- trial computations to determine the wave conditions along the NAP -5 m contour line in points with a spacing of 200 m for conditions with a probability of exceedance of 10^{-4} per year and 10^{-2} per year.

The project was carried out in cooperation with the Delft University of Technology (TUD). The sensitivity study, the validation and the trial computations were performed by Messrs. J. Dekker and J. Vis of DELFT HYDRAULICS. A few sensitivity computations for parameters not included in the scope of work were carried out by Mr. J. Andorka Gal of RWS-DGW. Mr. D.P. Hurdle was the project leader for DELFT HYDRAULICS. The analysis of the irregular behaviour of the HISWA-model was realised at the TUD by Dr. N. Booij. The study of the combined sensitivity was also carried out at the TUD by Mr. Y. Eldeberky under supervision of Dr. N. Booij. Messrs. Booij, Eldeberky en Dekker are also the authors of the respective parts of this report.

The study was carried out under project number H1355. The final report was completed in May 1993.

This report is arranged in the following way:

- The computer program HISWA, with which most of the study was carried out, is shortly described in Chapter 2.
- The investigation of the irregularities in HISWA-results of earlier studies and proposed changes in the program is summarized in Chapter 3. The full report by the TUD on this item is given in Appendix A.
- Chapter 4 describes the sensitivity studies. This includes the model set-up, the boundary conditions, the presentation of the results and an analysis of the most important factors for the wave conditions nearshore.
- The results of a validation of the HISWA-model using measurements in a profile near Egmond and in the tidal inlet is presented in Chapter 5.
- Finally Chapter 6 describes two trial computations performed to calculate the wave conditions along the NAP -10 m and NAP -5 m contour lines.

2 Description of HISWA

2.1 General

The wave model HISWA, acronym for HIndcast Shallow water WAves, is a numerical model developed by Delft University of Technology to simulate wave growth and propagation in areas of variable water depth and ambient current. HISWA models the wave 'action' (equivalent to wave energy when there is no current) in discrete directional sectors at points on a rectangular grid. Wave growth by the action of wind and dissipation by bottom friction and wave breaking are accounted for, as well as depth and current refraction. It is therefore suitable for application in large areas of shallow water where modelling of a directionally spread wave field is required.

In summary HISWA can model the following effects:

- Bottom and current refraction,
- Directional spreading of the waves,
- Wave growth due to wind action,
- Dissipation due to bottom friction,
- Dissipation due to wave breaking,
- Wave blocking by large opposing currents,
- Frequency changes due to dissipation and wind.

HISWA does not model the effects of wave diffraction and results should be interpreted with caution behind coastal structures and on other locations where large gradients in the wave height occur, e.g. due to concentration of wave energy by refraction along channels. At a larger distance behind such locations neglecting the diffraction effects is usually less severe, because local wave growth and the effect of directional spreading become more important. Further HISWA is a stationary model and applies incident wave conditions and a wind field which do not vary in time. Therefore it is suitable for application in areas which are small in comparison with those usually used with hindcast models (less than 100 km x 100 km).

The following sections of this chapter give a simplified description of the mathematical-physical background and the practical use of HISWA. A more detailed description of the theoretical background is given by Holthuijsen et al. (1989). The performance of HISWA has been extensively tested and the results have been compared with analytical solutions for academic situations, with wave measurements both in laboratory and field conditions and with other models. Examples can be found in Booij et al. (1988), Dingemans et al. (1987), Vogel et al. (1989), Den Adel et al. (1991) and DELFT HYDRAULICS (1987, 1990).

2.2 Physical background

2.2.1 Action balance equation

HISWA is based on the full action balance equation for each spectral component. The wave action A is related to the wave energy E according

$$A = E/\sigma \quad (2.1)$$

The relative frequency σ is defined as

$$\sigma = \omega - \underline{k} \cdot \underline{V} \quad (2.2)$$

where ω is the wave frequency, \underline{k} is the wave number vector and \underline{V} the current vector.

To limit the required computational effort, the equation is simplified by assuming that the wave field is stationary and that the frequency spectrum in each direction has a fixed shape and is characterised by one frequency. So in HISWA the wave spectrum is discrete in directions, but it is parametric in frequency. With these assumptions the evolution of the wave field can be described by two equations for each spectral direction:

$$\frac{\partial}{\partial x}(C_x^* A_0) + \frac{\partial}{\partial y}(C_y^* A_0) + \frac{\partial}{\partial \theta}(C_\theta^* A_0) = T_0 \quad (2.3)$$

$$\frac{\partial}{\partial x}(C_x^{**} A_1) + \frac{\partial}{\partial y}(C_y^{**} A_1) + \frac{\partial}{\partial \theta}(C_\theta^{**} A_1) = T_1 \quad (2.4)$$

These equations are the evolution equations for the zeroth-order and first-order moments A_0 and A_1 of the action density spectrum for that spectral direction. The left-hand sides of these equations represent the propagation of the waves and the terms T_0 and T_1 on the right hand side are the source terms representing the effects of wave generation and dissipation. The first two terms of each equation represent rectilinear propagation in space where C_x^* , C_y^* , C_x^{**} , C_y^{**} are the propagation velocities in x- and y- direction of action and mean frequency respectively. These propagation velocities are related to the group velocity \underline{C}_g which is defined as

$$\underline{C}_g = \frac{\partial \sigma}{\partial \underline{k}} \frac{\underline{k}}{k} + \underline{V} \quad (2.5)$$

The third term in the Eqs. (2.3) and (2.4) represents the effects of refraction.

2.2.2 Refraction

Refraction is commonly defined as the change in propagation direction due to variation in phase speed along the wave crest. This definition holds especially for regular, long-crested waves and the conventional ray-models are based on this principal. In the spectral description of an irregular, short-crested wave field refraction implies the transfer of energy from one spectral component to another and a change in the energy density function $E(f, \theta)$. In HISWA this transfer of energy is characterized by the propagation velocity C_θ which is defined as

$$C_\theta = -\frac{1}{k} \frac{\partial \sigma}{\partial h} \frac{\partial h}{\partial n} - \frac{k}{k} \frac{\partial V}{\partial n} \quad (2.6)$$

where h is the total water depth and n is the distance normal to the wave direction θ . Equation (2.6) shows that the refraction term includes both the effect of bottom refraction and the effect of a spatially varying current.

2.2.3 Wave growth by wind action

The model for wave growth by wind action is directionally decoupled and parametric, based on empirical models for wave growth in ideal circumstances. The meaning of directionally decoupled is that the wave growth in each direction sector is considered to be independent of the development in other direction sectors. To obtain the development of the wave energy and the mean frequency in that direction sector HISWA the wave energy to be part of a wave field in ideal conditions. The ideal circumstances refer to an open area with waves of initially zero height over which a constant wind blows. HISWA thus includes implicitly all processes of wave growth due to wind action on an unlimited, infinitely deep ocean without currents: atmospheric input, white-capping dissipation and non-linear wave-wave interactions. The evolution of the dimensionless total wave energy and the dimensionless average frequency is given by

$$E^* = A(t^*)^B \quad \text{for } t^* < t^*_{\max} \quad (2.7)$$

$$E^* = A(t^*_{\max})^B \quad \text{for } t^* \geq t^*_{\max}$$

$$f^* = P(t^*)^Q \quad \text{for } t^* < t^*_{\max} \quad (2.8)$$

$$f^* = P(t^*_{\max})^Q \quad \text{for } t^* \geq t^*_{\max}$$

where E^* is the dimensionless total energy, f^* the dimensionless average frequency, t^* the dimensionless time and t^*_{\max} the dimensionless time at which the maximum energy is reached. All variables are made dimensionless with the mean wind velocity at 10 m elevation (U_{10}) and the gravitational acceleration g . The coefficients A , B , P , Q and t^*_{\max} are chosen such that the HISWA results for fetch-limited growth agree well with the method given in the Shore Protection Manual (CERC, 1973). In ideal conditions for wave growth, wave energy and wave period are linked by the universal relationship (e.g. Hasselmann et al., 1976)

$$f^* = c(E^*)^d \quad (2.9)$$

The coefficients e and f follow easily from Eqs. (2.7) and (2.8). When HISWA predicts a combination of wave height and period which deviates from this ideal height/period relationship, a term is introduced which causes the period to move towards the ideal value.

2.2.4 Bottom dissipation

HISWA represents the effects of bottom friction using the conventional quadratic friction law to represent the bottom shear stress including the effect of a mean current. The corresponding energy dissipation is given by Putnam and Johnson (1949) for a regular wave. This was extended by Dingemans (DELFT HYDRAULICS, 1983) for irregular waves. In the directional version of this formulation it is assumed that the shear stress is directionally distributed in proportion to the square of the orbital velocity in each direction. The energy dissipation per unit of time (S) for one spectral direction is then calculated by

$$S(\theta) = -\frac{U_{bot1}^2}{g} (c_{fw} U_{bot2} + c_{fc} U_{cur}) \quad (2.10)$$

where c_{fw} and c_{fc} are the friction coefficients for the waves and currents respectively, U_{bot1} and U_{bot2} are measures for the orbital velocity at the bottom, U_{cur} is the current component in the direction θ and g is the gravitational acceleration.

HISWA can also represent the effect of bottom dissipation on the mean wave frequency. This frequency is expected to change because the dissipation has more effect on low frequency waves. However, it has been shown by various authors that this effect is often compensated in nearly equal measure by non-linear energy exchange between high and low frequency waves (see e.g. Bouws and Kooen, 1983). As the effect of non-linear energy exchange is not included in the HISWA model, this facility should be applied with care.

2.2.5 Surf dissipation

In HISWA the energy dissipation due to surf breaking is determined using the bore-model of Battjes and Janssen (1979). This model combines the effects of depth and steepness breaking in a single formulation. The corresponding directional distribution of the dissipation is considered to be proportional to the energy density in each direction. The computation of the dissipation due to wave breaking consists of three steps:

- computation of the maximum wave height H_m according

$$H_m = \frac{\gamma_d}{k} \tanh\left(\frac{\gamma_s kh}{\gamma_d}\right) \quad (2.11)$$

- determination of the fraction of breaking waves Q_b from

$$\frac{(1-Q_b)}{\ln(Q_b)} = -8 \frac{E_{tot}}{H_m^2} \quad (2.12)$$

computation of the dissipation for each directional component $S(\theta)$ using

$$S(\theta) = -\alpha Q_b f(\theta) H_m^2 \frac{E(\theta)}{8\pi E_{tot}} \quad (2.13)$$

where γ_s and γ_d are the coefficients for breaking in shallow and deep water respectively, k is the wave number, h the water depth, E_{tot} the total wave energy and $E(\theta)$ and $f(\theta)$ are the energy density and the mean wave frequency for the directional sector θ . A method to choose the coefficients γ_s and γ_d depending on the wave steepness on deep water was proposed by Battjes and Stive (1985).

In HISWA the mean wave frequency is not affected in the case of steepness induced breaking. When the wave breaking is caused by a decreasing water depth, a change in the mean frequency can optionally be modelled. In this procedure it is assumed that surf breaking dissipates energy mainly at the low frequency side of the spectrum. However, this option should be applied with care because the method to determine the breaking coefficients was derived for a fixed frequency.

2.2.6 Current dissipation

In a strong adverse current a part of the wave energy is carried away by the current. This is the energy in the frequencies which cannot travel against the current. For these frequencies the propagation velocity is smaller than the current velocity. The lowest frequency that cannot travel against the current is called the critical frequency f_c . In HISWA it is assumed that all energy carried by frequencies higher than the critical frequency is dissipated, so that the spectrum has the following shape:

$$\begin{aligned} E(f,\theta) &= C(\theta)f^{-n} && \text{for } f_p \leq f \leq f_c \\ E(f,\theta) &= 0 && \text{for } f < f_p \text{ and for } f_c < f \end{aligned} \quad (2.14)$$

where f_p is the peak frequency and $C(\theta)$ is a direction dependant constant. The mean wave frequency is modified accordingly.

2.3 Use of HISWA

For a computation with HISWA the user must provide on the bathymetry, the current field if present, the incoming wave conditions, the wind speed and direction and coefficients for the dissipation processes. Further is a suitable computational grid required, which is fine enough to provide accurate results without excessive computational effort.

The depth and the current velocity components have to be given on rectangular input grids. These grids need not to be identical and they neither need to coincide with the computational grid. The input grids should cover the computational area. The input grids must be chosen fine enough to represent all relevant details. In case of e.g. a sharp shallow ridge in the bathymetry, it is of importance that this ridge is included in the model bathymetry, otherwise the wave heights behind the ridge may be seriously over-predicted due to underestimation of the dissipation by wave breaking.

The computational grid is a grid in x -, y - and θ -space. The x -direction of the grid must be chosen in the direction of the main wave direction to obtain a good representation of the directional distribution of the wave field. Further should the resolution in x - and y -direction be sufficient to obtain accurate results, both for physical reasons (details in bathymetry) and numerical reasons (stable computations). The computational grid must usually be larger than the area of interest, because a region exists along the side boundaries where the wave field is disturbed.

The computational boundaries and resolution in θ -space must be chosen such that the directional distribution of wave energy is well represented, both at the incoming boundary and after possible refraction. The computational sector is usually taken about four times the standard deviation σ_d of the directional spectrum. For wind generated waves the directional sector of 120° is usually applied. The directional resolution is then taken between 5° and 10° . Both the sector and the directional resolution should be chosen much smaller for swell conditions with a narrow directional distribution.

The results of the computation can be presented in different types of tables and plots. The user can specify different types of point sets for output like points, lines and rectangular areas. Some of the possible output variables are:

- water depth
- current velocity components
- significant wave height
- mean wave period
- main wave direction
- directional spreading
- energy transport vector
- fraction of breaking waves.

Although HISWA has internal options to make contour and vector plots, DELFT HYDRAULICS uses tabled output to data files. These files are processed with separate plot programs to make colour plots, contour plots and vector plots of the computational results.

3 Irregular response

3.1 Introduction

In a recent sensitivity study in which HISWA was applied for several locations along the Dutch coast (Booy, Holthuijsen, 1991), it was found that in one of the shallow water areas the wave height did not always increase with an increasing water level. Because this irregular behaviour could not be explained from physical phenomena, this aspect was further studied as part of the present project. These studies were carried out by the group Fluid mechanics of the Delft University of Technology under supervision of Dr. N. Booij, co-author of the HISWA program. Their complete report concerning the irregular response of HISWA is given in Appendix A. The approach and most important conclusions are summarized in the sections below.

3.2 Approach and results

To assess the importance of various physical phenomena in the wave propagation process, corresponding to specific sections of the programming code, the series of computations with varying water level was repeated a number of times. In each series one other parameter was modified. No firm conclusions could be drawn based on the results of these computations. However, additional computations with slightly different versions of HISWA indicated that numerical problems could also be contributing to the irregular behaviour. Further investigations showed that the problems are (partly) related to points in the computational area where the action density in one of the directional sectors tends to zero and/or the wave frequency for one of the directions becomes very high. This occurs for instance at the lateral boundaries of the computational grid, if the default boundary condition is used. Problem default bounds course is used. The errors could be avoided to some extent. The extreme values for the wave action or wave frequency are caused by numerical effects, but are aggravated, because the high frequency induces wave breaking due to a large wave steepness. The high value of the wave frequency and the consequent errors are not damping out, but propagate into the computational area, because numerical diffusion has very little effect due to the extreme high frequency.

Further computations showed that the errors could be avoided to some extent by a modification of the default boundary condition at the lateral boundary of the computational grid. The generation of extreme steepness inside the computational grid appeared to be largely reduced by the use of a new test version. Apart from a few other modifications, the correction of a coefficient in the subroutine computing the dissipation due to wave breaking proved to have a beneficial effect. The modification of the lateral boundary condition and the changes and corrections introduced in the test version, will soon be implemented in the new production version.

4 Sensitivity study

4.1 General

An essential part of the present study is to analyse the sensitivity of the computational results for a number of input parameters of the HISWA-model. This analysis indicates which parameters have to be chosen with great care and for which a correct estimate is less critical in the final computations. This chapter describes the set-up and results of the sensitivity study. The results are important for the validation and calibration study (chapter 5). A few additional sensitivity computations outside the scope of work for the present study, were carried out by RWS-DGW. Some of the results are included in this report, the full details are presented in separate publications of RWS-DGW (Andorka, 1993).

4.2 Schematisations

4.2.1 Bottom topography

For the bottom topography of the area to be modelled in the sensitivity study a few different sources were available:

- the bathymetry of the HOKU-model,
- the survey-data of the coast line ("JARKUS profiles"),
- the survey-data of the coastal area ("long profiles"), and
- the bathymetry of the Zeegat van Texel and the Wadden Sea ("250x250 data").

The data were compared and checked and the most suitable parts were selected to compile an optimal set of bottom data for the present study.

The bottom data from the HOKU-model, a detailed flow model for the Dutch coast used to assess the flow conditions for morphological computations, cover nearly the whole relevant part of the North Sea. The bathymetry of this model was prepared in 1988, based on a large number of detailed maps from a few years earlier. The resolution of the bottom topography is approximately 1 km parallel to the coast; near IJmuiden and the Zeegat van Texel the distance is reduced to 400 m. Perpendicular to the coast the resolution is varying. Near the coast the distance between the points is about 150 m. Further from the coast the distance is gradually increased to 2 km. In the coastal zone and the area of the Zeegat van Texel seems too coarse to represent e.g. the bar in the profile accurately. The area covered by the HOKU-model is shown in Figure 4.1.

The survey data from the coastline are 1 km spaced profiles which are surveyed every five years. The profiles start near the high water line and extend 3 km seaward. The spacing of the soundings in the profile is about 20 m in the nearshore part and 40 m further offshore. For the present study the data from the most recent survey that had been validated, were selected. These are the results of the survey carried out in 1985. Figure 4.1 shows the JARKUS-profiles.

The data from the coastal area are available on profiles with a spacing of 5 km. These profiles, obtained by a one-off survey carried out in 1984, start close to the shore and extend to approximately 25 km offshore. The distance of the points in the profile is small compared to the distance between the profiles and varies from a few meters to about 60 m. These "long profiles" are indicated by dashed lines in Figure 4.1.

In the Zeegat van Texel and the adjacent areas of the North Sea and Wadden Sea a bathymetry is available on a regular 250x250 m grid. This bathymetry is based on data in the bathymetry data base of RWS. The "250x250 data" are based on surveys in 1984 and have also been used for the Wadden flow model. The area covered by these data is also shown in Figure 4.1.

The JARKUS-profiles and the survey data of the coastal area show a certain overlap. The agreement between the two was checked by plotting corresponding profiles in one graph. Figure 4.2 shows two such graphs. The profiles L33 and L35 of the coastal area are plotted with the adjacent JARKUS-profiles (J40/J41, resp. J30/J31). Both plots show good agreement. For the area close to the coast the JARKUS-profiles will be used for the bathymetry, because these are finer spaced. As the number of points in one profile is rather large, some tests were carried out to reduce the amount of data by averaging. In the averaging procedure the mean value of both the position and the depth is determined and written to the file with the reduced data set. Figure 4.3 shows the results for two of the JARKUS-profiles. The graphs show that an averaging procedure based on two points leads to only minor deviations compared to the original profile. A further reduction is not possible, because the bar/trough profile is then not properly represented any more.

Figure 4.1 shows that the long profiles and the bathymetry of the HOKU-model cover nearly the same area. The agreement between the two was again checked by plotting corresponding profiles into one graph for seven locations. A typical example is given in Figure 4.4. It shows that the two show a fair agreement in the part close to the coast, but further offshore the difference may be several meters with some ridges completely missing in the HOKU-bathymetry. This may be caused by the fact that the HOKU-bathymetry was obtained by digitisation from maps.

For the outer delta of the Zeegat van Texel the data from the HOKU-model and "Zeegat-bathymetry" were available. To compare these, a plot was made of both bathymetries in which each data point is represented by a coloured dot, the colour indicates the depth according to a chosen scale. Figure 4.5 and 4.6 show these plots for the HOKU-model and the "250x250 data". These plots show considerable differences, especially with regard to the shoal Noorderhaaks and the southern end of the island Texel.

Considering all points we decided to compile a bathymetry consisting of the following elements:

- the JARKUS-profiles for the coastline between IJmuiden and "Paal 10", about 3 km north of Callantsoog and from the "Witte Nol" to the north end of Texel,
- the profiles of the coastal area from approximately 3 km to 25 km offshore,
- the bathymetry of the HOKU-model in the area further offshore, and
- the "Zeegat-bathymetry for the Wadden Sea and the Zeegat van Texel up to approximately 10 km offshore.

For the area outside the HOKU-model additional data were digitised from the relevant nautical charts (Hydrographic Office, 1988, 1991a, 1991b). The areas are shown in Figure 4.7.

4.2.2 Current fields

The current fields in the area of the Zeegat van Texel were supplied by RWS-DGW. RWS-DGW has a whole series of models of different resolution, ranging from the Continental Shelf Model to the Wadden-model. For the flow conditions in the Zeegat van Texel the results of the Wadden-model are the most suitable. However, no computations were available for the extreme water levels used in the present wave computations. Additional computations were carried out to generate the current fields during a synthetic storm reaching a maximum wind speed of 35 m/s from north-west. For this simulation, the water levels and flow patterns were computed for a spring tide situation. A north-western storm was added reaching the maximum wind speed at low water and persisting for six hours (Figure 4.8). The computed maximum water level during this storm was close to NAP +4 m (Figure 4.8). This is still below the water level of NAP +5 m used in the wave computations, but the current fields are considered to be sufficiently representative for use in the sensitivity study. Two current fields were selected from the results: one for flood and one for ebb conditions, both close to the moment of high water. For flood time step $t = 20.00$ h was selected and for ebb $t = 01.00$ h (indicated in Figure 4.8). The current fields for these time steps are shown in Figure 4.9 and 4.10.

4.2.3 Computational grids

For the choice of the computational grids for the HISWA computations several factors are of importance. The size and orientation of the grid are mainly determined by the area of interest, the main wave direction and the position where the boundary conditions are known. The step sizes for the integration of the action balance equation depend on the variations in the bottom topography and the current field and on numerical considerations. The following aspects have to be considered:

- the computations must start on a position where the wave height can be assumed constant along the whole start line or where the variation along the incoming boundary is known,
- the side boundaries of the model should not affect the results in the area of interest,
- the direction of the X-axis of the computational grid may not deviate too much from the main wave direction and/or wind direction for a good representation of the directional spreading,
- the bottom topography must be modelled in sufficient detail; this applies especially in areas where the variations are large like near shoals and tidal channels,
- the ratio of the mesh sizes in X- and Y-direction should be small enough for stability of the computation.

For the schematisations in the present study it was further of importance that:

- the resolution of the computations should be sufficiently detailed to provide reliable results at 200 m intervals along the NAP -5 m contour line,
- the computations for the Zeegat van Texel were to include current refraction, whereas the computations for the area between IJmuiden and Callantssoog would be carried out without the effect of currents.

Measured wave conditions offshore are known at the locations IJmuiden and Eierlandse Gat. The wave direction in these points is assumed at 315°N . More close to the coast the direction is expected to change due to refraction. To avoid loss of wave energy due to refraction the grid was given an orientation at 300°N (-30° in HISWA conventions). The offshore boundary was taken between the two mentioned stations. The bottom level along the offshore boundary is rather uniform around NAP -25 m.

Along the coast between IJmuiden en Callantssoog most of the profiles show a bar near the NAP -5 m line (see e.g. Figures 4.2). The resolution of the computational grid in X-direction should sufficient to model these bars accurately. Due to the dimensions of the bar, the mesh size Δ_X was taken as 40 m. For reasons of numerical stability the step in Δ_Y was taken 100 m. With these mesh sizes a sufficient number of points in surf zone is obtained.

In the area of the Zeegat van Texel the required resolution is largely determined by the fact that the Molengat must be represented with a sufficient number of points for a correct modelling of the refraction in this relatively narrow channel. Because the effects of a current are taken into account in this model, the ratio between the mesh sizes Δ_X/Δ_Y was taken smaller than for the area along the coast.

Further offshore in deeper water, where the variations in depth and current are smaller, the resolution can be taken coarser to obtain sufficiently accurate results. For reasons of efficiency the area of interest is modelled in three computational grids:

- one large, coarser grid covering the whole area only meant to provide the boundary conditions for the other grids, referred to as the "BUITEN-model" (dutch for OUTER-model),
- a more fine grid along the coast between IJmuiden and Callantssoog, the "BINNEN-model" (INNER-model), and
- a model covering the Zeegat van Texel and the adjacent part of the North Sea, the "ZEEGAT-model").

The limits of the ZEEGAT-model in the North Sea were taken on positions where the flow pattern becomes more uniform and is not much influenced by the current into or out of the Zeegat van Texel. The limit of the BINNEN-model is taken in relative deep water (bottom level $<$ NAP -15 m). The model has a small overlap with the ZEEGAT-model. The orientation of the two detailed models is more eastward to account for expected refraction in the nearshore zone. The directional sector for these models was increased to 135° to obtain a sufficient overlap in the directional sectors of the BUITEN-model and the detailed models.

The dimensions and positions of the three models are:

BUITEN-model:

Dimensions : $L_x \times L_y$ = 37600 x 90000 m
 $\Delta_x \times \Delta_y$ = 160 x 400 m
 $N_x \times N_y$ = 236 x 226 points (53,336 points)
 N_θ = 17 (sectors 7.5°, computational sector 120°)
 Position : Origin : X = -97850.0 m, Y = 39350.0 m
 Orientation : $\alpha = -30^\circ$ (HISWA convention)

BINNEN-model:

Dimensions : $L_x \times L_y$ = 13200 x 48000 m
 $\Delta_x \times \Delta_y$ = 40 x 100 m
 $N_x \times N_y$ = 331 x 481 points (159,211 points)
 N_θ = 19 (sectors 7.5°, computational sector 135°)
 Position : Origin : X = -65000.0 m, Y = 35000.0 m
 Orientation : $\alpha = -8.746^\circ$

ZEEGAT-model:

Dimensions : $L_x \times L_y$ = 19500 x 21840 m
 $\Delta_x \times \Delta_y$ = 20 x 65 m
 $N_x \times N_y$ = 976 x 337 points (328,912 pts; abt. $\frac{3}{4}$ active)
 N_θ = 19 (sectors 7.5°, computational sector 135°)
 Position : Origin : X = -58076.92 m, Y = 80000.0 m
 Orientation : $\alpha = -8.746^\circ$

The position of the three models is shown in Figure 4.11.

4.3 Boundary conditions

4.3.1 General

In the sensitivity study for the hydraulic conditions the parameters with an exceedance frequency of 10^{-4} form the reference case. The boundary conditions for the reference case were assessed using several reports and guidelines. The information in these reports is often based on wave observations on a number of locations along the coast of the Netherlands. These stations are indicated in Figure 4.12. Each of the parameters is shortly discussed in the following sections.

Most of the parameters like water level, wave height, wave period, etc., are varied to assess the sensitivity for each of those parameters. For a number of the parameters the variations were specified in the tender documents, for the other parameters the variations were agreed upon in discussion with RWS-DGW and TUD. An overview of the parameters of the computations in the sensitivity study is given in Table 4.1.

4.3.2 Water levels

The design water level for the safety assessment of the coastal dunes is given by the Technical Advisory-committee for the Coastal Defense (TAW, 1984). These values are based on the design levels given by the Deltacommission (Deltacommission, 1960). The design level for a few relevant stations is:

Location	Design level (m + NAP)
IJmuiden	5,15
Den Helder	5,05
Texel	4,90

Because in HISWA only a constant water level with respect to the datum can be applied, the water level in the reference case was taken at NAP +5.0 m. In the sensitivity study computations were carried out for a water level of 1.0, 0.75, 0.5 and 0.25 m lower and 0.25, 0.5, 0.75 and 1.0 m higher than for the reference case.

4.3.3 Wave height

The corresponding significant wave height can be assessed from Figure 4.13 (TAW, 1984). It follows that for IJmuiden the significant wave height is $H_s = 8.1$ m and for the location Eierlandse Gat $H_s = 9.1$ m. In the HISWA computations the wave height along the incoming boundary was linearly varied between these two values.

Sensitivity computations were carried out for a 1.0, 0.75, 0.5 and 0.25 m lower wave height and for a 0.25, 0.5, 0.75 and 1.0 m higher significant wave height. The wave period was varied correspondingly, so that the wave steepness at the boundary remains constant (see also section 4.3.4).

4.3.4 Wave period

For the wave period a number of relations are given by Hoozemans (1988). As HISWA uses the mean wave period, the most obvious of these seems to be

$$T_{m01} = 4.55 H_s^{0.31} \quad (4.1)$$

with H_s in meters and T_{m01} in seconds. However, this formula leads to unacceptable low values of the wave period; the wave period corresponding to the wave height at IJmuiden for the reference case is e.g. $T_{m01} = 8.7$ s. Wave height and period exceedance curves given by Roskam (1988) give for a probability of exceedance of 0.01 at IJmuiden a significant wave height of 6.4 m and a wave period of 9.7 seconds. This difference may be caused by the fact that the relations in Hoozemans (1988) were derived for the Lichteiland Goeree, located further south in the North Sea.

Additional data from wave observations on the North Sea were available at RWS-DGW. Table 4.2 gives the averaged mean wave period \bar{T}_{m01} for each wave height class for the 8 locations in Figure 4.12. When a constant wave steepness is assumed, the relation between the wave period and the significant wave height is of the form $T = C\sqrt{H_s}$. The value of the constant C for each wave height class is also given in Table 4.2. It appears that the value of C is nearly constant for the higher wave height classes. The lower classes contain more swell observations, so that the constant is larger for these classes. From these results it follows that for the extreme conditions considered in this study the mean wave period is given by

$$T_{m01} = 3.6\sqrt{H_s} \quad \text{for Eierlandse Gat}$$

$$T_{m01} = 3.5\sqrt{H_s} \quad \text{for IJmuiden.}$$

Applying these relations for the wave heights derived in the previous section it follows that in the reference case the wave period at Eierlandse Gat is $T_{m01} = 10.9$ s and at IJmuiden $T_{m01} = 10.0$ s. The wave steepness at these locations related to the peak wave period, defined as $s = H_s/L_p$, is then $s = 0.044$.

In the sensitivity computations with varying wave height, the wave period was also changed, using the above relations. In the sensitivity runs for the wave period (varied wave steepness) computations were carried out for 3 and 1 s shorter wave periods and for wave periods 1 and 3 s longer. The wave steepness ranges in this way from 0.033 to 0.072.

4.3.5 Wave direction and directional spreading

In the available reports little information is given concerning the wave direction during the design conditions. However, the highest water levels and wave heights occur during north-western storms. The main wave direction for the reference case is set to 315°N . Sensitivity computations were carried out by RWS-DGW for 300°N , 285°N , 270°N (west). The wind direction is varied in the same direction as the wave direction. The wind speed was not varied for these cases.

The directional spreading of an ideal wave field in deep water is 32° , corresponding to a directional distribution of the form $\cos^2(\theta-\theta_0)$. Due to refraction the directional spreading at the model boundary will be slightly lower. In the reference case a directional spreading of 25° ($\cos^4(\theta-\theta_0)$) was used. This corresponds well with the directional spreading near the peak frequency measured during extreme conditions (Roskam, 1992; appendix 4). In the sensitivity study the directional spreading was varied to 32° ($\cos^2(\theta-\theta_0)$), 18° ($\cos^{10}(\theta-\theta_0)$) and 10° ($\cos^{30}(\theta-\theta_0)$).

4.3.6 Wind speed

Based on an assumed water depth of 30 m at IJmuiden and 35 m at Eierlandse Gat and the derived design values for the wave height on these locations, we estimate that the corresponding wind speed is 35 m/s. This value, which is class 12 on the Beaufort scale, seems a fair value for these conditions. The wind direction is taken equal to the main wave direction at 315°N .

Sensitivity computations were carried out for a 10 and 5 m/s lower wind speed and for a 5 and 10 m/s higher wind speed.

4.3.7 Bottom friction coefficient

The bottom friction coefficient during the design conditions was estimated using the theory of Nielsen (1979) and Jonsson (1978). In the deeper part of the area, where bottom friction is more important than wave breaking, the friction factor is around $f_w = 0.006$. For the variations it was considered that in the first part of the storm the bed may not be fully adapted to the wave conditions and ripples could be present. However, Ribberink (1992, personal communications) indicated that the bed forms are quickly (within a few minutes) washed out during storm conditions. The friction factor for waves was therefore more arbitrarily varied. The values applied for f_w are 0 (friction off), 0.012 and 0.018. These values cover the range of the expected values.

4.3.8 Frequency change due bottom friction

The frequency change due to bottom friction in HISWA is switched off in the reference case. This assumption is based on earlier experiences, that the effect of bottom friction on the frequency is counteracted and largely compensated by non-linear interactions. The effect of the non-linear interactions is not taken into account in HISWA and therefore switching the effect on the wave frequency off was considered most appropriate.

RWS-DGW carried out sensitivity computations for some of the wave conditions with the frequency change due to bottom friction on.

4.3.9 Wave breaking coefficient

The value for the coefficient for steepness induced breaking γ_d is based on Miche's criterion and derived for a steepness which is computed from the significant wave height and the peak wave period. HISWA uses the mean wave period as characteristic value. The computation of the wave number and the wave length are also based on this value. The value of γ_d must therefore be adapted. For the sensitivity study the coefficient for breaking due steepness was set to $\gamma_d = 1.13$. This parameter was not further modified during the computations.

The wave breaking coefficient for breaking caused by depth limitation was estimated from the wave steepness at the incoming boundary using the relation given by Battjes and Stive (1985). For the design conditions $\gamma_s = 0.80$ appeared to be a good choice for this coefficient. To cover the range of possible variations in the wave steepness the breaking coefficient was varied to $\gamma_s = 0.70$, $\gamma_s = 0.75$ and $\gamma_s = 0.85$.

4.3.10 Frequency change due to wave breaking

Until now, no full agreement exists with respect to the effect of wave breaking due to depth limitation on the wave frequency. It has been argued that since only the highest waves with the lowest frequencies are breaking, dissipation takes place at the low frequency side of the spectrum. However, recent literature indicates that energy is dissipated at all frequencies. In HISWA the first reasoning is adopted, so that wave breaking is causing the mean frequency to increase. The change of the frequency is of importance, e.g. because the computation of the run-up on a dike is rather sensitive to the wave period at the toe of the dike. Further the change in frequency is important in areas where the waves are breaking on a shoal and start growing again due to wind.

The frequency change due to wave breaking is switched on in the reference case. A sensitivity computation was carried out with the frequency change due to wave breaking switched off.

4.4 Presentation and discussion of results

4.4.1 General

For the presentation and analysis of the results several sets of output points were defined. To show the sensitivity of the wave conditions in one point for each varied parameter, a number of output points was specified. For the closed coast three points on the Egmond profile were selected: at the NAP -10 m, NAP -5 m and the NAP -0 m lines. In the area of the Zeegat van Texel one output point was defined in the middle of the Marsdiep and two points in the Wadden Sea on locations where wave measurements have been carried out.

For comparison of the results of different computations a number of output lines were defined. One output line was defined perpendicular to the coast through the buoy locations near Egmond ("Egmond profile"). This output line is considered to be representative for the sensitivity of the computations in the closed part of the coast. Because the variations in the Zeegat-area are expected to be rather large three output lines were defined in this area. One line (the "Breewijd profile") runs South-West to North-East through the deepest part of the Schulpengat and Breewijd to the location of the measurements at Bollen. The "Marsdiep profile" runs West to East across the Noorderhaaks into the Wadden Sea and the "Molengat profile" runs North-West to South-East through the Molengat to the shore near Den Helder. The variations of the quantities along these profiles are shown in graphs for each varied input parameter.

To check the differences caused by the currents two additional profiles were defined along the side boundaries of the ZEEGAT-model. These are indicated as "NHPAAL10" and "TXPAAL15". Results along these profiles are only presented for the reference case.

To obtain a general impression of the overall, 2-dimensional development of the wave field a number of rectangular areas was defined. For the BUITEN-model this output grid coincides with the computational grid. For the BINNEN-model only the northern part was selected to get sufficient detail in the plots. The results of the ZEEGAT-model are presented in three areas: one covering the whole computational grid, one detail of the entrance to the Marsdiep including the Noorderhaaks (indicated as "Haaks") and one detail of the Marsdiep including the adjacent part of the Wadden Sea (indicated as "Malzwin"). The results in these areas are presented in a number of colour plots (e.g. significant wave height) and vector-plots (wave direction). In this report we only included plots for the reference case. Colour plots showing the wave height distribution for the reference case and number of the sensitivity computations, usually the minimum and maximum value of the varied parameter, are presented in a separate appendix to this report.

All the output points, lines and areas are indicated in Figures 4.14 and 4.15.

In the next section we will first discuss the results of the reference case to indicate the most important phenomena in the computations. This is done using both colour plots showing the variation of the significant wave height in the whole area and graphs showing the results along the output profiles. In the following sections the effect of each parameter that has been varied in the sensitivity study will be discussed. This is illustrated with the results along the output profiles and a few selected points. Additional colour plots of the wave field for a number of the sensitivity computations are presented in a separate annex with a limited circulation. These plots are merely illustrative and not essential for the conclusions of this chapter.

4.4.2 Reference case

The results of the HISWA computations for the reference case are shown in Figures 4.16 to 4.24. The bathymetry of the BUITEN-model and the ZEEGAT-model is given in Figure 4.16 and 4.17. The background line indicating the coast of Texel and the Noorderhaaks in Figure 4.17 does not fully coincide with the NAP +0 m line, because the bathymetry is based on the 250x250 m data, whereas the background is digitised from a recent nautical chart. The current field in the ZEEGAT-model is plotted in Figure 4.18. Comparison with the given current field (Figure 4.9) shows that the representation in HISWA shows a good agreement.

Closed coast

The spatial variations of the computed significant wave height and main wave direction for the BUITEN-model are given in Figures 4.19a and 4.19b. Figure 4.19a shows that south of the Zeegat van Texel the wave height decreases gradually from the up-wave boundary towards the coast. This decrease is mainly caused by bottom friction. In the shallow waters near the coast the wave height decreases very rapidly. Surf breaking is the dominant process in this area. Note that the coastline is not properly followed by the colour areas because the bathymetry above the NAP line is not very accurate (limited data) and because the plot is based on the results in a selection of the computational points. Along the northeastern boundary of the BUITEN-model some boundary effects are visible. Figure 4.19b shows that more close to the coast the wave direction becomes more westerly due to refraction. A more detailed plot of the wave height and direction in the coastal zone near Egmond, computed using the BINNEN-model, is shown in Figures 4.20.

Tidal inlet

In the area of the Zeegat van Texel the wave height contours show more variations. Figures 4.21a and 4.21b show a detailed plot of the wave height contours and the main wave directions from the ZEEGAT-model. Figures 4.22 and 4.23 show wave heights and directions in more detail for the areas "Haaks" and "Malzwin". Please note the differences in the intervals of the colour scales. West of the Noorderhaaks and on this shoal the significant wave height decreases rapidly due to the limited depth. In the tidal inlets Molengat and Schulpengat/Breewijd the waves penetrate further. Figures 4.21b and 4.22b show that the main wave direction varies strongly on and east of the Noorderhaaks.

Agreement different models

The results along the Egmond profile for both the BUITEN-model and the BINNEN-model are shown in Figure 4.24a. From the offshore boundary of the model the wave height is gradually decreasing. It can also be seen that some energy is lost at the boundary of the BINNEN-model. This is caused by the fact that the directional sectors of the BINNEN- and BUITEN-model do not fully overlap. At km 28 the wave height in the BUITEN-model is even increasing, while it remains constant in the BINNEN-model. Looking into these differences in more detail, we found that it is caused by a larger energy in the most extreme directional sector of the BUITEN-model. However, this directional sector has an orientation parallel to the coast, so that the wave energy in this sector is not likely to reach the coast.

The results along the profiles in the area of the Zeegat van Texel are shown in Figure 4.24b to 4.24d. These graphs show a similar difference at the boundary of the ZEEGAT-model, partly caused by the fact that the directional sectors are not fully overlapping, but also due to the fact that in the ZEEGAT-model the current is taken into account and in the BUITEN-model not. This can be demonstrated with the results in the profile NHPAAL10 as shown in Figure 4.24e. In this graph the computed wave heights for all three models are plotted. It shows that the difference between the BINNEN-model and the ZEEGAT-model, which is entirely caused by the current, is of the same order as the difference between the BUITEN- and BINNEN-model.

4.4.3 Sensitivity for water level

Closed coast

The water level has a great effect on the wave heights. Figure 4.25a presents the variation of the significant wave height along the Egmond-profile from the model boundary to the coast line for the BUITEN-model. The graph shows a gradual increase of the differences; the highest water level leading to the highest wave heights. Figures 4.25b and 4.25c show the wave height and mean wave period in the last kilometres to the coast. Both wave height and wave period decrease sharply from the NAP -10 m contour to the coast (depth 14 to 16 m depending water level).

Figure 4.25d shows the variation of wave height and wave period for three positions along the Egmond-profile, respectively at NAP -10 m, NAP -5 m and NAP -0 m. The slope of the lines in this figure is increasing when approaching the coast. We therefore conclude that the dependence of wave height and wave period with respect to water level variations increases for decreasing water depth.

Tidal inlet

In the area outside the tidal inlet the effect of a change in the water level is similar to the effect for the closed coast. The significant wave height increases with increasing water level. Figures 4.25e and 4.25f show the variation along the Molengat-profile. Initially the differences increase along the profile; in deeper water slowly due to bottom friction and in shallow water more quickly by surf breaking. However, when the depth is again increasing, the differences decrease, though the wave height continues to decrease. The Marsdiep-profile shows the same phenomenon (Figure 4.25g to 4.25j), but the Breewijd-profile shows the

opposite effect (Figures 4.25k and 4.25l). These difference in behaviour along the profiles may be caused by 3-dimensional effects. All three profiles show that the effect of the water level variations is marginal further inside the tidal inlet and in the Wadden Sea.

Figure 4.25m shows the dependence of the significant wave height and mean wave period for the three selected points. The dependence is largest for the point in the Marsdiep. The behaviour in the point Malzwin is a bit irregular.

4.4.4 Sensitivity for wave height

Closed coast

The sensitivity of the wave height nearshore to the applied incoming wave height is not very strong. The differences in the wave height decrease gradually in the relatively deep water between the model boundary and the NAP -15 m contour (Figure 4.26a; approx. at 30 km), mainly due to bottom friction, but for the highest incoming waves surf breaking has also some effect. In the nearshore area, where the depth is more rapidly decreasing, the wave height reduces quickly and the differences between the various computations become very small (Figures 4.26b and 4.26c). Figure 4.26d shows that at the NAP -10 m line there is a small sensitivity which depends on the incoming wave height, but in more shallow water (NAP -0 m) the wave height is independent of the applied boundary condition. The wave period varies correspondingly.

Tidal inlet

Figures 4.26e to 4.26m show clearly that the wave height is only sensitive for the incoming wave height in the offshore areas beyond the NAP -10 m line. In more shallow waters the wave height is limited by the depth and surf breaking annihilates the differences between the various computations. In the deeper areas behind the shoals the wave height remains of course the same, as the generation and dissipation processes have the same effect in all computations.

4.4.5 Sensitivity for wave period

Closed coast

The computed wave heights along the coast are very sensitive for the wave period which is applied at the boundary. Because the wave height is not varying, the wave steepness increases with decreasing period. Figure 4.27a shows that for run TM1 the wave steepness at the boundary exceeds the maximum value, which results in a sharp decrease of the wave height due to steepness breaking (white capping). The latter can be deduced from Figures 4.27b and 4.27c which show that the mean wave period for TM1 is not changing while the steepness reduces. The criss-crossing of the lines in Figure 4.27a is caused by the fact that refraction and shoaling are also affected by the wave period. Figures 4.27d to 4.27f show that the differences are decreasing in more shallow water, but both the computed wave height and wave period are sensitive for the chosen period at the incoming boundary.

Tidal inlet

Figures 4.27g to 4.27o show a similar behaviour in the offshore area near the Zeegat van Texel. Figures 4.27h, 4.27k and 4.27n show that in the deeper parts behind the Noorderhaaks the wave height for the shortest wave period is highest and for the longest wave periods lowest. This reverse order in comparison with the values just before and on the shoal are caused by stronger refraction of the longer wave periods. Further inside the tidal inlet and in the Wadden Sea the wave height and wave period are not very sensitive to the wave period at the deep water boundary.

4.4.6 Sensitivity for wave/wind direction

The sensitivity computations for different wave/wind directions were carried out by RWS-DGW.

Closed coast

At the closed coast the wave height nearshore is mainly determined by the local depth and wave direction is not expected to have a significant effect. No sensitivity runs for varying wave direction were performed for the closed coast.

Tidal inlet

In the tidal inlet the direction of the incoming waves could have more effect, as waves from western directions may penetrate further into the Wadden Sea. Figures 4.28a to 4.28e show the results for waves from due west (270°N) in comparison with the reference case. Intermediate directions have also been computed, but did not show significant differences, as the results are between those of the shown directions. The graphs show that in deeper water offshore and on the shoals around the Noorderhaaks, the wave height is nearly the same for waves from west and waves from north-west. In the tidal inlet, just behind the shoal, the wave height is higher for the western direction (Figure 4.28b) as more wave energy penetrates through the channel of the Breewijd (Figure 4.28d). Locally the significant wave height is up to 1 m higher, see the Breewijd-profile at km 17 (Figure 4.28d) and the Molengat-profile km 23 (Figure 4.28a). In the tidal inlet the mean wave period is clearly higher for the western direction, because the part of the wave energy penetrating from open sea, that has a longer wave period, is larger than the locally generated wave components. Further into the Wadden Sea the wave heights are slightly lower for the western wind and wave direction. This is probably caused by the difference in the wave period, which affects the growth of the waves by the wind.

4.4.7 Sensitivity for directional spreading

Closed coast

Figure 4.29a shows that a smaller directional spreading of the waves (run SD3) leads to larger variations in the wave height along the profile. This is caused by the fact that more wave energy is carried by a small number of directions so that refraction has a stronger effect on the wave field. However, in the more shallow water the limitation by the depth is more important so that the wave heights are fairly insensitive for the directional spreading at the NAP -10 m, NAP -5 m and NAP -0 m lines (Figures 4.29b to 4.29d).

Tidal inlet

Figures 4.29e to 4.29m show that the directional spreading has also little effect on the wave heights in the area of the tidal inlet. Some differences occur in areas where refraction is of importance. Figure 4.29j (km16 and km21) shows that the wave period decreases more for the most narrow directional distribution (SD3), while the wave height is the same. This is caused by the fact that the dissipated wave energy is in HISWA assumed to be lost at the low frequency side of the spectrum. The same amount of energy is dissipated in all computations, but because the wave energy is concentrated in less directional sectors in computation SD3, more energy is dissipated in each sector, so that the wave period in each sector is changing more than for a wider directional distribution.

4.4.8 Sensitivity for wind speed

Closed coast

The influence of the wind speed on the wave heights is along the closed coast limited to the deeper parts. Figure 4.30a shows that the differences in wave height are gradually increasing from the deep water boundary and reach a maximum some 15 to 20 km from the coast (at km 15). Near the NAP -10 m line the differences decrease rapidly due to surf breaking and near the NAP -5 m line the wave height is equal for all wind speeds (Figures 4.30b to 4.30d).

Tidal inlet

In the deeper water offshore the wave height is slightly higher for higher wind speeds, but on the shoals of the outer delta the wave heights reduce sharply due to surf breaking and the wave height are about the same for all wind speeds (Figure 4.30e, 4.30g and 4.30k). In the deeper water in the entrance of the tidal inlet a higher wind speed causes a stronger increase of the wave height. Further in the tidal inlet and in the Wadden Sea wave growth due to wind generation is one of the dominant factors and wave heights depend strongly on the wind speed (Figure 4.30f, 4.30i, 4.30l and 4.30m). Figure 4.30j shows that in the Marsdiep the wave period is decreasing with increasing wind speed and wave height (Fig. 4.30i). This is caused by the fact that behind the shoal the spectrum consists of wave components that are penetrating over the shoal and components that are locally generated by the wind between the island Texel and the output profile. For the higher wind speed the locally-generated wave components that have a shorter wave period have a larger contribution in the total wave energy, so that the mean wave period is smaller than for a lower wind speed. Figure 4.30j shows that further into the Wadden Sea the contribution of the components penetrating from open sea, which have a longer period, becomes less important and the wave period increases again.

4.4.9 Sensitivity for current effects

Closed coast

The sensitivity for current effects was not studied for the closed coast.

Tidal inlet

In the deep water further offshore the current velocities are relatively small and changes in the current conditions have little effect on the wave height and wave period. In the tidal channels of the outer delta the currents are stronger and have more effect on the wave conditions. Figure 4.31b show that in the Molengat the mean wave period increases with the following current (run SSS) and decreases with an opposing current (run SR1). Consequently the wave height reduces with the following current (Fig. 4.31a) due to the effect of the current on wave propagation and due to refraction by the variations in the current velocities across the channel. For the opposing current the wave height is initially increasing, but when the current velocity increases near km 21 along the profile the wave height starts to decrease, while the wave period increases. At this point part of the wave energy is dissipated by the current (wave blocking, see section 2.2.6). Figures 4.31c to 4.31f show similar results for the Marsdiep and Breewijd profiles. The effect of current dissipation can be seen around km 26 in the Marsdiep profile and around km 25 in the Breewijd profile. Figure 4.31g shows that at the point Bollen the effect of variations in the current is very small, as this point is located outside the important tidal channels. In the middle of the Marsdiep the difference in significant wave height with a following and an opposing current is more than 0.5 m.

4.4.10 Sensitivity for bottom friction coefficient

Closed coast

The bottom friction coefficient has a very strong effect on the development of the wave height in the offshore area as can be seen in Figure 4.32a. Neglecting the effect of bottom dissipation leads to wave heights which are up to 0.5 m higher than for the reference case. Increasing the friction coefficient from $c_{fw} = 0.006$ (SSS) to $c_{fw} = 0.012$ (BW2) or $c_{fw} = 0.018$ (BW3) gives wave heights which are 0.5 to 1.5 m lower. Figure 4.32b shows that the differences decrease in the surf zone and at the NAP -0 m line the sensitivity for the friction coefficient is very small (Figure 4.32d). Figure 4.32c shows that the wave period is also affected by the change in friction coefficient, although the direct effect of bottom friction on the mean period is not switched on in these computations. However, the smaller dissipation by friction leads to an increased dissipation by wave breaking on deeper water. As the effect of wave breaking on the mean period is switched on, this leads to smaller wave periods when friction coefficient is reduced. For higher friction coefficients applies the opposite.

Tidal inlet

In the offshore area near the tidal inlet the effect of variations in the friction coefficient is again similar to the effects at the closed coast. However, the differences in wave height along the Molengat profile (Figure 4.32e) are smaller than along the Egmond profile, because the distance from the model boundary to the NAP -10 m line is much longer for the latter profile (approximately 14 and 35 km respectively). On the most shallow parts (bottom level above NAP -10 m) the friction coefficient has no effect on the wave height, but in the deeper areas behind the shoals a lower friction coefficient means a higher wave height. The effect is again negligible in the Wadden Sea (Figures 4.32f to 4.32m).

4.4.11 Sensitivity for frequency change due to bottom friction

The computations for the sensitivity of the results for the frequency change due to bottom friction were carried out by RWS-DGW.

Closed coast

Switching on the frequency change due to bottom friction has little effect on the wave height in the offshore area of the closed coast (Figure 4.33a), but considerably more on the wave period (Figure 4.33b). The wave period decreases gradually and is nearly 2 s lower just before the breaker zone. In the breaker zone the wave height decreases more due to breaking when the frequency change is switched on. Because the wave period is shorter, the waves are steeper and breaking has more effect. With the frequency change on the wave heights are up to 0.3 m lower. The breaking process decreases the difference in wave period.

Tidal inlet

In the offshore area of the tidal inlet the effect of frequency change is the same as for the closed coast (Figures 4.33d to 4.33h). Behind the shoal of the Noorderhaaks the depth increases and gives higher wave heights with the frequency change switched on. This is mainly caused by shoaling. A similar effect can be seen for the frequency change due to surf breaking (section 4.4.13). This effect gives a higher wave height (0.4 m) near the dike at Den Helder, see the Molengat-profile (Figure 4.33d). The wave period at this location is about 1 s lower, when the frequency change is switched on. Further inside the tidal inlet the differences in wave height and period disappear, because the conditions are determined by the locally generated waves with short wave periods, see the Breewijd-profile and Marsdiep-profile (Figures 4.33g and 4.33e).

4.4.12 Sensitivity for shallow water breaking coefficient

Closed coast

Figures 4.34a to 4.34d show that the shallow water breaking coefficient has a considerable influence on the significant wave height. Starting right from the model boundary the wave height decreases for decreasing γ_s . For the highest values of the breaking coefficient (BC3) the differences in deep water are smaller, but in more shallow water the difference between the runs SSS and BC3 are increasing. The differences decrease a little in the shallow waters near the coast, but at the NAP -0 m line the difference between the highest and lowest value is still in the order of 0.6 m.

Tidal inlet

In the offshore area of the tidal inlet the effect of changes in the breaking coefficient are the same as for the closed coast (Figures 4.34e, 4.34g and 4.34k). Behind the shoal the differences in wave height become very small (Figures 4.34f, 4.34i and 4.34l). The difference in wave period (Figures 4.34h and 4.34j) is larger than for e.g. a variation in incoming wave height or wind speed. This is caused by the combined effect of bottom dissipation and surf breaking. For a small wave breaking coefficient more wave energy is dissipated by surf breaking and less by bottom friction. As it is assumed that wave breaking affects the mean wave period and bottom dissipation not, the mean wave period is lower for a smaller coefficient γ_s . In the tidal inlet and the Wadden Sea the effect on wave height and wave period is negligible (Figure 4.34m).

4.4.13 Sensitivity for frequency change due to wave breaking

Closed coast

Switching off the frequency change due to surf breaking has very little effect on the wave height in the offshore area of the closed coast (Figure 4.35a). In this area only a very small amount of energy is dissipated by wave breaking due to depth limitation. Figure 4.35b and 4.35c show that the wave height just outside the surf zone is the same, but the wave period is about 0.5 s higher. In the surf zone the wave heights with the frequency change off are a few tens of centimetres higher, because the steepness is smaller in this case so that the amount of dissipation reduces (Figure 4.35d). Of course the difference in wave period increases rapidly towards the coast (Figure 4.35c).

Tidal inlet

A similar effect can be seen in Figures 4.35e to 4.35m in the parts where the depth is decreasing. Figure 4.35f, 4.35i and 4.35l show that when the depth increases again behind the shoal of the Noorderhaaks, the wave height is lower with the frequency change switched off. The higher wave period in this case causes more dissipation by friction, while the wave growth by wind generation has less effect due to the longer period. Further inside the tidal inlet the differences decrease again, not in the least because the wave period decreases sharply by the sheltering effect of the isle of Texel (Figure 4.35j).

4.4.14 Bottom variability

Closed coast

For the closed coast the sensitivity of the computations for variations in the bottom topography was analysed using the results of the run HS3 in five profiles perpendicular to the coast. The bathymetry in these profiles is shown in Figure 4.36a. The profiles look very much alike. Starting at a depth between NAP -20 m and NAP -15 m the depth first increases to NAP -20 m or more, then a gradual rise with a slope in the order of 1:1000 to NAP -15 m. Between NAP -15 m and NAP -0 m has a slope in the order of 1:100 with a bar and trough near the NAP -5 m line. Because the wave height in the shallow water is largely determined by the depth limitation, the significant wave height has been plotted against the actual water depth (including water level rise). Figure 4.36b shows that these curves agree very well for more shallow water. For a depth greater than 20 m the variations are quite large, but for

smaller depths wave breaking by depth limitation becomes the most important factor, so that the lines nearly coincide. Around a depth of 10 m (NAP -5 m contour) the lines are deviating due to the bar and trough, but in more shallow water the lines converge again. These results show that for the studied extreme conditions the wave height is not very sensitive for variations in the bathymetry. We expect that similar results would be found when variations of the bathymetry in time would have been studied.

Tidal inlet

To study the effect of the bathymetry in the tidal inlet on the results in this area, RWS-DGW has carried out several computations with a modified bottom topography, ranging from lowering the level of the Noorderhaaks to a completely flat bottom. The results have been presented in a separate document by Andorka (1993).

4.5 Combined sensitivity

4.5.1 General

In the previous sections the effect of each parameter was treated separately. However, the relative importance of the parameters and any indirect effects have not yet been considered. These are treated in this section by analysis of the total uncertainty in the computed significant wave height H_s and mean wave period T_m due to the uncertainty in a number of input parameters of the HISWA-model. The approach for this analysis is similar to the method applied in an earlier study for RWS-DGW by Digital Hydraulics Holland (1991).

The input parameters of the HISWA-model can be classified into external and internal parameters.

External parameters considered in this study include:

- water level (ws)
- incoming significant wave height (hi)
- incoming mean wave period (ti)
- directional spreading of incoming wave field (sd)
- wind speed (wi)
- current conditions (sr)

The wave direction was not varied in the basic set of computations and in the sensitivity study set to 315°N.

The internal parameters include the:

- breaking coefficient (bc)
- friction coefficient (bw)
- frequency change (fv)

In the following each parameter is indicated by the letters between parentheses.

The analysis is carried out for three profiles. The Egmond profile represents the situation at the closed part of the coast whereas the Molengat profile and the Marsdiep profile are used for the tidal inlet. The main difference between them with respect to the input parameters is the current conditions, which has not been varied for the Egmond profile.

The uncertainty analysis was extended to include the computation of wave run-up and dike height and their respective uncertainties. As this is beyond the scope of the present studies these results are given separately in Appendix C.

4.5.2 Method of analysis

Generally the uncertainty of the computational results (e.g. significant wave height H_s) due to the uncertainty of any input parameter Z_i can be described as follows

$$\sigma_{H_s} = \frac{\partial H_s}{\partial Z_i} \sigma_{Z_i}$$

where $\partial H_s / \partial Z_i$ is the rate of change of H_s with respect to parameter Z_i , and σ_{Z_i} is the uncertainty of parameter Z_i .

The overall uncertainty of H_s due to the uncertainty of the independent parameters Z_1, Z_2, \dots can be given by:

$$\sigma_{H_s}^2 = \left(\frac{\partial H_s}{\partial Z_1}\right)^2 \sigma_{Z_1}^2 + \left(\frac{\partial H_s}{\partial Z_2}\right)^2 \sigma_{Z_2}^2 + \dots$$

the uncertainty of H_s with respect to the input parameters Z_i can be normalized by the overall uncertainty as follows

$$\sigma^*\left(\frac{H_s}{Z_i}\right) = \frac{\partial H_s}{\partial Z_i} \sigma_{Z_i} / \sigma_{H_s}$$

where

$$\sum_i \{\sigma^*(H_s/Z_i)\}^2 = 1$$

in the computation the partial derivative of H_s with respect to the input parameter Z_i is approximated as follows

$$\frac{\partial H_s}{\partial Z_i} \approx \frac{\Delta H_s}{\Delta Z_i}$$

where $\Delta H_s / \Delta Z_i$ is computed at the reference case for the variation of parameter Z_i .

4.5.3 Method of computation

The computation of the uncertainty in the output results of the wave height and period is carried out for four groups of input parameters to see the effect of each of these group separately on the uncertainty of the output results. The four groups are classified with the labels in the figures as follows:

- 1 All input parameters (i.e. external and internal parameters) assuming mutual independency (labelled "all parameters").
- 2 External parameters only (labelled "external parameters")
- 3 Internal parameters only (labelled "internal parameters")
- 4 External parameters taking into account the interdependency (labelled "ext. with interdep")

In the computations two approaches have been followed to handle the uncertainty of the external parameters. Firstly, it is assumed that the external parameters are mutually independent. Secondly, it is assumed that the external parameters are dependent on some stochastic variables which affect the external parameters simultaneously. The corresponding interdependency between the external parameters will be explained in the next section.

Finally it has to be pointed out that the internal parameters are considered to be independent parameters (i.e. not influenced by either the external parameters or the stochastic variables).

4.5.4 Interdependency between the external parameters

The computed wave height H_s is dependent on a number of parameters as follows

$$H_s(D, h_i, t_i, w_i, s_r, s_d)$$

where:

- D = water depth
- h_i = incoming significant wave height
- t_i = incoming mean wave period
- w_i = wind speed
- s_r = current conditions
- s_d = directional spreading

These parameters are dependent on a number of stochastic variables such as:

- | | |
|-------------------|----------|
| sea level rise | S_{lr} |
| bottom level rise | B_{lr} |
| wind speed | w_i |
| storm surge level | S_{sl} |

The interdependency between the input parameters and the stochastic variables is given by the following relations:

$$\begin{aligned}
 D &= S_{lr} - B_{lr} + S_{sl} \\
 B_{lr} &= \alpha_B S_{lr} \\
 S_{sl} &= \alpha_{Ssl} w_i \\
 h_i &= \alpha_{hi} w_i \\
 t_i &= \alpha_{ti} h_i = \alpha_{ti} \alpha_{hi} w_i
 \end{aligned}$$

where

$$\alpha_{ti} = \text{constant} = t_i/h_i = 1.52$$

The arrangement of the dependency of the above mentioned parameters is given in Table 4.5. For the value which is assigned to each variable in this table is referred to Table 2.6 in the report by Digital Hydraulics Holland (1991).

The interdependency between the parameters can be expressed mathematically as follows:

for sea level rise

$$\frac{\partial H_s}{\partial S_{lr}} = \frac{\partial H_s}{\partial D} \frac{\partial D}{\partial S_{lr}} + \frac{\partial H_s}{\partial D} \frac{\partial D}{\partial B_{lr}} \frac{\partial B_{lr}}{\partial S_{lr}} = \frac{\partial H_s}{\partial D} (1 - \alpha_B)$$

$$\frac{\partial H_s}{\partial \alpha_B} = \frac{\partial H_s}{\partial D} \frac{\partial D}{\partial B_{lr}} \frac{\partial B_{lr}}{\partial \alpha_B} = - \frac{\partial H_s}{\partial D} S_{lr}$$

for wind speed

$$\frac{\partial H_s}{\partial w_i} \Big|_t = \frac{\partial H_s}{\partial w_i} \Big|_p + \frac{\partial H_s}{\partial h_i} \frac{\partial h_i}{\partial w_i} + \frac{\partial H_s}{\partial t_i} \frac{\partial t_i}{\partial w_i} + \frac{\partial H_s}{\partial D} \frac{\partial D}{\partial S_{sl}} \frac{\partial S_{sl}}{\partial w_i}$$

$$= \frac{\partial H_s}{\partial w_i} + \alpha_{hi} \frac{\partial H_s}{\partial h_i} + 1.52 \alpha_{hi} \frac{\partial H_s}{\partial t_i} + \alpha_{Ssl} \frac{\partial H_s}{\partial D}$$

$$\frac{\partial H_s}{\partial \alpha_{hi}} = \frac{\partial H_s}{\partial h_i} \frac{\partial h_i}{\partial \alpha_{hi}} + \frac{\partial H_s}{\partial t_i} \frac{\partial t_i}{\partial \alpha_{hi}} = w_i \frac{\partial H_s}{\partial h_i} + 1.52 w_i \frac{\partial H_s}{\partial t_i}$$

$$\frac{\partial H_s}{\partial \alpha_{Ssl}} = \frac{\partial H_s}{\partial D} \frac{\partial D}{\partial S_{sl}} \frac{\partial S_{sl}}{\partial \alpha_{Ssl}} = w_i \frac{\partial H_s}{\partial D}$$

The total uncertainty in H_s under the influence of the external parameters taking into account the interdependency is given by:

$$\begin{aligned}
 \sigma_{H_s}^2 &= \left(\frac{\partial H_s}{\partial S_{lr}} \right)^2 \sigma_{S_{lr}}^2 + \left(\frac{\partial H_s}{\partial \alpha_B} \right)^2 \sigma_{\alpha_B}^2 + \left(\frac{\partial H_s}{\partial w_i} \right)^2 \sigma_{w_i}^2 + \left(\frac{\partial H_s}{\partial \alpha_{hi}} \right)^2 \sigma_{\alpha_{hi}}^2 + \left(\frac{\partial H_s}{\partial \alpha_{Ssl}} \right)^2 \sigma_{\alpha_{Ssl}}^2 \\
 &+ \left(\frac{\partial H_s}{\partial s_r} \right)^2 \sigma_{s_r}^2 + \left(\frac{\partial H_s}{\partial s_d} \right)^2 \sigma_{s_d}^2
 \end{aligned}$$

and similarly the uncertainty in T_m by:

$$\begin{aligned} \sigma_{T_m}^2 = & \left(\frac{\partial T_m}{\partial S_{lr}}\right)^2 \sigma_{S_{lr}}^2 + \left(\frac{\partial T_m}{\partial \alpha_B}\right)^2 \sigma_{\alpha_B}^2 + \left(\frac{\partial T_m}{\partial W_i}\right)^2 \sigma_{W_i}^2 + \left(\frac{\partial T_m}{\partial \alpha_{hi}}\right)^2 \sigma_{\alpha_{hi}}^2 + \left(\frac{\partial T_m}{\partial \alpha_{ssl}}\right)^2 \sigma_{\alpha_{ssl}}^2 \\ & + \left(\frac{\partial T_m}{\partial sr}\right)^2 \sigma_{sr}^2 + \left(\frac{\partial T_m}{\partial sd}\right)^2 \sigma_{sd}^2 \end{aligned}$$

4.5.5 The uncertainty of the input parameters

For the computation of the uncertainty of the output results (H_s , T_m), certain values for the uncertainty in the input parameters have to be assigned. These values have been chosen to be in accordance with reality as much as we can. The reference case and the uncertainty in each input parameters are given in Table 4.6.

It has to be pointed out that the uncertainty in the current condition has been chosen to be a factor 1 (dimensionless). The reason is that the variation of the results is computed by taking the difference between the following and opposing current,

$$\frac{\partial H_s}{\partial sr} \approx \frac{\Delta H_s}{\Delta sr} = \Delta H_s$$

For the uncertainty of the frequency change (i.e. on or off), a factor 0.5 has been chosen since the knowledge to model the frequency change within the HISWA model is not complete yet. Similarly the variation of the output results (H_s , T_m) is computed by taking the difference between the results of frequency change on and off; so that

$$\frac{\partial H_s}{\partial fv} \approx \frac{\Delta H_s}{\Delta fv} = \Delta H_s$$

4.5.6 Presentation and discussion of the results

Egmond profile

The bottom topography along the Egmond profile is given in Figure 4.37a with the distribution of significant wave height and mean wave period for the reference case.

a) Uncertainty of the significant wave height

Figure 4.37b shows the uncertainty in the computed wave height along the Egmond profile. Considering the influence of all input parameters, the average value of the uncertainty is about 0.45 m in the offshore area. Nearshore the uncertainty is higher due the significant influence of the water level variation and about 0.55 m.

Figures 4.37c to 4.37e show the normalized uncertainty of each input parameters with respect to the total uncertainty of all parameters. Apparently in the nearshore area, the uncertainty in the water level variation and the breaking coefficient are the most important factor affecting the uncertainty in the computed significant wave height. Farther offshore the results are influenced by the uncertainty in the incoming wave height and period and the friction coefficient.

b) Uncertainty of the mean wave period

Figure 4.37f shows the uncertainty in the computed wave period along Egmond profile. In the offshore area, the uncertainty is about 1.5-1.7 s. In the nearshore area, the uncertainty due to all parameters shows an increase due to the effect of the internal parameters of frequency change. Without considering the effect of the internal parameters the uncertainty of the mean wave period is decreased.

Figures 4.37g to 4.37i show that most important parameter which influence the results. In the offshore area the effect of the incoming wave period is the most important one, and in nearshore area the effect of the frequency change is the predominant.

Molengat profile

The bottom topography along the Molengat profile is given in Figure 4.38a with the distribution of significant wave height and mean wave period for the reference case.

a) Uncertainty of the significant wave height

Figure 4.38b shows the uncertainty in the computed wave height along Molengat profile. In the area outside the tidal inlet the uncertainty is about 0.6-0.7 m and decreases slightly to about 0.4 m over the shoal due to the significant reduction of the wave height as the water depth decreases. Behind the shoal the uncertainty is increased to about 1 m mainly due to the variation in the current conditions, after that it decreases as it approaches the shoreline.

Figures 4.38c to 4.38e show that the most important parameters affecting the results along the profile. It is clear that the important parameters influencing the results are varied dramatically from one part to another along the profile. Outside the tidal inlet, the incoming wave height is most important, and over the shoaling area the influence is shared between the water level variation, incoming wave period and the breaking coefficient. However inside the tidal inlet the dominant parameter is the current condition.

Very near to the shore the influence of the incoming wave height and period is rather erratic. This might be due to the large steepness of the bottom slope which may cause numerical instability for the model.

b) Uncertainty of the mean wave period

Figure 4.38f shows the uncertainty in the computed wave period along Molengat profile. In the area outside the tidal inlet the uncertainty is about 1.5-2.0 s. As the water depth decreases the uncertainty increases due to the effect of frequency change, however it decreases for the cases which only consider the external parameters.

Figures 4.38g to 4.38i show that the most important parameters affecting the results. Outside the tidal inlet, the uncertainty in the incoming wave period is very significant. As the water depth decreases the effect of the frequency change is the most important one. Inside the tidal inlet the effect of the current condition is predominant.

Marsdiep profile

The bottom topography along the Marsdiep profile is given in Figure 4.39a with the distribution of significant wave height and mean wave period for the reference case.

a) Uncertainty of the significant wave height

Figure 4.39b shows the uncertainty of the significant wave height along the Marsdiep profile. It is clear that the important parameters influencing the results are varied dramatically from one part to another along the profile. In the offshore area the uncertainty is about 0.6-0.7 m and decreases to about 0.4 m as the water depth decrease due to the reduction of the wave height. Behind the shoal it increases again as the water depth increases and reaches about 0.7 m. The peak value of the uncertainty is about 1 m over the second shoal due to the uncertainty of the current condition.

Figures 4.39c to 4.39e show that in the offshore area the incoming wave height is the most important parameter affecting the uncertainty calculation. As the water depth decreases the influence is shared between the water level variation and the breaking coefficient. Behind the shoal the dominant parameter is the current condition.

b) Uncertainty of the mean wave period

Figure 4.39f shows the uncertainty of the mean wave period along the Marsdiep profile. In the offshore area the uncertainty is about 1.5-1.8 s and increases to about 3 s over the shoal mainly due to the effect of the uncertainty in frequency change. Behind the shoal, the uncertainty is decreased gradually and it reaches about 1 s over the second shoal.

Figures 4.39g to 4.39i show that in the offshore area the incoming wave period is the most important parameter affecting the uncertainty of the wave period. As the water depth decreases the effect of frequency change is predominant. Behind the shoal the effect of the current condition is significant.

Finally Table 4.7 gives a summary for the results at contours -5 m and -10 m NAP for the Egmond profile, and -25 m NAP for the Molengat profile. For the Molengat profile the -25 m NAP has been chosen to avoid the inaccurate results at the shallower areas. For the Marsdiep profile, the results are not tabulated because the end of the profile is deeper than -10 m NAP.

4.6 Conclusions

From the studies into the sensitivity of the computed wave conditions near the coast and in the tidal inlet for a number of external input parameters and internal coefficients of the HISWA-model, we draw the following conclusions with respect to the modelling of wave propagation in the area between deeper water (NAP -20 m contour) and the coast:

- In the deeper water further offshore the wave conditions are largely determined by the prescribed incoming wave conditions. When the interdependency of the parameters is taken into account, the wind speed is the most important factor in this area due to its effect on both the water level and the incoming wave conditions.
- The bottom friction coefficient is the most important internal parameter for the wave height in deeper water.
- The limitation of the wave height by the depth is the most important factor for the wave conditions in the shallow coastal area along the closed coast and on the outer-delta of the tidal inlet. The water level, the shallow water breaking coefficient and the frequency change due to wave breaking are the most important parameters for the wave conditions (both wave height and wave period) in this area.
- On the outer delta the current conditions have a significant effect in addition to the above mentioned parameters.
- The effect of wave breaking on the frequency spectrum is one of the most important factors for the computation of the mean wave period in shallow water.
- In the deep channels of the tidal inlet the current conditions and the frequency change due to wave breaking are the most important parameters for the computed wave conditions. The current conditions are the dominating factor for the wave height, whereas the frequency change largely determines the wave period, mainly due to breaking on the outer delta.
- Further into the Wadden Sea the current conditions and the wind speed become the parameters with the greatest significance. Their relative importance seems to vary with the location in the area. In the transition from the tidal inlet into the Wadden Sea the frequency change due to breaking has still some indirect effect as the wave growth due to wind is influenced by the wave period.
- Very close to the coast near Den Helder, at the end of Molengat-profile, the computed results are not very accurate due to numerical effects caused by the extremely steep bottom slope.
- From the assumed uncertainty in the input parameters and the adopted values for interdependency in the shallow water area of the Egmond profile the uncertainty in the significant wave height is about 0.55 m (H_s between 6 and 5 m). The uncertainty in the mean wave period is around 1.7 s (T_m between 10 and 9 s). In the Molengat profile near the coast at Den Helder the uncertainty in the significant wave height is also about 0.55 m ($H_s = 1.5$ m), but in the wave period the uncertainty is about 2.5 s ($T_m = 7$ s).

5 Validation

5.1 Storm selection

The results of all measurement campaigns carried out by RWS-DGW are stored in the database DTBEST. For the validation and calibration of the HISWA-model for the Dutch coast, RWS-DGW screened these records for wave data in the area of the models during storm conditions. A summary of the available measurements during four storms in 1981 and 1982 is given in Table 5.1. This table shows that data at the seaward boundary of the model (Eierlandse Gat and IJmuiden) are only available for two of the storms.

For the closed coast measurements are available for the storms of January 1981 (Bergen) and December 1982 (Egmond). In January 1981 the wave conditions have only been measured at the three points in the profile near Bergen. During the storm in December 1982, waves were measured both in the offshore locations Eierlandse Gat and IJmuiden and in the coastal zone near Egmond. Because these measurements provide the most complete dataset, the measurements during the storm of December 1982 were used for validation and calibration at the closed coast.

Unfortunately such a complete set of data is not available for the tidal inlet. During the storm of November 1981 waves were only measured just outside the tidal inlet (Schulpengat) and in the Wadden Sea (Bollen). In March 1982 measurements were carried at the offshore stations and just inside the tidal inlet (Malzwin). For December 1982 data are available offshore and just outside the tidal inlet. In spite of the lack of data at the offshore stations, the storm of November 1981 was selected for the validation in the tidal inlet, because the evolution of the wave field in the tidal inlet was considered the most important for this study. The boundary conditions for these computations have been estimated.

5.2 Computations Egmond profile

5.2.1 Description of measurements

The wave measurements at Eierlandse Gat and IJmuiden cover most of the month of December 1982. The data for the points in the Egmond profile cover, with some gaps, the period 10-24 December 1982. In this period the largest wave heights were measured on 15-17 December 1982 with peak values of 4.5 to 5.5 m for the significant wave height. This interval was scrutinised in more detail and three periods were selected to be computed with the HISWA-models. Figures 5.1 and 5.2 show the measured wave heights, periods, wind speed and direction as these are recorded in the DTBEST-files. The wave height and period at the offshore stations are given at a three-hourly interval (Figure 5.1a) and show that the wave height at IJmuiden is rather constant for more than 12 hours on December 16, 1982, but is more varying at Eierlandse Gat. For the stations in the Egmond profile the wave heights are given at an hourly interval, but gaps occur in the time series (Figure 5.1b). Especially for Egmond-6, the station closest to the coast, only a few measurements are available.

Figures 5.2 show that the wind direction and the wind speed are rather constant for most of the period, near 0.00 h on December 16, the recorded wind speeds show quite large variations between the different stations, which may be caused by spatial variations in the wind field. The sharp increase of the wave height at Eierlandse Gat and in two of the Egmond stations shortly after December 16 1982, 0.00 h, seems to be mainly caused by the change in wind direction from 240°N to 290°N . All measurements from the DTBEST-files in the period of interest are given in Table 5.2.

After initial computations trying to match to a single observation for each in each point, it was found that the variations in the measurements from hour to hour are sometimes rather large and both the input values at the offshore stations and the measured wave heights in the Egmond profile were averaged over a certain interval. The wave conditions simulated in the validation are the wave conditions on December 16, 1982 at 0.00 h, 6.00 h and 18.00 h. For the offshore stations the average wave conditions were computed using the values at the given moment and three hours earlier and later; for the stations near Egmond the averaged values were determined from the measurements in the intervals 21.00 h, 15/12/82 - 2.00 h, 16/12/82; 4.00 h - 8.30 h and 16.00 h - 20.30 h. The averaged values are included in Table 5.4, which shows the results of the computations.

5.2.2 Schematisation

The schematisations for the validation computations were slightly modified with respect to those for the sensitivity study. The bathymetry for the this computations was entirely the same as in the first set of computations and no currents were modelled for the closed coast. The computational grid of the BUITEN-model was modified to suit the direction of the incoming waves. The orientation of the BUITEN-model was taken the same as for the BINNEN- and ZEEGAT-model; the spatial resolution was the same as for the earlier computations. The position and dimensions of the model were:

BUITEN-model:

Dimensions:	$L_x \times L_y$	=	39040 x 90000 m
	$\Delta_x \times \Delta_y$	=	160 x 400 m
	$N_x \times N_y$	=	245 x 226 points (53,336 points)
	N_{θ}	=	17 (sectors 7.5° , computational sector 120°)
Position:	Origin	:	X = -95000.0 m, Y = 35000.0 m
	Orientation	:	$\alpha = -8.746^{\circ}$ (HISWA convention)

The position of the models is shown in Figure 5.3. The ZEEGAT-model was not used in the calibration for the closed coast.

5.2.3 Initial parameter settings

The water level for the computations was taken from the DTBEST-records. For the three selected conditions the water level was set at NAP +0.75 m (16/12/82, 0.00 h), NAP +1.90 m (16/12/82, 6.00 h) and NAP +1.20 m (16/12/82, 18.00 h).

For the incoming wave height and wave period the averaged values from the measurements at Eierlandse Gat and IJmuiden were used. The wave direction was taken equal to the wind direction in these points. For the calibration with the values for 0.00 h, the wave direction

was varied and taken equal to the wind direction in the preceding hours. For the directional spreading a value of 25° was adopted.

The wind conditions stored in DTBEST show a variation between the various stations. The wind speed and direction were chosen based on the values in all stations, but when the differences between these are large, the Egmond stations were given more weight.

The bottom friction coefficient was chosen based on the theory of Nielsen (1979) and Jonsson (1978) like for the sensitivity study. For the wave conditions of the validation runs a value of $f_w = 0.007$ was considered most appropriate. The wave breaking coefficient for depth limitation was again computed using the relation of Battjes and Stive (1985). The reference wave height on which this equation is based, is the wave height just outside the breaker zone. Because the boundary of the HISWA-models is much further offshore, a first estimate was made of the wave height closer to the coast. This value was used to estimate the shallow water breaking coefficient. This leads to slightly lower breaking coefficients. The initial value of the shallow water wave breaking coefficient was $\gamma_s = 0.78$.

The initial settings are summarized in Table 5.3. The first computation for each moment is with the initial settings. In following computations external conditions or internal parameters have been changed. These are discussed in the next section.

5.2.4 Results and calibration

The computed wave height and wave period along the Egmond-profile are shown in Figure 5.4 to 5.6 (note that some lines coincide over a considerable length). For the offshore stations Eierlandse Gat and IJmuiden and for the three stations in the Egmond-profile the measured and computed values are also given in Table 5.4. From the results it appears that the measurements at Egmond-8 and Egmond-7 of 6.00 h can not be matched in computations with reasonable values of the parameters. Increase of the wind speed (run B02), adaptation of the deep water breaking coefficients (run B03) or a lower friction coefficient lead not to a better agreement for this conditions. The agreement at Egmond-7 improves, but at Egmond-8 it deteriorates considerably. All computations and the measurements at 0.00 h and 18.00 h show that the wave height in Egmond-7 is usually a few centimetres lower than the wave height at Egmond-8. Further changes in the parameters of the computations to find a better agreement at 6.00 h would lead to values outside the ranges normally given and was not considered.

At 0.00 h, the initial setting of the parameters led to too high results at the stations Egmond-8 and Egmond-7. Changing the direction of the incoming waves to 250°N , which is more corresponding with the wind direction in the preceding hours, gives a better agreement of the computed and measured wave heights, but the computed periods are higher than the measured ones. Switching the frequency change due to friction on reduces the difference in wave period, but wave heights increase then again. At 18.00 h, the computed wave heights at Egmond-8 and Egmond-7 for the initial settings agree very well with the measured values. The wave periods are slightly higher than measured. It should be noted that although the measured mean wave period decreases strongly towards the coast (Figure 5.6), the peak wave period T_p of the spectrum remains nearly constant over the entire area or even increases a little (Roskam, 1993).

For station Egmond-6 the computed significant wave heights are for all three moments about 0.5 m higher than the measured values when the initial values are used, whereas the wave periods show a rather good agreement. Reduction of the wave height in this point is only obtained by a strong reduction of the wave breaking coefficient γ_s (run B09). Because Egmond-6 may be located in the zone where variations in the bathymetry are quite large, no further calibration was carried out for this point in this study. This is confirmed by a comparison of the bathymetry from successive years carried out by RWS-DGW. Figures 5.7 show the bathymetry in three profiles in the vicinity of the Egmond-profile for the years 1977 to 1984.

5.3 Computations Zeegat van Texel

5.3.1 Description of measurements

The wave measurements at Schulpengat and Bollen cover the period 18 - 31 November 1981. The storm of November 24, during which the significant wave height at Schulpengat reaches values between 4.5 and 5.0 m, is the most interesting part of this period. The measured wave heights, wave periods and wind conditions during the storm are shown in Figures 5.8a and 5.8b (note the difference in the vertical scale). Figure 5.8a shows that the wave height at Schulpengat is fairly constant during the first part of November 24. The increase of the wave height at the end of November 23 seems to take place in two steps: first from a wave height of 2.2 m to 3.2 m, then further to a value between 4 and 4.5 m. This seems to be caused by a change in wind speed followed by a change in wind direction a few hours later. The wave height at Bollen is fairly constant for most of the storm (Figure 5.8b). The wave period shows a very clear diurnal modulation caused by the tidal currents. Figures 5.9a and 5.9b show that the wind data in DTBEST are nearly equal for the two stations. These are probably based on the same coastal station (e.g. Den Helder).

5.3.2 Schematisation

For the validation in tidal inlet the bathymetry and the computational grid for the ZEEGAT-model was equal to those of the sensitivity computations. The BUITEN-model was the same as for the validation for the Egmond-profile, because the wind is from similar directions. As the propagation and generation of the waves are influenced by the currents, one current field was provided by RWS-DGW for November 24, 14.00 h. This current field, available from earlier computations with the ZUNOWAK-model, is shown in Figure 5.10.

5.3.3 Initial parameter settings

The DTBEST-records do not contain information on the water level during the storm of November 23-25, 1981, possibly due to a failure of the instrument. The water level was therefore assessed from a graph showing the water level as predicted with the ZUNOWAK-model, that was used to generate the current field. The water level at 14.00 h on November 24, 1981 was estimated at NAP +1.85 m.

As described before, no wave measurements were available at Eierlandse Gat and IJmuiden to provide the boundary condition to the models. The incoming wave conditions had to be assessed in a different way. The wave height and period generated by a wind of 18 m/s was

assessed for various fetch lengths and water depths using the formula given by Hurdle and Stive (1984). These are given in Table 5.5. Further are simultaneous measurements at Eierlandse Gat, IJmuiden and Schulpengat (but not for Bollen) available for the storm of March 11, 1982. During the peak of this storm, at a wind speed of about 16 m/s, the wave conditions given in Table 5.6 were measured. At November 24, 14.00 h, the moment selected for the validation, the wave height measured in Schulpengat was $H_{m0} = 4.14$ m. Considering the various sources, the following values were taken as a first estimate of the incoming wave conditions:

Eierlandse Gat	:	$H_s = 5.3$ m,	$T_{m01} = 8.3$ s
IJmuiden	:	$H_s = 4.9$ m,	$T_{m01} = 7.7$ s.

The wave direction was taken equal to the wind direction at 280°N. For the directional spreading a value of 25° was used.

The wind conditions in the area of the Zeegat van Texel were available as a spatially varying wind field from the ZUNOWAK-model. This wind field was used in the computations with the ZEEGAT-model. For the BUITEN-model the wind conditions were taken from the DTBEST-files. At 14.00 h the wind speed is 18 m/s and the wind direction 280°N, though it was 270°N the hours preceding the moment of 14.00 h.

Because the incoming wave conditions are in the same order of magnitude as for the storm of December 1982, the bottom friction and shallow water wave breaking coefficients were taken the same as for those computations. For the bottom friction coefficient the value of $f_w = 0.007$ was used, for the breaking coefficient $\gamma_s = 0.78$.

The initial settings and the conditions used in the following computations are given in Table 5.7.

5.3.4 Results and calibration

The wave height and wave period in the point Schulpengat show a fair agreement for the initial settings of the parameters. Because the conditions at the offshore boundary were not known from measurements no further calibration was done for this point. At the point Bollen the computed wave height is lower than measured; the wave period is higher than measured. Because it is known that wave growth after breaking is not very well modelled in HISWA, a computation was carried out with a part of the ZEEGAT-model. The incoming boundary for this model was situated just behind the Noorderhaaks (see Figure 5.3). No incoming waves were specified at this boundary. Table 5.8 shows that the computed wave height for this case (run A02) is a little higher than for the complete computation. The wave period is significantly lower.

In the sensitivity studies it was concluded that the wave height at Bollen is largely determined by local wind growth. The water level has also some influence on the wave height, but it is not expected that a possible inaccuracy in the water level will lead to large differences in wave height. Therefore only wind speed and direction were used for calibration. In the runs A03 and A04 the wind direction given in the wind field file was rotated 10° anti-clock wise, from approximately 290°N to around 280°N. The expected increase of the wave height at

Bollen due to the longer fetches in the Zeegat van Texel appeared to be a small decrease, probably caused by smaller waves generated in more northern sectors of the computational grid.

In the last two computations (A05 and A06) the wind direction was kept at the original value, but the wind speed was increased with 10%. Because the values used for calibration were measured in November, a justification for such an increase is the probable difference in temperature between water and air. In November the air will usually be colder than the water, causing an unstable boundary layer. The Shore Protection Manual (CERC, 1984), based on results of Resio and Vincent (1977), prescribes for such situations to use a higher wind speed to compute the generated wave height. This correction applies especially for Bretschneider-type growth curves. In earlier studies with HISWA for the northern Adriatic, it was found that the use of a corrected wind speed improved the agreement between computed and measured values of the wave height (De Girolamo et al., 1993). Because the actual temperatures of air and water on November 24, 1981, were not known, an arbitrary increase of the wind speed with 10% was used. According to Figure 5.11 this corresponds to a difference in temperature of only 3 degrees. Table 5.8 shows that the increase in wind speed of 10% leads at Bollen to waves that are more than 10% higher, both for the computation starting at the offshore boundary and for local wave growth. The computed wave periods show also a better agreement with the measured values. It is concluded that in the estuaries the wind speed is the most important parameter for calibration. The difference in temperature between air and water is in this respect a significant factor.

5.4 Conclusions

From the validation study we draw the following conclusions:

- Considering that the measurements show sometimes important variations and may also contain inaccuracies, the results of computations with the initial parameter settings show a fair agreement with the measurements;
- The procedure to assess the friction coefficient gives reliable values, as the wave height in the stations Egmond-8 and Egmond-7 show fair agreement;
- The wind speed has only a small influence on the wave heights on open sea for the selected conditions;
- For the closed coast wave breaking is the most relevant process for calibration. The formula of Battjes and Stive (1985) may overestimate the breaking coefficient, thus leading to too high waves in the breaker zone;
- The prediction of the wave period, which is also an important parameter for e.g. wave run-up computations, is a weak point of the present HISWA-model. This is mainly caused by a poor modelling of the change of the frequency due to wave breaking; There are, however, no other operational models that give a good prediction of the wave period in the surf zone.
- The data available in DTBEST for the four selected storms are not sufficient for a complete calibration in the tidal inlet, due to a lack of simultaneous measurements offshore and in the inlet;
- In the tidal inlets local wave growth is an important factor. Wind speed is the most relevant parameter for calibration in relatively deep water;

- The difference in temperature between air and water is a major element in the growth of waves by wind;
- The mean wave period for wave growth after wave breaking is overestimated due to the parametric representation of the frequency in HISWA.

6 Trial computations

6.1 General

To complete the study for the methodology for future computations, trial computations were carried out for two wave conditions. The main purpose of these computations is to calculate the wave conditions at regular intervals along the coast in a form suitable for use in computations of dune-erosion during extreme storms or wave run-up on the dikes. Awaiting the results of the statistical studies of the HYDRA-project, the conditions were determined by RWS-DGW using the guidelines for dune-erosion (TAW, 1984) like for the reference case of the sensitivity study. In deviation to the specifications in the proposal the computations were carried out for conditions with a probability of exceedance of 10^{-4} and 10^{-2} per year.

6.2 Schematisations

For the trial computations the same schematisations were used as for the sensitivity study, because the most relevant factors like wave direction and required accuracy are the same in these trial computations. The bathymetry was equal in both computations and the computational grids were identical to those in the sensitivity study. The current patterns during the storm with an exceedance probability of 10^{-2} per year will be different from the conditions during the synthetic extreme storm due to a lower wind speed and water level (section 4.2.2). However, the computed water level during this storm was still well below the water level determined using the graphs of TAW (TAW, 1984). The current field for flood conditions from the synthetic extreme storm was therefore used for both trial computations.

6.3 Boundary conditions

As stated above, the boundary conditions were determined by RWS-DGW using the same method as for the reference case of the sensitivity computations. For the condition with a probability of exceedance of 10^{-4} all external conditions were the same as for the reference case of the sensitivity study. The water level with a probability of exceedance of 10^{-2} is NAP +3.75 m and the corresponding significant wave heights at Eierlandse Gat and IJmuiden are 8.20 m and 7.10 m (see Figure 4.13). The wave period was computed according Eqs. 4.2. Except for the breaking coefficient, all other parameters were taken the same as in the reference case of the sensitivity computations. The wave breaking coefficient for breaking caused by depth limitation was again assessed using the relation given by Battjes and Stive (1985). However, the reference wave heights on which this relation has been calibrated, were measured on a relatively short distance from the breaker zone. Because the boundary of the HISWA-model is farther offshore, the wave height and period at the boundary are not the most suitable values to determine the breaking coefficient. From earlier computations the values just outside the breaker zone were used to compute this coefficient. The result of $\gamma_s = 0.75$ was used in both trial computations. All input parameters are summarized in Table 6.1.

6.4 Discussion of results

For the requested output along the NAP -10 m and NAP -5 m contours, the RAY and DEPTH commands from HISWA were used to generate the output points. The rays were specified in such a way that the interval between two rays at the NAP -5 m contour was approximately 200 m. Because the cross-shore profile shows a bar near the NAP -5 m along most of the coast of North-Holland and the DEPTH command locates only the first point of the given depth along the rays, each of the contour lines was determined in two ways: starting from the seaward side and from the landward end of the rays. Figures 6.1 to 6.4 show the output points generated in this way. Figure 6.1 shows that along most of the North-Holland coast there is a single NAP -10 m contour, but at the shoal of the Pettemer Polder and near the Schulpengat different lines are found. The NAP -5 m contour (Figure 6.2) shows small deviations all along the coast due to the presence of the bar around this depth. If the top of the bar is below the NAP -5 m contour and the trough above, the two lines coincide. If this is not the case, different positions in the ray are found. Larger differences can be seen near the Schulpengat. Figures 6.3 and 6.4 show similar results for the part of the coast of Texel within the ZEEGAT-model. In this area the large differences are caused by the shoal north of the Noorderhaaks.

The results of the computations along the defined output-lines are shown in Figures 6.5 to 6.8 for the conditions with a probability of exceedance of 10^{-4} and in Figures 6.9 to 6.12 for 10^{-2} . For the coast of North-Holland the graphs are compiled from the results for the BINNEN-model and the ZEEGAT-model. In the area where the two models overlap, a suitable point was selected where the output-lines of the two models coincide and the results were combined. The figures show that the output-lines follow the contour lines properly along a large part of the coast of North-Holland, but that considerable deviations occur in the entrance of the tidal inlet. This is most likely caused by the steep gradients in the bathymetry along the side of the Breewijk near Den Helder.

Figures 6.5 and 6.9 show that the results along the NAP -10 m contour line are rather constant. Between the profiles 140 and 160 some deviations occur due to the shoal of the Pettemer Polder. From profile 200 to the north, the wave height decreases due to the sheltering effect of the outer delta of the tidal inlet. Due to the presence of the bar on several places along the coast, the results for the NAP -5 m contour are more irregular between the profiles 0 and 140 (Figures 6.6 and 6.10). Further north the results change more gradually. Along the coast of Texel the results along the most seaward contour lines is nearly constant (Figures 6.7, 6.8, 6.11 and 6.12). In the Molengat (profiles 0 to 8) the results along the NAP -10 m and NAP -5 m contours are nearly the same. The results along the NAP -5 m contour show a gradual decrease of the wave height towards the south.

The difference between the results for the conditions with a probability of exceedance of 10^{-4} and those for 10^{-2} is approximately 0.5 m for the wave height and 0.5 s for the wave period, both at the coast of North-Holland and at the coast of Texel.

6.5 Conclusions

From the trial computations carried out for the area between IJmuiden and the island of Texel we conclude that the results along the NAP -10 m and NAP -5 m contour lines are rather constant. The HISWA option to create these output contours is suitable for the NAP -10 m contour which exists, except for a few locations with larger shoals, only once in the cross-shore profile. This method is not very suitable for the NAP -5 m contour. The cross-shore profile is usually a bar-trough profile, of which the bar is located around the NAP -5 m contour. Because of this fact, the output points generated by HISWA are not in a smooth line. This leads to irregular variations in the computed wave height and period, depending on the fact whether the generated output point is just before or just after the bar. This may be avoided by defining the output line manually. The upper envelope of the values computed along the NAP -5 m contour are a fair first estimate for the wave conditions just before the most seaward bar. However, we doubt whether the use of the NAP -5 m contour line or another line near this position is suitable as an interface between the wave propagation model and the models for dune erosion or wave run-up, because the bathymetry at this location can vary considerably from year to year. We suggest to discuss this item before the operationalisation of the models with the users.

References

- Aalst, W. van, 1983: Golfhoogte-waterstandsrelaties t.p.v. de NAP -20m lijn langs de Nederlandse kust. Notitie WWKZ-83G.218, Deltadienst Rijkswaterstaat, 12 p. + 23 bijl.
- Andorka, J.H., 1993: onderzoek naar golfdoordringing in het Zeegat van Texel met numerieke modellen. Werkdocument GWAO-92.212X, Rijkswaterstaat, DGW
- Battjes, J.A., J.P.F.M. Jansen, 1979: Energy loss and set-up due to breaking of random waves. Proc. 16th Int. Conf. on Coastal Engineering, Hamburg, 1978. ASCE, New York, N.Y., pp 569-587.
- Battjes, J.A., M.J.F. Stive, 1985: Calibration and Verification of a Dissipation Model for Random Breaking Waves. J. of Geophysical Research, Vol. 90, No. C5, pp 9159-9167.
- Booij, N., L.H. Holthuijsen, J. Dekker, R. Schoonbeek, 1988: Standard tests for the shallow water wave model HISWA, Rep. No. 6-88, Delft University of Technology, Dept. of Civil Engineering, Group of Hydraulic and Geotechnical Engineering, 43 p.
- Bouws, Koomen, 1983: On the Balance between Growth and Dissipation in an Extreme Depth-Limited Wind-Sea in the Southern North Sea. J. of Phys. Oceanography, Vol. 13, No. 9, September 1983.
- CERC, 1973: Shore Protection Manual, third edition. Coastal Engineering Research Center, U.S. Department of the Army.
- CERC, 1984: Shore Protection Manual, fourth edition. Coastal Engineering Research Center, U.S. Department of the Army.
- DELFT HYDRAULICS, 1983: Verification of numerical wave propagation models with field measurements; CREDIZ verification Haringvliet. Report W488.
- DELFT HYDRAULICS, 1987: Verification of numerical wave propagation models with laboratory measurements; HISWA verification in the directional wave basin. Report H228, Part 1A to 1D, November 1987.
- DELFT HYDRAULICS, 1990: Verification of the HISWA model. Annex to 'Investigation of the Wave Behaviour at Lido, Malamocco and Choggia Inlets of the Venice Lagoon, Report on numerical study, HISWA modelling of outer sea area'. Report H54, Vol. IA to IIIA, December 1990.
- De Girolamo, P., G. Passacantando, D.P. Hurdle, A. Noli, 1993: Evaluation of design waves along the coast and at the inlets of the Venice Lagoon. Proc. 23rd Int. Conf. on Coastal Engineering, Venice, 1992, ASCE, New York, N.Y., pp. 1851-1864.
- Deltacommissie, 1960: Rapport Deltacommissie; deel I: Eindverslagen en Interimadviezen. Staatsuitgeverij.
- Den Adel, J.D., A. Franken, H.D. Niemeijer, N. Booij, M.J.F. Stive, J.A. Vogel, 1991: Wave model application on a Wadden Sea area. Proc. 22th Int. Conf. on Coastal Engineering, Delft, 1990, ASCE, New York, N.Y., pp 530-543.
- Digital Hydraulics Holland, 1991. Het golfveld langs de Nederlandse kust bij een zeespiegelrijzing. Digital Hydraulics Holland, report 902, April 1991, Zwijndrecht, the Netherlands.
- Dingemans, M.W., M.J.F. Stive, J. Bosma, H.J. de Vriend, J.A. Vogel, 1986: Directional nearshore wave propagation and induced currents. Proc. 20th Int. Conf. on Coastal Engineering, Taipei, 1986. ASCE, New York, N.Y., pp 1092-1106.
- Hasselmann, K., D.B. Ross, P. Müller, W. Sell, 1976: A parametric wave prediction model. J. Phys. Oceanography, 6: pp.200-228.
- Holthuijsen, L.H., N. Booij, T.H.C. Herbers, 1989: A Prediction Model for Stationary, Short-crested Waves in Shallow Water with Ambient Currents. Coastal Engineering, Vol 13, pp 23-54.
- Hoozemans, F.M.J., 1988: Golfklimaat ter hoogte van het eiland Texel. Notitie GWAO-88.243, Rijkswaterstaat, DGW, 9 p. + 3 fig.
- Hydrographic Office, 1988: North Sea, The Netherlands, Zeegat van Texel to Friesche Zeegat, Chart 2593, scale 1:150.000, edition 1988.
- Hydrographic Office, 1991a: Netherlands, Goeree to Texel, Chart 2322 (INT 1415), scale 1:150.000, edition 1991.
- Hydrographic Office, 1991b: North Sea, Netherlands Gas Fields, Chart 1505, scale 1:150.000, edition 1991.
- Jonsson, I.G., 1978: A new approach to oscillatory rough turbulent boundary layers. Series Paper No. 17, Inst. of Hydrodynamics and Hydraulic Engng., Tech. Univ. of Denmark, 79 p.
- Nielsen, P., 1979: Some basic concepts of wave sediment transport. Series Paper No. 20, Inst. of Hydrodynamics and Hydraulic Engng., Tech. Univ. of Denmark, 160 p.
- Putnam, J.A., J.W. Johnson, 1949: The Dissipation of Wave Energy by Bottom Friction. Trans. Am. Geoph. Union, Vol. 30, No. 1.
- Resio, D.T., C.L. Vincent, 1977: Estimation of winds over the Great Lakes. J. of the Waterways, Port, Coastal and Ocean Division, ASCE, Vol. 103, No. WW2, pp. 265-283.
- Roskam, A., 1988: Golfklimaten voor de Nederlandse kust. Notitie GWAO-88.046, Rijkswaterstaat, DGW, 21 p. + 24 bijl.

References (continued)

- Roskam, A., 1992: Eerste resultaten van golfrichtingsmetingen in de Noordzee met de Wavec-boei; periode 1985-1989. Notitie GWAO-92.126x, Rijkswaterstaat, DGW, 62 p. + 8 bijl.
- Roskam, A., 1993: Verwerking Egmond 1982 meting EG2320 t.b.v. projekt HYDRA. Werkdocument GWAO-93.112x, Rijkswaterstaat, DGW, 7 p. + 27 bijl.
- TAW, 1984: Leidraad voor de beoordeling van de veiligheid van duinen als waterkering. Technische Adviescommissie voor de Waterstaat (TAW), Staatsuitgeverij, 's-Gravenhage, 38 pp.
- Vogel, J.A., A.C. Radder, J.H. de Reus, 1989: Verification of numerical wave propagation models in tidal inlets. Proc. 21th Int. Conf. on Coastal Engineering, Malaga, 1988, ASCE, New York, N.Y., pp 433-447.

Run	Water level above NAP (m)	Wind dir. (°N)	Wind speed (m/s)	Wave conditions Umuiden			Wave conditions Eierlandse Gat			C _w (-)	T _s (-)	Remarks		
				H _s (m)	T _{m01} (s)	Dir (°N)	m (-)	H _s (m)	T _{m01} (s)				Dir (°N)	m (-)
Reference case														
SSS	5.00	315	35	8.10	10.0	315	4	9.10	10.9	315	4	.006	.800	Frequency change breaking on; ZEEGAT model: flood currents
Variation of water level														
WS1	4.00	315	35	8.10	10.0	315	4	9.10	10.9	315	4	.006	.800	Variation in water level
WS2	4.25	315	35	8.10	10.0	315	4	9.10	10.9	315	4	.006	.800	
WS3	4.50	315	35	8.10	10.0	315	4	9.10	10.9	315	4	.006	.800	
WS4	4.75	315	35	8.10	10.0	315	4	9.10	10.9	315	4	.006	.800	
WS5	5.25	315	35	8.10	10.0	315	4	9.10	10.9	315	4	.006	.800	
WS6	5.50	315	35	8.10	10.0	315	4	9.10	10.9	315	4	.006	.800	
WS7	5.75	315	35	8.10	10.0	315	4	9.10	10.9	315	4	.006	.800	
WS8	6.00	315	35	8.10	10.0	315	4	9.10	10.9	315	4	.006	.800	
Variation of wave height														
HS1	5.00	315	35	7.10	9.3	315	4	8.10	10.2	315	4	.006	.800	Variation of wave height
HS2	5.00	315	35	7.35	9.5	315	4	8.35	10.4	315	4	.006	.800	
HS3	5.00	315	35	7.60	9.6	315	4	8.60	10.6	315	4	.006	.800	
HS4	5.00	315	35	7.85	9.8	315	4	8.85	10.7	315	4	.006	.800	
HS5	5.00	315	35	8.35	10.1	315	4	9.35	11.0	315	4	.006	.800	
HS6	5.00	315	35	8.60	10.3	315	4	9.60	11.2	315	4	.006	.800	
HS7	5.00	315	35	8.85	10.4	315	4	9.85	11.3	315	4	.006	.800	
HS8	5.00	315	35	9.10	10.6	315	4	10.10	11.4	315	4	.006	.800	
TM1	5.00	315	35	8.10	7.0	315	4	9.10	7.9	315	4	.006	.800	Variation of wave period
TM2	5.00	315	35	8.10	9.0	315	4	9.10	9.9	315	4	.006	.800	
TM3	5.00	315	35	8.10	11.0	315	4	9.10	11.9	315	4	.006	.800	
TM4	5.00	315	35	8.10	13.0	315	4	9.10	13.9	315	4	.006	.800	

Table 4.1 Boundary conditions HISWA-computations sensitivity study

Run	Water level above NAP (m)	Wind dir. (°N)	Wind speed (m/s)	Wave conditions Umliden				Wave conditions Eierlandse Gat				C _{iw} (-)	T _s (-)	Remarks
				H _s (m)	T _{m01} (s)	Dir (°N)	m (-)	H _s (m)	T _{m01} (s)	Dir (°N)	m (-)			
WR1	5.00	300	35	8.10	10.0	300	4	9.10	10.9	300	4	.006	.800	Carried out by RMS-DGW
WR2	5.00	285	35	8.10	10.0	285	4	9.10	10.9	285	4	.006	.800	Carried out by RMS-DGW
WR3	5.00	270	35	8.10	10.0	270	4	9.10	10.9	270	4	.006	.800	Carried out by RMS-DGW
SD1	5.00	315	35	8.10	10.0	315	2	9.10	10.9	315	2	.006	.800	sd = 32°
SD2	5.00	315	35	8.10	10.0	315	10	9.10	10.9	315	10	.006	.800	sd = 18°
SD3	5.00	315	35	8.10	10.0	315	30	9.10	10.9	315	30	.006	.800	sd = 10°
WI1	5.00	315	25	8.10	10.0	315	4	9.10	10.9	315	4	.006	.800	Variation of wind speed
WI2	5.00	315	30	8.10	10.0	315	4	9.10	10.9	315	4	.006	.800	
WI3	5.00	315	40	8.10	10.0	315	4	9.10	10.9	315	4	.006	.800	
WI4	5.00	315	45	8.10	10.0	315	4	9.10	10.9	315	4	.006	.800	
SR1	5.00	315	35	8.10	10.0	315	4	9.10	10.9	315	4	.006	.800	Zeegat model: ebb currents
SR2	5.00	315	35	8.10	10.0	315	4	9.10	10.9	315	4	.006	.800	Zeegat model: no currents
BW1	5.00	315	35	8.10	10.0	315	4	9.10	10.9	315	4	.000	.800	No bottom dissipation
BW2	5.00	315	35	8.10	10.0	315	4	9.10	10.9	315	4	.012	.800	
BW3	5.00	315	35	8.10	10.0	315	4	9.10	10.9	315	4	.018	.800	
BC1	5.00	315	35	8.10	10.0	315	4	9.10	10.9	315	4	.006	.700	Variation of breaking coefficients
BC2	5.00	315	35	8.10	10.0	315	4	9.10	10.9	315	4	.006	.750	
BC3	5.00	315	35	8.10	10.0	315	4	9.10	10.9	315	4	.006	.850	
FV1	5.00	315	35	8.10	10.0	315	4	9.10	10.9	315	4	.006	.800	Frequency change breaking off
FV2	5.00	315	35	8.10	10.0	315	4	9.10	10.9	315	4	.006	.800	Frequency change friction on Carried out by RMS-DGW

Table 4.1 Boundary conditions HRWA-computations sensitivity study (continued)

H_{m0} (m)	Averaged mean wave period T_{m01} (in s)										Ratio $T_{m01}/\sqrt{H_{m0}}$ (in $s/m^{0.5}$)									
	SON	ELD	K13	YM6	MPN	EUR	LEG	SWB	SON	ELD	K13	YM6	MPN	EUR	LEG	SWB				
.50	4.20	4.30	4.10	4.00	4.10	3.80	4.00	4.00	5.94	6.08	5.80	5.66	5.80	5.37	5.66	5.66				
1.00	4.80	4.80	4.60	4.50	4.60	4.30	4.40	4.40	4.80	4.80	4.60	4.50	4.60	4.30	4.40	4.40				
1.50	5.30	5.30	5.20	4.90	5.10	4.70	4.80	4.90	4.33	4.33	4.25	4.00	4.16	3.84	3.92	4.00				
2.00	5.80	5.60	5.50	5.40	5.50	5.10	5.20	5.30	4.10	3.96	3.89	3.82	3.89	3.61	3.68	3.75				
2.50	6.30	6.10	5.90	5.80	6.00	5.40	5.60	5.70	3.98	3.86	3.73	3.67	3.79	3.42	3.54	3.60				
3.00	6.70	6.40	6.30	6.30	6.40	5.80	6.00	6.10	3.87	3.70	3.64	3.64	3.70	3.35	3.46	3.52				
3.50	7.20	6.70	6.80	6.70	6.90	6.30	6.40	6.60	3.85	3.58	3.63	3.58	3.69	3.37	3.42	3.53				
4.00	7.70	7.20	7.10	7.10	7.30	6.60	6.70	6.90	3.85	3.60	3.55	3.55	3.65	3.30	3.35	3.45				
4.50	8.10	7.70	7.40	7.40	7.70	6.90	7.00	7.20	3.82	3.63	3.49	3.49	3.63	3.25	3.30	3.39				
5.00	8.60	8.00	7.90	7.80	8.10	7.30	7.20		3.85	3.58	3.53	3.49	3.62	3.26						
5.50	8.90	8.40	8.30	8.30	8.30				3.79	3.58	3.54	3.54	3.54							
6.00	9.30	8.80	8.70	8.50					3.80	3.59	3.55	3.47								
6.50	9.80								3.84											
7.00																				

SON: Schiermonnikoog Noord
ELD: Eierlandse Gat
K13: Platform K13
YM6: IJmuiden
MPN: Meetpost Noordwijk
EUR: Euro-0
LEG: Lichteiland Goeree
SWB: Schouwenbank

Table 4.2 Averaged mean wave period T_{m01} for a few stations along the Dutch coast (for position see Figure 4.12)

Runid	NAP -10 m contour			NAP -5 m contour			NAP +0 m contour		
	Hs (m)	Tm (s)	θ_o ("N)	Hs (m)	Tm (s)	θ_o ("N)	Hs (m)	Tm (s)	θ_o ("N)
sss	6.16	9.98	303.0	5.05	8.83	298.6	2.98	7.08	292.7
ws1	5.87	9.78	302.6	4.62	8.48	298.1	2.48	6.65	292.1
ws2	5.95	9.83	302.7	4.73	8.57	298.2	2.60	6.76	292.2
ws3	6.02	9.88	302.8	4.83	8.66	298.4	2.73	6.87	292.4
ws4	6.09	9.93	302.9	4.94	8.74	298.5	2.86	6.97	292.5
sss	6.16	9.98	303.0	5.05	8.83	298.6	2.98	7.08	292.7
ws5	6.23	10.06	303.0	5.15	8.91	298.8	3.11	7.19	292.8
ws6	6.30	10.11	303.1	5.25	8.99	298.9	3.23	7.29	293.0
ws7	6.37	10.15	303.2	5.35	9.08	299.0	3.36	7.40	293.2
ws8	6.43	10.15	303.3	5.45	9.15	299.2	3.48	7.50	293.3
hs1	6.02	9.70	303.1	4.99	8.66	298.8	2.96	6.98	292.8
hs2	6.07	9.80	303.1	5.01	8.72	298.7	2.97	7.02	292.8
hs3	6.10	9.84	303.0	5.02	8.74	298.7	2.97	7.02	292.8
hs4	6.13	9.89	303.0	5.03	8.77	298.7	2.97	7.04	292.7
sss	6.16	9.98	303.0	5.05	8.83	298.6	2.98	7.08	292.7
hs5	6.17	9.96	303.0	5.04	8.81	298.6	2.98	7.07	292.7
hs6	6.20	10.04	303.0	5.06	8.87	298.7	2.99	7.10	292.7
hs7	6.21	10.02	302.9	5.06	8.84	298.6	2.98	7.09	292.7
hs8	6.22	10.07	303.0	5.07	8.88	298.7	2.99	7.11	292.7
tm1	5.53	7.92	304.0	4.57	7.27	299.9	2.77	6.11	293.8
tm2	5.96	9.05	303.4	4.86	8.10	299.1	2.89	6.62	293.1
sss	6.16	9.98	303.0	5.05	8.83	298.6	2.98	7.08	292.7
tm3	6.30	10.99	302.7	5.21	9.66	298.3	3.07	7.62	292.4
tm4	6.41	13.09	302.4	5.46	11.51	298.0	3.23	8.84	292.1
wi1	6.08	9.94	303.1	5.03	8.84	298.8	2.98	7.10	292.8
wi2	6.12	9.97	303.1	5.04	8.85	298.7	2.98	7.10	292.8
sss	6.16	9.98	303.0	5.05	8.83	298.6	2.98	7.08	292.7
wi3	6.15	9.95	302.8	5.04	8.81	298.5	2.98	7.07	292.6
wi4	6.26	9.91	302.8	5.04	8.71	298.5	2.97	7.00	292.6
sr1	-	-	-	-	-	-	-	-	-
sr2	-	-	-	-	-	-	-	-	-
sss	6.16	9.98	303.0	5.05	8.83	298.6	2.98	7.08	292.7
fv1	6.18	10.66	302.9	5.18	10.65	298.5	3.26	10.63	292.1
sd1	6.13	10.05	300.7	5.06	8.92	296.7	3.00	7.13	291.1
sss	6.16	9.98	303.0	5.05	8.83	298.6	2.98	7.08	292.7
sd2	6.18	9.87	305.8	5.02	8.72	301.2	2.96	7.02	295.0
sd3	6.21	9.81	307.7	5.01	8.63	303.1	2.94	6.97	296.7
bw1	6.29	9.12	303.5	4.92	7.97	299.1	2.89	6.48	293.2
sss	6.16	9.98	303.0	5.05	8.83	298.6	2.98	7.08	292.7
bw2	5.57	10.51	302.7	4.98	9.76	298.4	3.06	7.87	292.4
bw3	4.81	10.61	302.5	4.61	10.34	298.2	3.08	8.63	292.1
bc1	5.53	9.25	303.2	4.40	8.09	298.9	2.57	6.52	293.0
bc2	5.86	9.65	303.1	4.73	8.48	298.8	2.78	6.81	292.9
sss	6.16	9.98	303.0	5.05	8.83	298.6	2.98	7.08	292.7
bc3	6.41	10.24	302.9	5.35	9.15	298.6	3.18	7.34	292.6

Table 4.3 Computed significant wave height, mean wave period and main wave direction of sensitivity runs in selected points in the Egmond profile

Runid	Marsdiep			Bollen			Malzwin		
	Hs (m)	Tm (s)	θ_o (°N)	Hs (m)	Tm (s)	θ_o (°N)	Hs (m)	Tm (s)	θ_o (°N)
sss	1.28	4.99	284.3	1.70	4.06	309.5	1.18	4.28	314.6
ws1	1.20	4.61	289.6	1.68	4.02	309.7	1.10	4.28	313.5
ws2	1.22	4.71	288.4	1.69	4.03	309.3	1.18	4.22	314.3
ws3	1.23	4.82	286.4	1.70	4.04	309.5	1.18	4.24	314.4
ws4	1.25	4.93	285.0	1.70	4.05	309.3	1.12	4.34	313.8
sss	1.28	4.99	284.3	1.70	4.06	309.5	1.18	4.28	314.6
ws5	1.29	5.15	282.2	1.70	4.08	309.3	1.14	4.37	314.1
ws6	1.32	5.20	281.8	1.71	4.09	309.6	1.17	4.35	314.3
ws7	1.35	5.32	280.7	1.71	4.11	309.6	1.14	4.46	314.1
ws8	1.36	5.44	278.8	1.72	4.12	308.9	1.17	4.42	314.5
hs1	1.28	4.97	284.5	1.70	4.06	309.5	1.17	4.29	314.2
hs2	1.28	4.98	284.4	1.70	4.06	309.6	1.13	4.36	313.8
hs3	1.28	4.98	284.4	1.70	4.06	309.5	1.17	4.32	314.2
hs4	1.28	4.98	284.3	1.70	4.06	309.5	1.17	4.31	314.2
sss	1.28	4.99	284.3	1.70	4.06	309.5	1.18	4.28	314.6
hs5	1.28	4.99	284.3	1.70	4.06	309.6	1.16	4.33	314.2
hs6	1.28	5.00	284.2	1.70	4.06	309.5	1.16	4.32	314.2
hs7	1.28	5.00	284.2	1.70	4.06	309.5	1.17	4.30	314.3
hs8	1.29	5.00	284.5	1.70	4.06	309.6	1.13	4.37	313.7
tm1	1.33	4.66	284.4	1.72	4.04	308.8	1.24	4.22	314.0
tm2	1.30	4.86	284.0	1.71	4.05	309.1	1.22	4.25	314.7
sss	1.28	4.99	284.3	1.70	4.06	309.5	1.18	4.28	314.6
tm3	1.25	5.13	285.0	1.70	4.06	309.5	1.19	4.27	315.5
tm4	1.19	5.49	286.0	1.69	4.07	310.0	1.17	4.30	316.3
wi1	1.04	5.43	271.8	1.15	3.56	309.4	.75	4.02	314.0
wi2	1.15	5.18	278.1	1.42	3.81	309.4	.95	4.16	314.2
sss	1.28	4.99	284.3	1.70	4.06	309.5	1.18	4.28	314.6
wi3	1.43	4.90	288.8	1.98	4.31	309.3	1.39	4.51	313.9
wi4	1.59	4.86	292.5	2.28	4.54	309.3	1.64	4.67	313.8
sr1	1.95	5.88	276.3	1.88	4.47	303.2	1.81	5.19	307.4
sr2	1.63	5.18	289.0	1.87	4.22	307.0	1.73	4.49	314.5
sss	1.28	4.99	284.3	1.70	4.06	309.5	1.18	4.28	314.6
sss	1.28	4.99	284.3	1.70	4.06	309.5	1.18	4.28	314.6
fv1	.91	7.34	294.2	1.66	4.08	311.7	1.03	4.49	318.3
sd1	1.29	5.08	283.8	1.70	4.07	309.5	1.17	4.31	314.5
sss	1.28	4.99	284.3	1.70	4.06	309.5	1.18	4.28	314.6
sd2	1.26	4.89	285.4	1.70	4.06	309.6	1.16	4.32	314.0
sd3	1.24	4.81	286.4	1.70	4.05	309.5	1.18	4.26	314.3
bw1	1.33	4.90	283.3	1.70	4.06	309.1	1.20	4.28	313.9
sss	1.28	4.99	284.3	1.70	4.06	309.5	1.18	4.28	314.6
bw2	1.21	5.12	287.2	1.69	4.06	310.0	1.14	4.33	314.8
bw3	1.12	5.22	293.3	1.68	4.06	310.5	1.14	4.28	315.8
bc1	1.26	4.69	286.7	1.70	4.04	309.3	1.20	4.23	313.9
bc2	1.27	4.87	285.3	1.70	4.05	309.3	1.17	4.28	313.8
sss	1.28	4.99	284.3	1.70	4.06	309.5	1.18	4.28	314.6
bc3	1.29	5.16	283.5	1.70	4.07	309.7	1.15	4.36	314.4

Table 4.4 Computed significant wave height, mean wave period and main wave direction of sensitivity runs in selected points in the tidal inlet

Primary(x)			Secondary(y)		Interdependency			
	x	σ_x	y	σ_y^*	α	σ_α	γ_{xy}	σ_y
sea level rise	0.6	0.5						
	bottom level rise		0.3	0.12	0.5	0.2	0.85	0.29
wind speed	30	3						
	storm surge level		5.0	0.5	0.1667	0.01667	0.7	0.71
	hi (deep water)		6.0	0.72	0.2	0.024	0.64	0.94
	ti (ti=1.52hi)		9.1	0	-	-	-	-

Table 4.5 Mean value and standard deviation of primary and related secondary parameters and the assumed interdependency (note: $y = \alpha x$)

Σ_i	reference case	σ_z
------------	----------------	------------

External parameters

ws	5.0 m	0.92 m
hi	8.35 m	0.94 m
ti	10.2 s	1.4 s
wi	35 m/s	3 m/s
sr	following	1
sd	25 deg.	7 deg.

Internal parameters

fv	on	0.5
bw	0.006	0.002
bc	0.80	0.05

Table 4.6 Reference values and assumed uncertainty of the input parameters

Egmond profile		Molengat profile
-5 m NAP	-10 m NAP	-25 m NAP

the uncertainty in the computational results of significant wave height and mean wave period

	H_s (m)	T_m (s)	H_s (m)	T_m (s)	H_s (m)	T_m (s)
σ_{all}	0.55	1.64	0.47	1.47	0.53	2.47
σ_{ext}	0.46	1.01	0.36	1.37	0.45	0.67
σ_{int}	0.30	1.28	0.30	0.51	0.27	2.38
$\sigma_{ext.dep}$	0.48	1.16	0.47	1.57	0.45	0.66
$\sigma_{all.dep}$	0.57	1.73	0.56	1.65	0.53	2.47

the normalized uncertainty due to each independent parameter

ws	0.75	0.21	0.55	0.11	0.21	0.19
hi	0.33	0.04	0.17	0.09	0.01	0.01
ti	0.37	0.58	0.50	0.92	-0.15	0.18
wi	0.00	-0.09	0.07	0.00	0.15	-0.05
sd	0.03	0.06	-0.06	0.06	0.04	0.06
sr	-	-	-	-	0.81	0.02
fv	-0.18	-0.74	-0.02	-0.23	0.50	-0.95
bw	0.05	0.18	-0.26	0.16	-0.08	0.06
bc	0.52	0.19	0.59	0.20	0.00	0.11

the normalized uncertainty due to each external parameter with interdependency

Slr	0.23	0.08	0.15	0.03	0.07	0.19
α_b	-0.11	-0.04	-0.07	-0.01	-0.03	-0.09
wi	0.76	0.71	0.78	0.67	0.20	0.67
α_{hi}	0.36	0.67	0.51	0.74	-0.13	0.55
α_{Ssl}	0.46	0.16	0.30	0.06	0.13	0.38
sd	0.03	0.08	0.06	0.06	0.02	0.22
sr	-	-	-	-	0.96	0.07

$\sigma_{all.dep}$ is the uncertainty due to all parameters taking into account the interdependency between the external parameters.

Table 4.7 Absolute and relative uncertainty at two locations in the Egmond profile and one point in the Molengat profile

Station	Depth (m)	Position				Available measurements			
		Paris-coordinates		Amersfoort-coordinates		Storm 1/81	Storm 11/81	Storm 3/82	Storm 12/82
		X (km)	Y (km)	X (km)	Y (km)				
Eierlandse Gat	27.	101.594	579.527	-53.406	116.527			X	X
Bollen	7.5	118.550	556.620	-36.450	93.620		X		
Malzwin	4.5	116.125	553.310	-38.875	90.310			X	
Schulpengat	10.	104.967	545.648	-50.033	82.648		X		X
Bergen-1	6.	103.300	521.510	-51.700	58.510	X			
Bergen-3	15.	101.310	521.600	-53.690	58.600	X			
Bergen-4	20.	97.820	521.800	-57.180	58.800	X			
Egmond-6	7.	102.223	514.764	-52.777	51.764				X
Egmond-7	15.	99.930	515.098	-55.070	52.098				X
Egmond-8	20.	96.004	515.638	-58.996	52.638				X
Mun.stort. IJmuiden*)	21.	64.500	506.600	-90.500	43.600			X	X
Meetpost Noordwijk	18.	80.512	476.658	-74.488	13.658				X

*) Position estimated from nautical chart for 52°33'N, 4°04'E.

Table 5.1 Wind and wave measurements available for validation in DTBEST-files

Date	Time (hh. mm)	Water level (m+NAP)	Wind Dir. (°N)	Wind speed (m/s)	Eierlandse Gat		Umsuiden		Egmond-8		Egmond-7		Egmond-6	
					H _{m0}	T _{m01}	H _{m0}	T _{m01}	H _{m0}	T _{m01}	H _{m0}	T _{m01}	H _{m0}	T _{m01}
821215	12.00	0.05	245	17	2.69	5.8	2.86	5.7					2.10	5.5
	12.15	0.06	245	17							2.41	5.5		
	12.30	0.21	245	16					2.42	5.7				
	12.45													
	13.00													
	13.15													
	13.30													
	13.45													
	14.00													
	14.15													
	14.30	1.71		235	19					3.31	6.2			
	14.45													
	15.00					3.91	6.4	3.51	6.1					
	15.15	1.60		235	19							3.37	6.4	
	15.30	1.51		235	18					3.05	6.0			
	15.45													
	16.00													
	16.15	1.43		235	19							3.78	6.4	
	16.30	1.41		235	21					3.76	6.6			
	16.45													
	17.00													
	17.15	1.29		235	21							4.08	6.7	
	17.30													
	17.45													
	18.00					3.87	6.6	3.80	6.8					
	18.15	1.33		235	20							3.46	6.6	
	18.30	1.32		235	21					3.64	6.9			
	18.45													
	19.00													
	19.15	1.37		240	22							3.89	6.8	
19.30	1.35		240	22					3.63	6.8				
19.45														
20.00														
20.15	1.20		240	21							3.86	6.8		
20.30	1.18		240	21					3.86	6.9				
20.45														
21.00	1.00		245	20	3.49	6.6	4.30	7.5					3.17	6.9
21.15	0.90		245	21							3.73	6.6		
21.30	0.79		245	21					3.84	7.0				
21.45														
22.00														
22.15	0.65		250	18							3.66	7.1		
22.30	0.55		270	17					3.59	6.9				
22.45														
23.00	0.51		265	16									3.12	6.9
23.15	0.57		290	17							3.73	7.0		
23.30	0.64		295	19					3.66	6.8				
23.45														
821216	.00	0.75	295	19	4.30	7.3	4.37	7.0					3.04	6.6

Table 5.2 Measured wave conditions during storm of December 1982

Date	Time (hh. mm)	Water level (m+NAP)	Wind Dir. (°N)	Wind speed (m/s)	Eierlandse Gat		Umuiden		Egmond-8		Egmond-7		Egmond-6	
					H _{m0}	T _{m01}	H _{m0}	T _{m01}	H _{m0}	T _{m01}	H _{m0}	T _{m01}	H _{m0}	T _{m01}
821216	0.00	.75	295	19	4.30	7.3	4.37	7.0					3.04	6.6
	0.15	.81	295	18							3.51	6.6		
	0.30	.91	295	22					3.78	6.8				
	0.45													
	1.00													
	1.15	1.20	290	20							3.90	6.7		
	1.30	1.39	285	20					3.98	7.0				
	1.45													
	2.00													
	2.15	1.84	280	19							5.14	7.9		
	2.30	2.06	275	19					5.14	8.0				
	2.45													
	3.00					5.28	7.9	4.39	7.2					
	3.15	2.20	280	18							5.00	8.0		
	3.30	2.19	280	17					4.50	8.0				
	3.45													
	4.00													
	4.15	2.15	270	18							4.79	8.0		
	4.30	2.21	275	18					4.16	7.4				
	4.45													
	5.00													
	5.15	2.16	280	19							5.16	8.1		
	5.30	2.08	280	19					4.31	7.7				
	5.45													
	6.00					5.36	7.8	4.51	7.4					
	6.15	1.90	275	19							4.73	8.2		
	6.30	1.86	275	18					5.02	8.0				
	6.45													
	7.00	1.76	275	19									3.63	7.4
	7.15	1.69	280	19							4.64	7.8		
7.30	1.65	280	18					4.47	7.5					
7.45														
8.00														
8.15	1.41	270	19							4.65	7.7			
8.30	1.37	270	18					4.27	7.7					
8.45														
9.00					5.53	8.3	4.54	7.6						
9.15	1.01	270	19							3.98	7.4			
9.30														
9.45														
10.00														
10.15														
10.30														
10.45														
11.00														
11.15														
11.30														
11.45														
821216	12.00				4.93	7.9	4.59	7.6						

Table 5.2 Measured wave conditions during storm of December 1982 (continued)

Date	Time (hh. mm)	Water level (m+NAP)	Wind Dir. ("N)	Wind speed (m/s)	Eierlandse Gat		Umuiden		Egmond-8		Egmond-7		Egmond-6		
					H _{m0}	T _{m01}	H _{m0}	T _{m01}	H _{m0}	T _{m01}	H _{m0}	T _{m01}	H _{m0}	T _{m01}	
821216	12.00				4.93	7.9	4.59	7.6							
	12.15														
	12.30														
	12.45														
	13.00														
	13.15														
	13.30														
	13.45														
	14.00														
	14.15														
	14.30	1.50	255	16					4.56	7.8					
	14.45														
	15.00					4.82	7.5	4.08	7.0						
	15.15	1.97	260	17							4.26	7.5			
	15.30	1.97	260	17					4.42	7.5					
	15.45														
	16.00														
	16.15														
	16.30	1.72	260	18					3.88	7.3					
	16.45														
	17.00														
	17.15	1.52	265	17							3.92	7.2			
	17.30	1.47	260	18					4.00	7.3					
	17.45														
	18.00					4.95	7.7	3.77	6.6						
	18.15	1.31	265	18							3.87	7.1			
	18.30	1.22	270	18					3.75	6.9					
	18.45														
	19.00	1.11	270	18									3.15	7.1	
	19.15	1.05	265	17							4.30	7.5			
19.30	1.00	275	16					4.69	7.4						
19.45															
20.00															
20.15	.99									3.85	7.2				
20.30	.93							3.88	7.4						
20.45															
21.00					4.86	7.8	4.05	7.4							
21.15	.71									3.86	7.4				
21.30	.63							4.03	7.4						
21.45															
22.00															
22.15															
22.30															
22.45															
23.00															
23.15															
23.30															
23.45															
821217	0.00		275	17	3.92	7.4	4.30	7.6							

Table 5.2 Measured wave conditions during storm of December 1982 (continued)

Run	Water level above NAP (m)	Wind dir. (°N)	Wind speed (m/s)	Wave conditions IJmuiden			Wave conditions Eierlandse Gat			C _{fw} (-)	γ _s (-)	Remarks		
				H _s (m)	T _{m01} (s)	Dir (°N)	m (-)	H _s (m)	T _{m01} (s)				Dir (°N)	m (-)
December 16, 1982, 0.00 h														
B06	0.75	290	19.8	4.35	7.2	290	4	4.36	7.3	280	4	.007	.78	Averages 821216, 0.00 h θ _{wave} = θ _{wind} , 21.00h B07, frequency change friction on B08, γ _s lower
B07	0.75	290	19.8	4.35	7.2	250	4	4.36	7.3	250	4	.007	.78	
B08	0.75	290	19.8	4.35	7.2	250	4	4.36	7.3	250	4	.007	.78	
B09	0.75	290	19.8	4.35	7.2	250	4	4.36	7.3	250	4	.007	.70	
December 16, 1982, 6.00 h														
B01	1.90	275	19.0	4.51	7.4	280	4	5.36	7.8	270	4	.007	.78	Averages 821216, 6.00 h Wind speed 10% higher Breaking: α = 0.83, γ _d = 1.13 Friction coefficient lower
B02	1.90	275	20.9	4.51	7.4	280	4	5.36	7.8	270	4	.007	.78	
B03	1.90	275	20.9	4.51	7.4	280	4	5.36	7.8	270	4	.007	.793	
B04	1.90	275	20.9	4.51	7.4	280	4	5.36	7.8	270	4	.005	.78	
December 16, 1982, 18.00 h														
B05	1.20	265	18.7	3.97	7.0	270	4	4.88	7.7	260	4	.007	.780	Averages 821216, 18.00 h

Table 5.3 Boundary conditions validation computations Egmond

Run	Eierlands Gat			IJmuiden			Egmond-8			Egmond-7			Egmond-6		
	H _s (m)	T _{m01} (s)	θ ₀ (°N)	H _s (m)	T _{m01} (s)	θ ₀ (°N)	H _s (m)	T _{m01} (s)	θ ₀ (°N)	H _s (m)	T _{m01} (s)	θ ₀ (°N)	H _s (m)	T _{m01} (s)	θ ₀ (°N)
0.00 h, averaged															
Meas.	4.36	7.27	-	4.35	7.23	-	3.77	6.90	-	3.70	6.85	-	3.11	6.8	-
B06	4.36	7.50	280.2	4.33	7.28	288.1	4.21	7.61	288.7	4.15	7.65	289.0	3.62	7.13	285.4
B07	4.22	7.60	259.5	4.34	7.28	264.9	3.95	7.58	266.7	3.92	7.61	268.9	3.56	7.19	270.6
B08	4.25	7.55	259.2	4.35	7.24	264.9	4.14	7.20	266.3	4.14	7.13	268.4	3.51	6.48	270.3
B09	4.25	7.55	259.2	4.35	7.24	264.9	4.14	7.20	266.3	4.12	7.11	268.5	3.24	6.27	270.4
6.00 h, averaged															
Meas.	5.39	8.00	-	4.48	7.40	-	4.45	7.66	-	4.79	7.96	-	3.63	7.40	-
B01	5.07	7.98	272.3	4.59	7.47	279.2	4.47	7.81	281.3	4.41	7.84	282.3	4.01	7.46	280.8
B02	5.16	8.02	273.0	4.59	7.48	279.1	4.52	7.87	281.3	4.47	7.91	282.2	4.04	7.49	280.7
B03	5.16	8.02	273.0	4.59	7.48	279.1	4.52	7.87	281.3	4.47	7.91	282.2	4.12	7.56	280.7
B04	5.19	8.02	272.9	4.60	7.48	279.1	4.64	7.87	281.2	4.62	7.91	282.2	4.08	7.40	280.7
18.00 h, averaged															
Meas.	4.88	7.67	-	3.97	7.00	-	4.04	7.26	-	3.99	7.25	-	3.15	7.10	-
B05	4.89	7.81	280.2	4.07	7.10	270.1	4.01	7.47	274.2	3.98	7.50	275.7	3.67	7.18	275.9

Table 5.4 Measured and computed wave conditions at offshore and Egmond-stations, storm December 16, 1982

Fetch (km)	Water depth 25 m		Water depth 30 m		Water depth 35 m	
	H_s (m)	T_p (s)	H_s (m)	T_p (s)	H_s (m)	T_p (s)
150	4.19	9.07	4.46	9.22	4.63	9.32
200	4.41	9.59	4.80	9.83	5.07	10.00
250	4.50	9.89	4.98	10.23	5.34	10.47
500	4.58	10.30	5.20	10.85	5.76	11.30
1000	4.59	10.33	5.21	10.92	5.79	11.43

Table 5.5 Wave conditions predicted using Hurdle and Stive (1984) for a wind speed of 18 m/s

Date (yyymmdd)	Time (hh.mm)	Water level (m + NAP)	Wind speed (m/s)	Wind direction (°N)	Eierlandse Gat		Umuiden		Schulpengat	
					H _{m0} (m)	T _{m01} (s)	H _{m0} (m)	T _{m01} (s)	H _{m0} (m)	T _{m01} (s)
820311	03.00	0.46	14	280	3.55	6.3	3.94	6.8	3.66	6.6
	04.00	1.26	15	280					3.73	7.0
	05.00	1.32	15	280					4.36	7.6
	06.00	1.58	16	280	4.32	7.4	4.39	7.2	4.43	7.7
	07.00	1.70	16	280					4.48	7.8
	08.00	1.79	15	280					4.91	8.0
	09.00	1.67	14	280	4.51	7.6	4.07	7.3	3.93	7.7

Table 5.6 Wave conditions measured during storm of March 11, 1982

Run	Water level above NAP (m)	Wind dir. (°N)	Wind speed (m/s)	Wave conditions IJmuiden			Wave conditions Eierlandse Gat			c _w	γ _s	Remarks		
				H _s (m)	T _{md01} (s)	Dir (°N)	H _s (m)	T _{md01} (s)	Dir (°N)					
				m	m	m	m	m	m					
November 24, 1981, 14.00 h														
A01	1.85	280	18.0	4.90	7.7	280	4	5.30	8.3	280	4	.007	.78	ZEEGAT-model wind field RMS
A02	1.85	*	*	0.00	-	-	-	0.00	-	-	-	.007	.78	part ZEEGAT-model, local wave growth
A03	1.85	*	*	0.00	-	-	-	0.00	-	-	-	.007	.78	Local wave growth, wind 10° rotated
A04	1.85	*	*	4.90	7.7	280	4	5.30	8.3	280	4	.007	.78	Wind field ZEEGAT-model 10° rotated
A05	1.85	280	19.8	4.90	7.7	280	4	5.30	8.3	280	4	.007	.78	Wind speed 10% higher
A06	1.85	*	*	0.00	-	-	-	0.00	-	-	-	.007	.78	Local wave growth, wind speed 10% higher

Table 5.7 Boundary conditions validation computations Zeegat van Texel

Run	Eierlands Gat			Umuiden			Schulpengat			Bollen			Malzwin		
	H _s (m)	T _{m01} (s)	θ ₀ (°N)	H _s (m)	T _{m01} (s)	θ ₀ (°N)	H _s (m)	T _{m01} (s)	θ ₀ (°N)	H _s (m)	T _{m01} (s)	θ ₀ (°N)	H _s (m)	T _{m01} (s)	θ ₀ (°N)
14.00 h															
Meas.	-	-	-	-	-	-	4.14	8.10	-	0.80	3.00	-	-	-	-
A01	3.95	8.31	264.3	4.92	7.79	280.1	4.20	7.97	272.8	0.63	3.41	292.2	0.41	3.81	311.7
A02	-	-	-	-	-	-	-	-	-	0.66	2.68	287.5	0.47	2.60	310.5
A03	-	-	-	-	-	-	-	-	-	0.64	2.69	277.1	0.44	2.51	305.6
A04	-	-	-	-	-	-	4.20	7.92	273.4	0.59	3.54	284.0	0.38	3.93	305.2
A05	5.14	8.40	279.0	4.92	7.79	280.1	4.22	7.94	273.5	0.71	3.39	292.5	0.47	3.76	311.3
A06	-	-	-	-	-	-	-	-	-	0.75	2.82	287.3	0.53	2.75	309.8

Table 5.8 Measured and computed wave conditions at offshore-stations and stations in the Zeegat van Texel, storm November 24, 1981

Run	Water level above NAP (m)	Wind dir. (°N)	Wind speed (m/s)	Wave conditions IJmuiden				Wave conditions Eierlandse Gat				c_{fw} (-)	γ_s (-)	Remarks
				H_s (m)	T_{m01} (s)	Dir (°N)	m (-)	H_s (m)	T_{m01} (s)	Dir (°N)	m (-)			
Z01	5.00	315	35	8.10	10.0	315	4	9.10	10.9	315	4	.006	.750	Conditions 10^{-4} per year
Z02	3.75	315	27	7.10	9.3	315	4	8.20	10.3	315	4	.006	.750	Conditions 10^{-2} per year

Table 6.1 Boundary conditions trial computations

Appendix A

Irregularities in HISWA results

1 Introduction

It was found in a previous sensitivity study (Booij and Holthuijsen, 1991) that HISWA results sometimes show irregular behaviour; in particular this was the case in the entrance to the Westerschelde estuary. Experience showed that the predicted wave height and period did not always vary smoothly with the water level. This was found in particular for very high water levels (the study was concerned with extreme storm surges).

To gain further insight into the problems, further computations were done for the Westerschelde area (for the bathymetry see Figure A1), again for waves at storm surge levels.

2 Search for an explanation

In the sensitivity study by Booij and Holthuijsen (1991) it was found that the wave height in the Westerschelde region did not vary smoothly with water level. This behaviour is illustrated by Figure A2 where the wave height along the line "As" (indicated in Figure A1) is shown for three different water levels.

When the irregular behaviour was found, it was initially attributed to refraction. The reason is that from earlier ray computations in such areas it was known that wave rays do behave chaotically. In a model like HISWA which takes the integral of the wave energy over many spectral directions, this chaotic behaviour is suppressed. However, it may be that in a milder form the effects of the chaotic behaviour may still show up. This may be particularly so if the dissipative effects are not dominant. It would explain why the irregularities were not found for lower water levels, because there dissipation is so strong that refraction is only a minor effect. It must be admitted, however, that refraction also becomes weaker with increasing depth.

A sensitivity analysis was carried out in order to try to find the cause for this behaviour. In this analysis the water level was varied in the range of 5 to 6.4 m above datum (N.A.P.). In the basic case all the effects of refraction, breaking, friction, frequency change due to dissipation and wind were taken into account. In each of the subsequent computations one of these effects was switched off, and it was studied whether this had an effect on the irregularities.

The effect of currents was not considered in this study.

The output of HISWA was considered along three lines, one line (called "As") parallel to the main axis of the channel from deep water (appr. 20 m) to a point appr. 10 km east of Vlissingen, and two lines perpendicular to "As", viz. a line "B1" 2 km West of the line Vlissingen-Breskens, and "B2" 2 km East of the line Vlissingen-Breskens (see Figure A1). The quantities considered in the sensitivity study are the significant wave height (H_s) and mean wave period (T_m).

The following observations were made:

- Refraction off: The effect of disabling refraction is a smoother variation of both H_s and T along the line "As"; the behaviour as function of water level is also smoother. Further inland larger values of H_s are probably due to absence of the scattering effect of refraction.
- Breaking off: The results in the case without breaking seem slightly smoother than in the basic case.
- Friction off: At some places H_s is larger than in the basic case. The behaviour is sometimes more irregular than in the basic case. From a comparison with the basic case and other cases it seems that the frequency change along "As" is largely due to friction.
- Freq. change off: The wave heights are consistently lower than in the basic case, probably due to the property that dissipation is larger for larger wave period (as is the case if frequency change is disabled), and that wind input is smaller for larger period.
- Wind off: No particulars. The effect of the wind turned out to be small, both on the results as such and on the irregularities.
- Larger period: A larger period of the incoming waves does not lead to significantly larger irregularities; since refraction is stronger for larger periods, this seems to contradict the importance of refraction.
- Narrower distr: A narrower directional distribution does not lead to significantly larger irregularities which also seems to contradict the importance of refraction.

The results seem to indicate that refraction plays a role in the existence of irregular behaviour of the wave parameters as function of water level. However, contra-indications are present, and for instance breaking may also contribute to the phenomenon.

In search of other sources of irregularities two computations were done with two (slightly) different versions of HISWA. The locations where the irregularities occurred changed considerably. Apparently the irregularities are very sensitive to minor changes in the computational procedure. This suggests that there are numerical causes for the phenomenon. When studying isoline plots for the wave steepness it was confirmed that extreme wave steepness occurred at isolated points and that this high steepness propagates along diagonal lines of the computational grid; Figure A3 presents an example of such lines. These lines are seen to be parallel to the directional limits of the computation.

In an isoline figure of the significant wave height it can be seen that along the lines with extreme steepness the dissipation is larger than elsewhere. The large steepness causes a large (whitecapping) dissipation. Such extreme dissipation results in the unexplained differences in wave height observed in the study by Booij and Holthuijsen (1991).

3 Causes for extreme steepness

It proved to be difficult to find the cause for the generation and propagation of the above indicated extreme steepness. It was found in such cases that for a spectral direction at or near the directional limit the wave frequency was extremely high. This was found after a facility was added to HISWA to visualise the action density or the average frequency for each individual spectral direction, the so-called "star" plot. An example of a "star" plot is shown in Figure A5. The length of the line in a certain direction is proportional to the frequency associated with that direction; a similar facility exists for the action density.

The problem seems to arise when the wave action density tends to zero; if this occurs the frequency becomes indeterminate, and can therefore attain very high values. The action density can go to zero if the refraction term moves action away from a direction in which the action density is already small; this is the case usually near the directional boundaries of the computational sector (where moreover no energy is imported across the limiting direction). The direction of the refractive transfer of energy is determined by the sign of c_{θ} , i.e. the velocity of energy transfer over directions, associated with the curvature of rays in a ray model. The situation is sketched in Figure A4.

The problem may be aggravated if the above effect is combined with bottom friction and/or shallow-water breaking, i.e. dissipation effects which have a tendency to increase the average frequency. Bottom friction, however, can hardly play a role in this respect; friction does increase the frequency but as soon as the frequency is higher for one direction than for others the dissipation for that direction decreases dramatically. Wave breaking is a more serious candidate since in a grid point the ratio of dissipation vs existing energy is dependent on integrated wave parameters. The breaking dissipation (but not the friction dissipation) is proportional to the action density; therefore relative breaking dissipation in a direction can be considerable also if the energy associated with that direction is small. The frequency shift is associated with the relative dissipation and is the same for all directions. Thus the frequency shift can be considerable also for directions in which there is little energy and a high frequency.

The above assumptions are supported to a certain extent by the findings from the sensitivity analysis discussed in the previous section. It was seen that the presence of a refraction term was crucial, but that a change in spectral shape did not have a large influence. Also breaking dissipation was seen to have some, albeit minor effect. Other effects have hardly any influence which seems in accordance with the above hypothesis.

From the "star" plots it was also found that often the lines of extreme steepness originated at the lateral boundaries. The area shown in Figure A5 is located along the right lateral boundary (the Southwest boundary); it is seen that the high frequencies exist already on the boundary itself. This is attributed to the assumption of a fully absorbing lateral boundary which is the standard option in the present version of HISWA. Wave action propagating towards such a boundary is absorbed and no action is coming in while the frequency is set at a rather high value. However, with zero action for the incoming directions the frequency is in fact indeterminate for these directions.

Propagation of the high steepness would normally be difficult due to the presence of numerical diffusion over directions. If the action density in a certain direction is very small numerical diffusion would tend to smoothen both the action density and the frequency and would therefore transport action to the considered direction from neighbouring directions. In our case, however, this mechanism does not work, because for the considered directions c_{θ} was close to zero (as a result of the high frequency) and this caused the numerical diffusion over direction (which is proportional to c_{θ}) to be small.

4 Possible remedies

Several possibilities were tested to improve the robustness of the model. One way is to prevent the generation of the high frequencies (a). The second way is to modify the formulation of the numerical diffusion over directions slightly so that the differences in frequency would be smoothed out (b).

- (a) One possibility to prevent generation of high frequencies is to make the lateral boundary slightly reflecting, because then the directions away from the boundary will carry some energy and a physically feasible frequency. A computation was done with reflection coefficient 0.2 on the open boundaries. Figure A6 shows the isolines of the wave steepness and indeed some of the lines with too high steepness have disappeared. The value of the reflection coefficient has little influence on the resulting wave parameters as long as it is a (small) positive value.

Another improvement resulted from using the last test version of HISWA (update number 100.09). Although the modifications and corrections involved are not aiming at preventing high steepness values, this version proves to be more stable than the previous one and thus generates less cases of high steepness. In particular the correction of a coefficient used in the subroutine which computes breaking dissipation proved to be effective. This correction has no noticeable effect in regions with smooth bathymetry, but it does make the results smoother in regions with steeper slopes. It is stressed that in the new version the formulation of the numerical diffusion over directions was unchanged with respect to previous versions. The improvement is illustrated in Figure A7, where it is shown how the significant wave height in 4 points A, B, C and D depends on the water level when the production version of March 1992 is used (upper panel) and when the above mentioned test version is used (lower panel). It is concluded that the behaviour has improved to such an extent that a sensitivity analysis of the type described by Booij and Holthuijsen (1991) becomes feasible.

A further contribution in preventing the generation of high frequencies can be expected from a reformulation of the frequency change in very shallow water; research is being done to arrive at a formulation which is decoupled from the breaking dissipation and which is based on nonlinear transfer of energy in the spectrum by 3-wave interactions. Such nonlinear transfer will probably be considered for every spectral direction separately, and will be very small if the average frequency is high, so that the problems with frequency change due to breaking, mentioned in the previous section, are avoided.

- (b) The formulation of the numerical diffusion over directions was modified by developing an experimental version of HISWA. In this version the diffusion was made dependent on an average c_g rather than on the local value. This does help in making the propagation of errors more difficult but it has a disadvantage. It was found that this formulation of the numerical diffusion led to a substantially larger smearing of action over directions also in cases where this was not necessary. For instance in the case of a narrow wave field propagating over a bar, it turned out that the directional spread did not decrease over the bar as it should and that it tended to a too high value behind the bar.

5 Comparison with fully spectral model

In view of the irregular behaviour a comparison was made with the fully spectral wave model of Won (1991), see also Neu and Won (1990). This model is described in more detail in Appendix B. For one case a computation was made with Won's model and with HISWA. It was not possible to use one of the existing HISWA computations because of the following limitations of the fully spectral model. This model was developed for intermediate depths and not for coastal applications, so shallow water breaking is not included. Also various dissipation terms were formulated differently. The computations with HISWA and Won's model were therefore done with dissipation completely neglected.

Because of memory limitations of the computer on which Won's model was to be run, the resolution was quite coarse. The spatial steps were 1 km in both directions, the circle was covered with 12 spectral directions, i.e. a directional step size of 30 degrees, and 12 discrete frequencies were used. The resolution in the HISWA run was finer, the step sizes were the same as for all other runs: step size in computational direction: 278 m, step size in cross-direction 533 m, directional step: 10°. Both computations were done for a water level of NAP +6 m, and waves from the NW. Isolines for the significant wave height resulting from the two computations are shown in Figure A9.

Bearing in mind the differences in resolution between the two computations it can be concluded that the overall pattern of the isolines is much the same in both computations. Apparently there is no reason to mistrust the HISWA results apart from the points where irregularities occur.

6 Conclusion

To prevent unrealistically high steepness values in HISWA it is helpful to choose a (completely or partially) reflecting boundary on the lateral boundaries of the computational area. This does not seem to have negative effects and it is therefore planned to replace the present default boundary condition by a partially reflecting boundary condition in the next production version of HISWA.

The increased robustness of the test version 100.09 helps to prevent to a large extent the generation of high steepness in the interior of the computational region. The positive effect is mainly due to a correction in the computation of breaking dissipation. These changes will soon be implemented on the production version. Further improvement is expected from a

reformulation of frequency change in very shallow water. Such a reformulation should be based on 3-wave nonlinear energy transfer within the spectrum; this is planned for the fully spectral wave models SWAN and PHIDIAS. It is uncertain whether a simplified version fitting in the HISWA framework can be developed.

Modification of the numerical diffusion over directions is helpful in preventing the propagation of extremely high frequencies. However, since this leads to considerable errors in the directional spread it is not considered to be a useful modification for future production versions of HISWA.

The propagation results by HISWA in the case studied are in good agreement with those of a fully spectral model.

References

- Booij, N. and L.H. Holthuijsen, "Het golfveld langs de Nederlandse kust bij een zeespiegelrijzing", Digital Hydraulics Holland, report 902, Zwijndrecht 1991.
- Neu, W.L. and Y.S. Won (1990), "Propagation schemes for wind wave models with finite depth and current", Proc. of CAMS (Canad. Appl. Math. Soc.) Conference, pp. 947-954.
- Won, Y.S. (1991), "Higher order numerical schemes for propagation of wind wave spectra", dissertation, Virginia Polytechnic Institute, Blacksburg, VA.

Appendix B

Fully spectral propagation scheme

1 Introduction

The HISWA results are compared with those calculated from a full spectrum model (Neu and Won, 1990; Won, 1991). To make the comparison simple and fair, all the source terms are disabled and only the propagation including depth refraction is allowed. The full spectrum model has been developed to provide a higher order propagation scheme which can perform reasonable accuracy for a coarse grid.

The 1st order schemes have severe numerical dispersion at transient stage, resulting in a very smooth distribution of incident waves. Among the 2nd order schemes, Lax-Wendroff schemes are investigated which are successfully used in a meteorology field. The drawbacks of the Lax-Wendroff scheme (Lax and Wendroff, 1960) are phase lagging errors and spurious oscillations. The modified Lax-Wendroff scheme (Gadd, 1978; Gadd, 1980) shows good performance for both steady and transient cases, except for the spurious oscillations. Another problem of the Lax-Wendroff schemes is that they become unstable when used in both the spatial and directional dimensions.

In this chapter, some methods to remedy the spurious oscillations and the instability problem of the Lax-Wendroff schemes are introduced, and by integrating these methods a new scheme is proposed. The new scheme is designed to take the performance of the modified Lax-Wendroff scheme, reducing the spurious oscillations and avoiding the instability problem by the use of a limiter and time splitting. This scheme as well as the 1st order upwind scheme are tested for the Wester Schelde case.

2 The Limiter

According to Godunov's theorem, no second order scheme can be monotone-preserving (Roe, 1986). In other words, the spurious oscillation is an inherent problem of second order schemes which do not possess the *total variation diminishing* (TVD) property as discussed in Morton and Sweby (1987). A limiter is used to retain the TVD property for the higher order schemes by adopting first order schemes where the spurious oscillation is expected. There are various types of limiters to do this work.

For linear advection equations, Sweby(1984) rearranged several second order schemes into the first order upwind scheme and a *limited* flux called an additional anti-diffusive flux. A limiter is the parameter which controls the amount of the *limited* flux. He compared a class of limiters which can be transformed into his expression, and showed the range of values which the limiters may take to keep the scheme oscillation-free. Its application to non-linear equations, however, is quite complicated and the modified Lax-Wendroff scheme, which is our choice, cannot be transformed into his expression. His expression is based on a three-point approximation while the modified Lax-Wendroff scheme uses a five-point approximation for a one-dimensional advection equation.

Therefore, we will use a rather simple kind of limiter which yields a weighted average of two schemes, i.e., the 1st order upwind scheme and the modified Lax-Wendroff scheme. That is,

$$A_j^{n+1} = A_j^n + s_j^n \Delta A_{j,LWG}^n + (1-s_j^n) \Delta A_{j,UPI}^n \quad (\text{B.1})$$

where $\Delta A_{j,LWG}^n$ is an increment of A_j^n during one time step as found from the modified Lax-Wendroff scheme and $\Delta A_{j,UPI}^n$ is the corresponding increment from the 1st order upwind scheme. These are combined using a weighting determined by the limiter, s_j^n .

The limiter, s_j^n , varies from 0 to 1, depending on the shape of the variation of A_n near the j -th grid point. The extreme values of s_j^n , 0 and 1, result in the 1st order upwind scheme and the modified Lax-Wendroff scheme, respectively. After testing various types of limiters, we found that the following limiter gives stable and reasonably accurate results.

$$s_j = \frac{|2r_j|}{1+r_j^2} \quad (\text{B.2})$$

where $r_j = (A_{j+1} - A_j) / (A_j - A_{j-1})$. The above limiter without the absolute value corresponds to the Van Albada's continuously differential limiter (Van Albada et al., 1982), which when used with the modified Lax-Wendroff scheme produced unstable results.

The limiter, s_j , is a function of r_j which represents the ratio between two consecutive gradients of A . If a gradient of A at one side is dominant, the limiter has a small value which gives more weight to the 1st order upwind scheme to reduce the spurious oscillation. When both sides have comparable gradients, then the result is closer to that of the modified Lax-Wendroff scheme. Note that this limiter satisfies a reciprocal symmetry, i.e., $s(r_j) = s(1/r_j)$, which means that the limiter has the same value for a pair of gradients regardless of their order of appearance.

3 Time-Splitting Method

Dimensional extension requires tremendous efforts for the numerical schemes which use the *staggered point* approximation such as Lax-Wendroff schemes. Since wind wave models have usually three or four dimensions, the use of the modified Lax-Wendroff scheme for all dimensions is quite difficult.

A time-splitting method (Yanenko, 1971) developed by Soviet mathematicians provides an easier way to solve a multi-dimensional equation. It solves a series of one-dimensional equations instead of one multi-dimensional equation. As a simple example, consider a two-dimensional linear advection equation.

$$\frac{\partial A}{\partial t} + \dot{x} \frac{\partial A}{\partial x} + \dot{y} \frac{\partial A}{\partial y} = 0 \quad (\text{B.3})$$

For explicit schemes, the finite difference equation can be written as follows using an operator notation.

$$A_{j,k}^{n+1} = L_{xy}(\Delta t) A_{j,k}^n \quad (\text{B.4})$$

The form of the operator, $L_{xy}(t)$, depends on the numerical scheme being used. For example, if the 1st order upwind scheme is used, the operator becomes

$$L_{xy}^{UPI}(\Delta t)A_{j,k}^n = A_{j,k}^n - \frac{\dot{x}\Delta t}{\Delta x}(A_{j,k}^n - A_{j-1,k}^n) - \frac{\dot{y}\Delta t}{\Delta y}(A_{j,k}^n - A_{j,k-1}^n) \quad (\text{B.5})$$

The time-splitting method *splits* one equation (B.4) into a couple of one-dimensional equations.

$$\begin{aligned} A_{j,k}^{n+\frac{1}{2}} &= L_x(\Delta t)A_{j,k}^n \\ A_{j,k}^{n+1} &= L_y(\Delta t)A_{j,k}^{n+\frac{1}{2}} \end{aligned} \quad (\text{B.6})$$

One-dimensional operators, $L_x(t)$ and $L_y(\Delta t)$, are defined in the same manner as the two-dimensional operator, $L_{xy}(\Delta t)$. For the case of the 1st order upwind scheme, they are defined as

$$\begin{aligned} L_x^{UPI}(\Delta t)A_{j,k}^n &= A_{j,k}^n - \frac{\dot{x}\Delta t}{\Delta x}(A_{j,k}^n - A_{j-1,k}^n) \\ L_y^{UPI}(\Delta t)A_{j,k}^n &= A_{j,k}^n - \frac{\dot{y}\Delta t}{\Delta y}(A_{j,k}^n - A_{j,k-1}^n) \end{aligned} \quad (\text{B.7})$$

This is also called a fractional step method since one time step is divided into several fractional time steps as we *split* the equations. Besides the ease of handling multi-dimensional equations, this method also provides a wider stability region for numerical schemes. Note that more grid points are used in calculating the split form. For the above example of the 1st order upwind scheme, one more grid point value, $A_{j-1,k-1}^n$, is included in the split form.

When applying the time-splitting method to a second order scheme, the sequence of operators should be symmetric to keep its second order accuracy (Warming and Beam, 1976; Anderson et al., 1984), for example,

$$A_{j,k}^{n+1} = L_x\left(\frac{\Delta t}{2}\right)L_y\left(\frac{\Delta t}{2}\right)L_y\left(\frac{\Delta t}{2}\right)L_x\left(\frac{\Delta t}{2}\right)A_{j,k}^n \quad (\text{B.8})$$

In the proposed scheme, we have adopted the following sequence to reduce the amount of computation necessary for each time step.

$$A_{j,k}^{n+1} = L_x\left(\frac{\Delta t}{2}\right)L_y(\Delta t)L_x\left(\frac{\Delta t}{2}\right)A_{j,k}^n \quad (\text{B.9})$$

Although this is an approximation of (B.8), we retain the second order accuracy.

4 New Propagation Scheme

Among the numerical schemes being tested, the modified Lax-Wendroff scheme shows the best performance for both steady and transient cases. The new scheme is based on the modified Lax-Wendroff scheme, adopting the limiter and the time-splitting method to resolve the spurious oscillation and the instability problem described above.

First, the four-dimensional action conservation equation can be *split* into the following three equations which represent propagation in a spatial, a frequency, and a directional dimension, respectively.

$$\begin{aligned}\frac{\partial A}{\partial t} + \frac{\partial}{\partial x}(\dot{x}A) + \frac{\partial}{\partial y}(\dot{y}A) &= 0 \\ \frac{\partial A}{\partial t} + \frac{\partial}{\partial \omega}(\dot{\omega}A) &= 0 \\ \frac{\partial A}{\partial t} + \frac{\partial}{\partial \theta}(\dot{\theta}A) &= 0\end{aligned}\tag{B.10}$$

The spatial advection equation may be also split into two equations, but we keep this in one equation since the same physical domain is involved. These equations are solved sequentially at each time step.

If we use the operator notations as before, the finite difference equation becomes

$$\begin{aligned}A^{n+\frac{1}{3}} &= L_{xy}(\Delta t)A^n \\ A^{n+\frac{2}{3}} &= L_{\omega}(\Delta t)A^{n+\frac{1}{3}} \\ A^{n+1} &= L_{\theta}(\Delta t)A^{n+\frac{2}{3}}\end{aligned}\tag{B.11}$$

Operators are defined according to the numerical schemes being used. For example, when the 1st order upwind scheme is applied, the formula of the two-dimensional operator, $L_{xy}(\Delta t)$, is shown in the previous section. Although the details are not described here, the modified Lax-Wendroff scheme implies two step operations for each operator.

The 1st order upwind scheme and the modified Lax-Wendroff scheme are then combined by a limiter at each level of the time split equations. The values of the limiters are calculated at the beginning of each time step Δt , and remain unchanged through the fractional time steps. For example, the last level of the above equations becomes

$$A^{n+1} = \left(1 + s_{\theta}^n [L_{\theta}^{LWG}(\Delta t) - 1] + (1 - s_{\theta}^n) [L_{\theta}^{UPI}(\Delta t) - 1]\right) A^{n+\frac{2}{3}}\tag{B.12}$$

where s_{θ}^n is the limiter defined by (B.2) in the θ direction.

Since the limiter has a different value for each dimension, the updated value using the two-dimensional spatial operator should be decomposed into x and y components to be combined with the corresponding limiters, s_x^n and s_y^n , which is quite straightforward. The sequence of operators is taken to be symmetric as shown in (B.9) to keep the second order accuracy. Another advantage of the use of the limiter is to be able to avoid erroneous results of the central differencing such as the Lax-Wendroff schemes near a fixed value point (e.g., land boundary, wave breaking point). In this region, the schemes which involve the fixed point often fail to converge due to the constant value being forced at the fixed point. By setting $s_j = 0$ at the adjacent points, this undesirable effect of the fixed point can be avoided.

References

- Andersson, D.A., J.C. Tannehill and R.H. Pletcher (1984), *Computational fluid mechanics and heat transfer*, Hemisphere.
- Gadd, A.J. (1978), "A numerical advection scheme with small phase speed errors", *Quart. J. R. Met. Soc.*, 104, pp. 583-594.
- Gadd, A.J. (1980), "Two refinements of the split explicit integration scheme", *Quart. J. R. Met. Soc.*, 106, pp. 215-220.
- Lax, P.D. and B. Wendroff (1960), "Systems of conservation laws", *Comm. Pure Appl. Math.*, 13, pp. 217-237.
- Morton, K.W. and P.K. Sweby (1987), "A comparison of flux limited difference methods and characteristic Galerkin methods for shock modelling", *J. Comput. Phys.*, 73, pp. 203-230.
- Neu, W.L. and Y.S. Won (1990), "Propagation schemes for wind wave models with finite depth and current", *Proc. of CAMS (Canad. Appl. Math. Soc.) Conference*, pp. 947-954.
- Roe, P.L. (1986), "characteristic-based schemes for the Euler equations", *Ann. Rev. Fluid Mech.*, 18, pp. 337-365.
- Sweby, P.K. (1984), "High resolution schemes using flux limiters for hyperbolic conservation laws", *SIAM J. Numer. Anal.*, 21, no. 5, pp.995-1011.
- Van Albada, G.D., B. van Leer and W.W. Roberts Jr (1982), "A comparative study of computational methods in cosmic gas dynamics", *Astron. Astrophys.*, 108, pp. 76-84.
- Warming, R.F. and R.M. Beam (1976), "Upwind second-order difference schemes and applications in aerodynamic flows", *AIAA Journal*, 14, no. 9, pp. 1241-1249.
- Won, Y.S. (1991), "Higher order numerical schemes for propagation of wind wave spectra", dissertation, Virginia Polytechnic Institute, Blacksburg, VA.
- Yanenko, N.N. (1971), *The method of fractional steps, The solution of problems of mathematical physics in several variables*, Springer.

Appendix C

Analysis of uncertainty for wave run-up and dike height

1 General

The calculations of the wave run-up and the its uncertainty are very essential for the design height of the dikes. The calculation of wave run-up and its sensitivity are carried out for location NAP 0 m for the Egmond profile, however for the Molengat profile where the dike toe is located in deep water, the NAP -25 m has been chosen for the design condition to avoid the unreliable results at the very nearshore area.

2 Calculation of wave run-up

For the wave run-up, two formulae are available:

$$h_r = 8 H_s \tan \alpha$$

$$h_r = 1.5 H_s \tan \alpha \sqrt{\frac{g T_p^2}{2 \pi H_s}}$$

where

- h_r = vertical run-up height
- H_s = significant wave height at the dike toe
- T_p = peak wave period at the dike toe (= 1.05 T_m assumed in this study as T_m is calculated by HISWA)
- $\tan \alpha$ = 1/5 (mild slope)
- = 1/3 (steep slope)

The wave run-up calculation is given in Table C1 (The values of H_s and T_m are based on the reference case)

	Egmond		Molengat	
H_s (m)	2.98		1.46	
T_m (s)	7.08		6.07	
slope	mild	steep	mild	steep
for formula 1 (m)	4.77	7.95	2.34	3.89
for formula 2 (m)	4.81	8.01	2.75	4.58

Table C1 Calculation of wave run-up

3 Uncertainty of wave run-up

The uncertainty of wave run-up can be expressed as follows for the above mentioned two formulae:

$$h_r = 8 H_s \tan \alpha$$

$$\sigma_{h_r} = \left(\frac{\partial h_r}{\partial H_s} \right) \sigma_{H_s}$$

$$\frac{\partial h_r}{\partial H_s} = 8 \tan \alpha$$

$$h_r = 1.5 H_s \tan \alpha \sqrt{\frac{g T_p^2}{2 \pi H_s}}$$

$$= c H_s^{0.5} T_m \tan \alpha$$

since $T_p = 1.05 T_m$ then

$$c = 1.5 \times 1.05 \sqrt{\frac{g}{2 \pi}} = 1.97$$

assuming independency between H_s and T_m , the uncertainty in the wave run-up is given by:

$$\sigma_{h_r}^2 = \left(\frac{\partial h_r}{\partial H_s} \right)^2 \sigma_{H_s}^2 + \left(\frac{\partial h_r}{\partial T_m} \right)^2 \sigma_{T_m}^2$$

where

$$\frac{\partial h_r}{\partial H_s} = 0.5 c H_s^{-0.5} T_m \tan \alpha$$

$$\frac{\partial h_r}{\partial T_m} = c H_s^{0.5} \tan \alpha$$

The calculation of uncertainty in the wave run-up is given in Table C2.

	Egmond		Molengat	
H_s (m)	2.98		1.46	
T_m (s)	7.08		6.07	
	σ_{H_s}	σ_{T_m}	σ_{H_s}	σ_{T_m}
all parameters	0.54	1.98	0.52	2.47
external par.	0.47	0.80	0.45	0.67
internal par.	0.25	1.81	0.27	2.38
ext. with dep.	0.45	0.93	0.45	0.66
all parameters with dep.	0.52	2.03	0.52	2.47

formula 1	mild	steep	mild	steep
$\partial h / \partial H_s$	1.60	2.67	1.60	2.67
σ_{all}	0.86	1.44	0.83	1.39
σ_{ext}	0.75	1.26	0.72	1.20
σ_{int}	0.40	0.67	0.43	0.72
$\sigma_{ex.dep}$	0.74	1.23	0.72	1.20
$\sigma_{all dep}$	0.83	1.39	0.83	1.39

formula 2	mild	steep	mild	steep
$\partial h / \partial H_s$	0.81	1.35	0.99	1.65
$\partial h / \partial T_m$	0.68	1.13	0.48	0.79
σ_{all}	1.42	2.35	1.29	2.13
σ_{ext}	0.66	1.11	0.55	0.91
σ_{int}	1.25	2.07	1.17	1.93
$\sigma_{ex.dep}$	0.73	1.22	0.55	0.91
$\sigma_{all dep}$	1.45	2.40	1.29	2.13

Table C2 The uncertainty of the wave run-up (in meters)

4 Calculation of the design height of the dike and its uncertainty

The design height of the dike can be obtained using the following expression

$$\text{dikeheight}(h_d) = \text{waterlevel}(w_s) + \text{run-up height}(h_r)$$

The run-up height is a function of the significant wave height in front of the dike, and since the wave height is a parameter dependent on the water level in front of the dike, the uncertainty analysis for the dike height will be carried out assuming interdependency between the run-up height and the water level.

By assuming a full correlation between the significant wave height and the water level, the following relation can be found

$$H_s = \beta_{H_s} w_s$$

and similarly for the mean wave period:

$$T_m = \beta_{T_m} w_s$$

a) analysis for formula 1

$$h_d = w_s + 8 \beta_{H_s} w_s \tan \alpha$$

$$\sigma_{h_d}^2 = \left(\frac{\partial h_d}{\partial w_s}\right)^2 \sigma_{w_s}^2 + \left(\frac{\partial h_d}{\partial \beta_{H_s}}\right)^2 \sigma_{\beta_{H_s}}^2$$

where

$$\frac{\partial h_d}{\partial w_s} = 1 + 8 \beta_{H_s} \tan \alpha$$

$$\frac{\partial h_d}{\partial \beta_{H_s}} = 8 w_s \tan \alpha$$

b) analysis for formula 2

$$h_d = w_s + c H_s^{0.5} T_m \tan \alpha$$

$$= w_s + c (\beta_{H_s} w_s)^{0.5} (\beta_{T_m} w_s) \tan \alpha$$

$$= w_s + c \beta_{H_s}^{0.5} \beta_{T_m} w_s^{1.5} \tan \alpha$$

$$\sigma_{h_d}^2 = \left(\frac{\partial h_d}{\partial w_s}\right)^2 \sigma_{w_s}^2 + \left(\frac{\partial h_d}{\partial \beta_{H_s}}\right)^2 \sigma_{\beta_{H_s}}^2 + \left(\frac{\partial h_d}{\partial \beta_{T_m}}\right)^2 \sigma_{\beta_{T_m}}^2$$

where

$$\frac{\partial h_d}{\partial w_s} = 1 + c \beta_{H_s}^{0.5} \beta_{T_m} (1.5 w_s^{0.5}) \tan \alpha$$

$$\frac{\partial h_d}{\partial \beta_{H_s}} = 0.5 c \beta_{H_s}^{-0.5} \beta_{T_m} w_s^{1.5} \tan \alpha$$

$$\frac{\partial h_d}{\partial \beta_{T_m}} = c \beta_{H_s}^{0.5} w_s^{1.5} \tan \alpha$$

The factor β_{H_s} (and β_{T_m}) can be obtained from the model results from the relation between the water level and significant wave height (and mean wave period). The values are summarized in Table C3:

	Egmond	Molengat
β_{H_s}	0.59	0.29
β_{T_m}	1.40	1.21
$\sigma_{\beta_{H_s}}$	0.032	0.09
$\sigma_{\beta_{T_m}}$	0.23	0.44

Table C3 Correlation between significant wave height, resp. mean wave period and the water level and the uncertainty

The design height of the dike and its uncertainty is given in meters in Table C4, where the reference value of the water level is NAP 5.0 meter and the uncertainty is 0.92 m.

	Egmond		Molengat	
H_s (m)	2.98		1.46	
T_m (s)	7.08		6.07	
slope	mild	steep	mild	steep
h_d (formula 1)	9.77	12.95	7.34	8.89
σ_{h_d} (formula 1)	1.80	2.40	1.52	2.03
h_d (formula 2)	9.81	13.01	7.75	9.58
σ_{h_d} (formula 2)	2.40	3.37	2.05	2.93

Table C4 The design height of the dike and its uncertainty

5 Conclusion

From Table C4 with respect to the uncertainty in the dike height it is concluded that:

- The design height for the conditions in the Egmond profile is about the same for both formulae, but the uncertainty in the design height is larger for formula 2, due to the effect of the wave period on the results.
- For the Molengat-profile formula 2 leads to a higher design dike height than formula 1. However, the values are well within the range of uncertainty.
- For the dike at the Egmond profile with mild slope, the height is about 9.81 m with uncertainty about 1.73 m.
- For the dike at the Molengat profile with mild slope, the height is about 8.31 m with uncertainty about 2.05 m.



main office
Rotterdamseweg 185
p.o. box 177
2600 MH Delft
The Netherlands
telephone (31) 15 - 56 93 53
telefax (31) 15 - 61 96 74
telex 38176 hydel-nl

location 'De Voorst'
Voorsterweg 28, Marknesse
p.o. box 152
8300 AD Emmeloord
The Netherlands
telephone (31) 5274 - 29 22
telefax (31) 5274 - 35 73
telex 42290 hylvo-nl

